MARIE-GABRIELLE BRAUNBRUCK

PREPARATION, CHARACTERIZATION AND SIMULATION OF FUNCTIONALIZED MONOLITHIC MATERIALS FOR ELECTROCHROMATOGRAPHY

Dissertation

Zu Erlangung des akademischen Grades einer

Doktorin der technischen Wissenschaften

Betreuer:

Univ.-Prof. Dipl.-Ing. Dr.techn. Johannes G. Khinast

Dipl.-Ing. Dr.techn. Heidrun Gruber-Wölfler

Institut für Prozess- und Partikeltechnik

Technische Universität Graz

Graz, 2013

ACKNOWLEDGMENT

First of all, I like to thank my advisor Johannes Khinast who gave me the possibility to work at the Institute of Process and Particle Engineering of the TU Graz. I wish to thank him for the support and to give me the chance to participate in different scientific congresses and meetings.

Furthermore, I am very grateful for the guidance of my supervisor Heidi Gruber-Wölfler. She helped me in every possible situation and even in times of her absence she always had an open ear and assisted with ingenious advice.

I like to thank the European Union and all cooperation partners of the CAEC project for funding and fruitful collaboration. I am very thankful for the work with René Laskowski in Kaiserslautern.

Moreover, my special thanks goes to Martin Schmid and Stefan Mohr of the Department of Pharmaceutical Chemistry of the KFU. Their help with questions in chromatography did not leave any of these open.

Additionally, I wish to thank all my colleges of the Institute of Process and Particle Engineering. The work atmosphere and the possibility to discuss difficult topics over a good cup of coffee supported me in every situation. Special thanks go to Peter Feenstra, who accompanied me from the beginning of my work and to Michael Gruber, who was very patient in helping me with the simulation project.

I wish to thank my family who encouraged me all along the way and who gave me the possibility to do what I want in life.

I am grateful for the support of my love, Roland, who probably knows best about me and my struggles. I like to thank my flat mates, Emily and Simone, who both know of the different stages during a long project like this dissertation and all my friends who were there for me when I needed them.

ABSTRACT

In the last decade trends in pharmaceutical industry have been transformed from batch towards continuous processes due to the promise of a constant product quality and the facilitation of operation automation. One example for this transition is chromatography, which is a popular tool in pharmaceutical industry for the purification process of an active pharmaceutical ingredient, API. However, this step is very cost-intensive, therefore the development of a continuous mode of operation with maintaining the same separation efficiencies is preferable and could lead to more effective ways to design new drugs.

One afford in this area is the project of continuous annular electrochromatography, CAEC.[i] This project is a cooperation of several academic research institutes and partners from industry and is co-financed by the European Union.

The main goal of this work is the development of a prototype, which combines the advantages of capillary electrochromatography and liquid annular chromatography. This prototype consists of a stationary phase fixed in two glass cylinders, a moving feed rotating at the top and the option to collect fractions at the bottom. Furthermore, two electrodes are embedded on top and at the bottom to be able to apply high-voltage. This device can be operated continuously and can therefore

- ensure a high through-put
- maintain a high separation efficiency
- and is equipped with an online detection system to ensure high quality control.

In this thesis the development of the stationary phase for the CAEC device is documented. The stationary phase is based on a macroporous material functionalized with octyl-chains and supported by porous silica particles to prevent shrinking. This so-called monolithic material is characterized with FTIR spectroscopy, nitrogen physisorption, mercury intrusion porosimetry and elemental analysis.

Furthermore, the material was filled into capillaries for capillary electrochromatography, a planar test cell and the annular device.

[i] www.caec-eu.de/

The separation efficiency of the monolith in all three molds was investigated with a standard test system, namely thiourea, naphthalene and anthracene, a mixture of polycyclic aromatic hydrocarbons, a mixture of phenols and a mixture of alkylbenzenes.

In the capillaries, plate numbers of up to 39 000 per meter could be achieved. The volume flow in the planar test cell could be increased from 10 ml/h in a 0.3 mm gap to more than 40 ml/h in a 1 mm gap. Furthermore, the polycyclic aromatic hydrocarbons could be separated in the planar test cell and the standard test system could be separated in the planar test cell and the annular geometry. A volume flow of more than 300 ml/h could be obtained in the annular device.

The second part of this thesis deals with the development of a simulation program in MATLAB to predict the interactions of the analyte molecules in the mobile phase with the stationary phase. For this purpose, algorithms of diffusion, convection and retentions are incorporated in the program and the separation can be operated in a pressure-driven or electroosmotic flow mode. After the program is fed with data of a specific separation problem, rate constants are calculated and an actual chromatogram is simulated. Additionally, through adjusting the parameters of the stationary phase, different kinds of stationary phases can be tested for a given separation problem.

All in all the stationary phase developed and the supporting simulation program are powerful tools for future demanding separation tasks in the development of new drugs. The presented CAEC device is a starting point towards new production methods in pharmaceutical industry.

KURZFASSUNG

Bei der Entwicklung eines Medikamentes ist eine Vielzahl von Schritten notwendig. Die meisten dieser Schritte werden immer noch in kostintensiven, zeitraubendenden Prozessen umgesetzt. Ein gutes Beispiel hierfür ist die Aufarbeitung biosynthetischer Wirkstoffe, welche vorwiegend mit der diskontinuierlichen Methode der Chromatographie durchgeführt wird. Der Trend zu kontinuierlichen Verfahren birgt die Vorteile einer konstanten Produktqualität, einer möglichen Online-Überwachung des Ablaufs und einer erhöhten Flexibilität bezüglich neuer Nischenprodukte.

Obwohl Chromatographie im Bereich der Analytik bereits gut erforscht ist, gibt es in der Anwendung der präparativen Chromatographie noch Möglichkeiten zur Effizienzsteigerung.

Ein Ansatz hierzu ist die Entwicklung eines kontinuierlichen Ringspalt-Elektrochromatographen.[ii] Dieser wurde in einer Kooperation verschiedener Industrie- und Universitätspartner entwickelt und verbindet die hohe Trenneffizienz der Elektrochromatographie mit dem hohen Durchsatz der kontinuierlichen Flüssigphasenchromatographie. In dieser Arbeit wird die Entwicklung der stationären Phase für dieses Verfahren präsentiert.

Die stationäre Phase ist ein Monolith basierend auf Kieselgel. Dieses makroporöse Material kann durch Funktionalisierung an unterschiedliche Trennprobleme angepasst werden und ist in der Kapillar – Elektrochromatographie bereits weit verbreitet, wird aber in größeren Dimensionen nicht angewendet, da das Material schrumpfen und anschwellen kann.

Im Rahmen dieser Arbeit wurde durch eine Verstärkung des Materials mit Siliziumpartikeln ein stabiler C_8-funktionalisierter Monolith, welcher in einem Stück synthetisiert werden kann, für den Ringspalt – Elektrochromatograph hergestellt. Das monolithische Material wurde mit FTIR Spektroskopie vermessen und die Porenverteilung wurde mit Quecksilberporosimetrie und Stickstoffabsorption ermittelt. Die stationäre Phase wurde in Kapillaren für Kapillar – Elektrochromatographie, eine planare Testzelle und die annulare Einheit gefüllt und auf ihre Trenneffizienz getestet.

Komplexe Testsysteme wie eine Mischung aus polyzyklischen aromatischen Kohlenwasserstoffen, eine Mischung aus Alkylbenzenen und eine Mischung aus Phenolen

[ii] www.caec-eu.de/

konnten mit einer Trenneffizienz von bis zu 39 000 pro Meter in den Kapillaren getrennt werden. In der planaren Testzelle war eine Trennung der polyzyklischen aromatischen Kohlenwasserstoffen mit einem Durchfluss von über 40 ml/h möglich.

Im Ringspalt-Elektrochromatographen konnte ein Standard Testsystem, Harnstoff, Naphthalin und Anthrazen, erfolgreich getrennt und ein Durchfluss von über 300 ml/h erreicht werden.

Neben der Entwicklung der stationären Phase wurde ein Programm zur Simulation der Wechselwirkungen von Analyten in der mobilen Phase mit der stationären Phase erstellt. Durch Anpassung der Parameter der gewünschten Analyten und der stationären Phase können für definierte Trennprobleme die Geschwindigkeitskonstanten errechnet und Chromatogramme simuliert werden. Dies führt zu einer Erleichterung bei der Auswahl einer stationären Phase bei gegebenen Trennproblemen.

Der kontinuierliche Ringspalt-Elektrochromatograph kann somit durch den hohen Durchsatz und der effizienten Trennleistung sowie durch die Möglichkeit der Online-Überwachung eine deutliche Vereinfachung in der Aufreinigung von pharmazeutischen Wirkstoffen ermöglichen.

Table of Content

List of Figures

List of Tables

GOALS AND MOTIVATION

In pharmaceutical industry, a major goal of developing new drugs is adaption on changes in society and an increase in easily accessible medication.[1] Chromatography is used both as an analytical and as a preparative tool in the development of a new drug, from the discovery to the production.[2] Bigelow mentions several chromatographic techniques, which have been used in pharmaceutical industry since 1900.[3] Among others, the most important ones are gas chromatography, thin layer chromatography, capillary electrophoresis and high-performance liquid chromatography, HPLC. Here, HPLC is the method mostly used for preparative applications. However, there are certain drawbacks to this method:

- there is still potential to improve separation efficiency[4] of HPLC,
- the purification step with chromatography in a drug development process is very cost-intensive.

Therefore, the industry looks for alternatives to ensure higher cost-effectiveness and is ambitious to follow the trend towards "Green Chemistry". One possibility to do so is the implementation of continuous processes.[5]
All these aspects and the fact that the pharmaceutical industry is going from large scale bulk drugs towards the small-scale production of high value-added products countenance the development of new flexible separation systems.

An attempt to facilitate and accelerate the purification step of active pharmaceutical ingredients, APIs, in pharmaceutical industry is the project to establish **Continuous Annular Electrochromatography**, short **CAEC**. This CAEC project is one of the small or medium-scale focused research projects co-financed by the European Commission in the *7th Framework Programme Theme 4 – NMP Nanosciences, Nanotechnologies, Materials and new Production Technologies*. The cooperation assigned with this task is a combination of different honorable research institutes and partners of the industry.

The main objective of the CAEC project is the

- combination of continuous annular chromatography to ensure a high through-put while
- maintaining the separation efficiency of capillary electrochromatography.

The prototype developed is able to separate a multiplicity of separations and can easily be adapted to new tasks.

In detail the project involves the manufacturing of a prototype, which includes two glass cylinders assembled in a device, where the stationary phase for the separation problem is fixed between the glass cylinders, the annulus. The feed is rotating on top of the annulus and the fractions can be collected at the bottom. To increase separation efficiency, two electrodes are implanted on top and at the bottom of the annulus and a voltage of up to 20 kV can be applied. Furthermore, the development of the prototype is supported by the implementation of adaptive process control and by providing a predictive steady state model for process design and optimization.

In the following, the different challenges of the cooperation members are going to be presented.

The **Kaiserslautern University of Technology** is assigned with the development of the equipment design and testing of the prototype for continuous annular electrochromatography.

The **University of Dortmund** is responsible of the development of a predictive steady state model for progress design and optimization as well as an adaptive process control, furthermore of the development of on-line sensors and the management of the project.

Microinnova Engineering GmbH provides the equipment of the prototype to obtain a fully functional CAEC unit.

The **Institut für Mikrotechnik Mainz GmbH** is instructed to design and manufacture the prototype.

Additionally, **Galileous Oy** and **Novartis** are industrial partners and provide support defining test systems and directions in industrial testing.

Our task in the project, the task of the **Graz University of Technology**, is the

- **preparation**
- **characterization and**
- **functionalization of a stationary phase** for this prototype for continuous annular electrochromatography.

This work is the description of a C_8-functionalized silica-based stationary phase implemented into different molds, namely capillaries for capillary electrochromatography, a planar test cell and a glass annulus for the prototype. Furthermore, a detailed characterization procedure of this stationary phase and different separation problems are discussed.

An additional part is the **simulation of the interactions of solute molecules with a reversed phase stationary phase**. The program developed is validated and the separation of a standard test system, namely naphthalene and anthracene, is calculated.

A) INTRODUCTION

1. The monolith

In pharmaceutical industry, the most cost-intensive step in the production of a new active pharmaceutical ingredient, API, is the purification process. The technique predominantly used for that step is chromatography. There are more and more complex systems, which have to be separated and therefore, the separation efficiency has to be increased. This is directly coupled with the decrease of the diameter of particles used in chromatography.

The need to decrease the size of particles in chromatography promoted the development of new materials for the stationary phase. Therefore, the application of macroporous materials in one piece lies near. These materials are called monolithic materials. Monoliths have the right requirements and can easily be adapted to certain molds and problems due to their high versatility in the distribution of pores and the adaption of functional groups. Due to the large through-pores a high flow velocity is ensured, because of the micro- and mesopores high separation efficiency can be obtained.

The beginnings of the implementation of monolithic materials for chromatography lay in the 1980s.[6] The first compounds used were organic monomers, whereas the use of inorganic silica-based materials only started in 1996.[7] Today, besides organic and inorganic, also hybrid monolithic materials are used in chromatography. Besides chromatography also other areas of interest use the advantages of monolithic materials, i.e., catalytic applications,[8] monolithic membranes[9,10] and micro extractions[11-13].

As the majority used in capillary electrochromatography (CEC) is organic polymer-based materials, a short overview of these materials and their application will be given. However, in this work the focus will be laid on the silica-based monoliths, which did suit our application better.

1.1. Organic polymer monolithic materials

There are several ways to synthesize organic polymeric monoliths for capillary electrochromatography. To begin with, there is the possibility to prepare a monolith from an

aqueous monomer solution. For this approach, acrylamide, piperazine diacrylamide and vinylsulfonic acid are mixed and stearyl methacrylate or butyl methacrylate are added for hydrophobicity.[14] To ensure mixing of the components, also a surfactant has to be induced. The solution is sonicated and immediately drawn into the capillary for polymerization.[15] Besides the monomers, also a catalyst, like tetramethylethylenediamide, has to be added. The acid mentioned induces precipitation and can be replaced by a porogen, like polyethylenglycol.

To avoid the problem of the insoluble monomers in aqueous solutions polymers can also be prepared in organic solvents. Considering the different possibilities to combine polar and non-polar solvents, one can tailor the solubility of the starting material. It can be distinguished between three organic monomers: acrylamide, methacrylate ester and polystyrene. Again, a porogen and a catalyst, like azobisisobutyronitrile, have to be added to initiate polymerization.

In other words, polymer monoliths can be grouped into hydrophilic, like the ones synthesized by Hjertén[6], and hydrophobic polymers, prepared in organic solvents like the ones of Švec et al.[7] To be more precise, the water-soluble monomers are polymerized in presence of a salt, whereas the hydrophobic monomers are polymerized in the presence of a co-solvent, the porogen. Therefore, the classification is based on the different phase-separation principles.[16]

According to Guiochon[17], there are three major steps to prepare a polymer monolithic column: the first is to activate the walls, i.e., to cover the inner wall of the capillary with a binding agent for the monolith polymerized later in the capillary, which can be defined as the second step. The third step may include surface modification to obtain the desired functionality of the monolithic column. A good overview of the different polymerization techniques is given by Buchmeister.[18]

In addition to the common polymer monoliths, there are also porous layer open tubular (PLOT) columns and molecular imprinted polymers (MIP). The PLOT columns can only be used in gas chromatography due to their low specific surfaces which lead to low retention and low capacities.[19] The MIP principle consists of the key – lock system, where a specific problem can be targeted. The analytes are enclosed in the polymer matrix during gelation and can be washed out when the material is rigid.[20,21]

In contrast to silica monoliths, a wide variety of different recipes for polymer monoliths can be found in the literature. Due to the widespread approaches, no significant characterization procedures are described. However, the separation of biomolecules seems to be more promising on organic polymer-based columns although there are just a few commercially available ones.[17] Organic monolithic materials show good pH stability but they tend to swell and shrink when certain organic solvents are used. This affects the mechanical stability and results in a shorter lifetime.[22-24]

1.2. Silica-based monoliths

As mentioned, the beginnings of the silica-based monolithic columns lie in the early 1990s in Japan.[25] This procedure was transferred into a patent and led to intensified research in this field. Today, Merck (Darmstadt, Germany) offers a monolithic column for high performance liquid chromatography, namely the Chromolith® column.

1.1.1. Preparation

Silica-based monoliths are formed via the Sol-Gel process. Larry Hench has given a detailed review on the steps and aspects of the process.[26] There are three ways how to obtain monolithic materials: gelation of solutions of colloidal powders, hydrolysis and polycondensation by alkoxide or nitrate precursors followed by hypercritical drying or hydrolysis and polycondensation of alkoxide precursors followed by drying and aging under ambient conditions. The focus of this introduction will be laid on the last one.

A sol is a colloidal dispersion of a solid species in a liquid[27], whereas a gel is an interconnected rigid network[26]. Furthermore, one can distinguish between (i) aerogels – where the liquid from the pores is removed by critical drying and the gel maintains its size; (ii) xerogels – where the gels are dried and ambient temperature and the gel shrinks; and (iii) alcogels – where the pore liquid is alcohol based.

To prepare a silica-based monolith silicon alkoxides like tetramethoxysilanes (TMOS) and tetraethoxysilanes (TEOS) are used. Depending on the desired functionality of the monolith, one can add other silicon alkoxides like aminopropyltriethoxysilane (APTES) to introduce amino groups or n-octyltriethoxysilane (C_8-TEOS) to obtain a reversed phase functionalization. In addition to that a porogen to tailor the porosity is needed. In general polyethyleneglycole (PEG) or cetyltrimethylammonium bromide (CTAB) are used. The start

of the polymerization is initiated with the change of the pH-value of the solution. The formation of a gel will be discussed in detail in the following.

The first step of the monolith preparation is the mixing of the reagents. The process is started by hydrolysis of the components which can only be performed by solving the alkoxides in alcohol and adding water and a catalyst like acid or base in a second step. Polycondensation starts delayed but happens simultaneously and competes with the hydrolysis. Aggarwal et al. define the process as beginning spinodal decomposition, where solvent-rich and solvent-poor domains are formed and frozen by gelation.[28] There are several factors, which influence the rates of hydrolysis and condensation. The major ones are temperature, concentration of electrolyte, nature of solvent, pressure and the type of precursor.[29,30] A detailed overview is given by Hench.[26] The gelation point, however, is not easy to measure but may be determined by measuring the viscoelastic behavior of the gel as a function of the shear rate.[30]

Another important parameter to consider is the porogen added. Depending on type and amount the matrix of the gel can be strengthened or weakened due to the different pore sizes generated.[31] Furthermore, the direction of the eletroosmotic flow during the separation in the monolithic column can be influenced. This will be explained in more detail in the chapter *Electrophoresis*.

After gelation, the gel is aged for the appropriate amount of time. Aging is also called syneresis and increases the strength of the network tremendously. Additionally, the porosity can be tailored by changing the aging solvent to a basic solution; an acidic or neutral solution does not have any influence.[17]

The following drying step is highly important concerning the structure and the stiffness of the monolith. Depending on the drying method, the gel will maintain its size or will shrink drastically due to the capillary stresses. The monolith may be decreased in size by a factor of 10. The amount of shrinkage can be described by the relation between capillary pressure and modulus of the network[27]:

$$P_c = -2\gamma_{LV} \cos\frac{\Theta}{r_h} \quad (1)$$

where $\gamma_{(LV)}$ is the surface tension of the pore liquid at the liquid vapor interphase, Θ is the contact angle of the liquid and r_h is the hydraulic radius, the ratio between two times the

pore volume and the pore surface. There are several drying methods, i.e. supercritical drying, where the liquid is replaced by critical CO_2, changing the drying liquid or using ionic liquids.

Depending on the application intended for the monolithic material, a further treatment can be densification. The material is dried at temperatures between 1000° and 1700° C and therefore, the process can also be called sintering. With this step, the gel is transformed into a glass. In the combination with TiO_2 particles, sintered SiO_2 monoliths are considered as bone replacement materials.[32]

To use the monolithic columns for chromatographic applications, the problem of shrinkage has to be overcome. Therefore, the solution of Merck – one of the few commercial distributors of monolithic columns – is to enclose the monolithic rod with a PEEK shell. This so called cladding ensures that there is no void between the monolith and the outer cover. In this work, we present a way how to prepare stable monolithic columns and how to avoid the cladding step.

1.1.2. Properties of the monolithic columns

As already mentioned, the main advantage compared to particle-packed columns in chromatography is the increased porosity and surface area of the monolithic columns. Therefore, the characterization of this property is a major issue. In this special case, the porosity is an indication for the through-put of mobile phase and therefore for the productivity of the system. However, before one can determine the porosity and similar characteristics, one has to agree over a universal terminology. The most important variables are D [m], the pore mean diameter, S [m^2/g], the specific surface area of the material and V_P [cm^3/g] the specific pore volume of the material.

The mean diameter has to be handled with care because it does not represent more than one maximum. If the pore size distribution (PSD) is bimodal, which is often the case with mesoporous materials, D only gives a mean value.[33] Furthermore, on one hand the larger the specific surface area, the smaller is the pore diameter whereas $S < 10\ m^2/g$ indicates a macroporous sample.

The pore volume on the other hand can serve to calculate the internal porosity, ε_P, of the material, which is expressed as

$$\varepsilon_P(\%) = \frac{V_P}{V_P + V_S} \cdot 100 \quad (2)$$

V_S is the volume of the pure solid. The internal porosity added to the external porosity ε_e gives the total porosity ε_t.[34] The total porosity can also be calculated via

$$\varepsilon_t = \frac{4F_v}{\pi d_c^2 u} = \frac{4F_v t_0}{\pi d_c^2 L} \quad (3)$$

where F_v is the volume flow-rate, d_c is the column diameter, L is the length of the column and t_0 is elution time of an unretained solute.

The boundaries between external ε_e and the internal porosity ε_P, also referred to ε_i, are not easily drawn, one of the definition most popular in literature[35,36] is the following: ε_e is the fractional volume of the cavities between and around the particles or of the through-pores whereas ε_P is the volume fraction occupied by the mesopores inside the particles or in the monolithic rod.

There are different ways to determine total porosity of a sample. Firstly, one can calculate the porosity via the density of the sample measured with helium pycnometry and the total pore volume, secondly it can be determined with mercury intrusion and nitrogen physisorption and thirdly, in chromatography one can determine the porosity with inverse size exclusion chromatography.[37] IUPAC divides pores into different categories, namely micropores with a diameter smaller than 2 nm, mesopores in a range of 2 – 50 nm and macropores larger than 50 nm.[38] Monolithic columns usually have a bimodal pore size distribution due to their fraction of mesopores.[39]

Directly correlated with the porosity is the density of the material. Depending on the characterization method one can determine either the true density or the apparent density. The true density is the ratio of mass to volume excluding open and closed pores, which is rather difficult to determine. Apparent density only excludes open pores and can be measured with gas pycnometry.[40] The sample is placed into a sample chamber of a known volume. After evacuation the sample is purged with helium and due to the pressure differences the density volume can by calculated via the ideal gas equation.

The pore size distribution and pore volume can be determined with the classical methods, i.e. nitrogen physisorption and mercury intrusion. Depending on the pore size, either of these methods will give more accurate results. Both theories will be explained in detail in the next section.

1.3. Nitrogen physisorption

To determine the pore size distribution, the pore volume and the pore diameter of a porous material, several methods can be used. The most important one is to use the relation of relative pressure to adsorbed gas molecules on a surface and in the pores.[41] The gas taken up by the solid is called adsorbate, whereas the solid taking up the gas is the adsorbent. The relationship is expressed in adsorption isotherms and Brunauer classified different types of isotherms[42], which are now assigned into the IUPAC classification body.[38] The six types of adsorption isotherms are significant for different porosities of the solid material (see Figure 1.1).

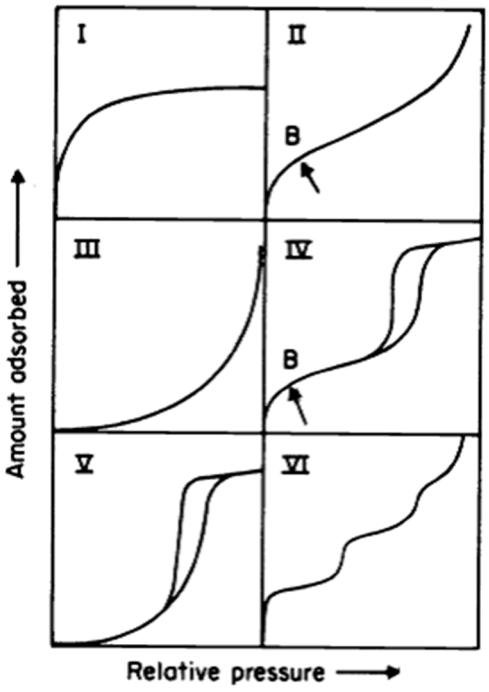

Figure 1.1: The six types of adsorption according to IUPAC[38]

The Type I isotherm is typical for microporous materials with a small external surface. In the literature these isotherms are also referred to as Langmuir Isotherms. The Type II isotherm is formed by non-porous or macroporous materials, where B indicates the point of monolayer adsorption. Type III isotherms are not common, but these are related to materials which

only have an indistinctive point B. In comparison of the first three types, which are reversible, Type IV shows a hysteresis loop. This loop is assigned to the capillary condensation in mesoporous materials. Type V is rarely recorded and Type VI shows the stepwise adsorption of multilayers on a uniform non-porous surface. A sub class of these isotherms is the differentiation in four types of hysteresis loops, see Figure 1.2.

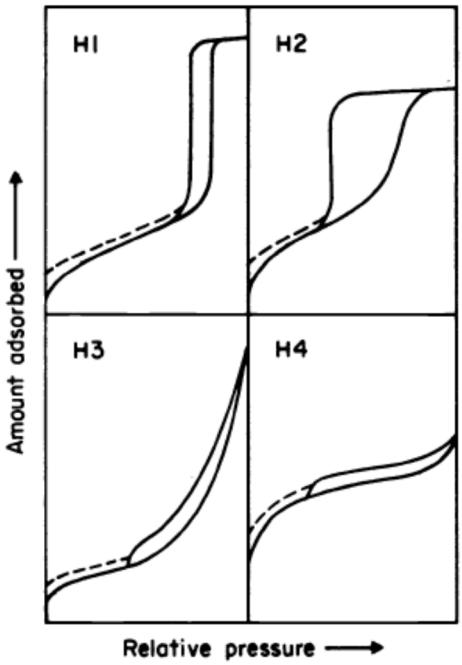

Figure 1.2: Hysteresis types after IUPAC[38]

H1 and H4 are two extreme types of hysteresis whereas H2 and H3 are intermediates. The type of hysteresis is dependent on specific pore structures. H1 is given by porous networks formed of agglomerates, so there are no interconnecting channels.[43] In the systems showing a H2 hysteresis, the pore network is not well defined, there are narrow and wide sections. However, in literature pores of these networks are referred to as “ink bottle” pores. H3 is given by aggregates of plate shaped particles, which give slit-shaped pores and H4 hysteresis are observed with narrow slit-shaped pores for a network with regular pores. The dashed lines in Figure 1.2 are indications for low pressure hysteresis. These can be associated with the swelling of non-rigid porous structures, with non-reversible uptake of molecules in pores or with chemical reactions of adsorbate with the adsorbent.

To derive the specific surface area, the most common method is still the popular BET plot[44], i.e. the Brunauer, Emmett and Teller theory for *Adsorption of Gases in Multimolecular Layers*[42].

The equation derived by these authors is

$$\frac{p}{n^a\left(p^0 - p\right)} = \frac{1}{n_m^a C} + \frac{\left(C-1\right)}{n_m^a C}\frac{p}{p^0} \qquad (4)$$

where p is the pressure, p^0 is the saturation pressure, n^a is the is the gas amount adsorbed at the relative pressure p/p^0 and n^a_m is the monolayer capacity. The BET constant C depends on the enthalpy of adsorption of the first layer. To be able to calculate the surface area, a BET plot as mentioned has to be performed. It requires a linear relation between $p/(n^a(p^0-p)$ and p/p^0 in the range of 0.05 and 0.30. The reason for this range is C, which has to be a constant and at lower pressures the adsorption energy generated by the first molecules adsorbed on the surface is higher than that one adsorbed by the following ones.[44,45]

Via the interception and the slope of the plot one can determine the monolayer capacity and the BET constant. By knowing these values the specific surface area, a_s, can be calculated with following equation

$$a_s = \frac{n_m^a N_a A_x}{M} \qquad (5)$$

where N_a is the Avogadro constant, A_x is the cross-sectional adsorbate area and M is the molecular mass of the adsorbent. Nowadays, the measurements are carried out with nitrogen as an adsorbate at a temperature of 77 K. With nitrogen as the only adsorbing gas, the static-volumetric method is used. After the sample chamber is evacuated, it is filled with nitrogen and the first layer of molecules is adsorbed on the sample surface. As more and more molecules adsorb, the pressure in the chamber becomes larger and can be compared to the gas added to generate the adsorption isotherm.

1.4. Mercury intrusion porosimetry

The basic idea of intrusion porosimetry measurements is to force a non-wetting liquid into the porous material. If one knows the volume of liquid, in this case mercury, and the pressure applied, one can calculate the pore distribution via the Washburn equation[46]:

$$p = -\frac{4\gamma\cos\Theta}{D_w} \qquad (6)$$

where p is the minimal pressure needed to force mercury into a pore, γ is the surface tension of mercury and Θ is the contact angle between mercury and surface. D_w is the corresponding diameter of the pore due to the Washburn equation. As γ is equivalent to 0.48 N/m at 293 K, Θ equates to 140° at 293 K and both values are considered to be constant, i.e. are independent of the pressure applied and of the curvature of the walls, the equation is simplified to

$$p = \frac{14.708}{D_w} \qquad (7)$$

when p is 1 bar, the diameter of the pores filled is ≥ 15 µm, when 1000 bars are applied, pores with a diameter ≥ 15 nm are completely filled with mercury.[33,46]

As the materials have to be dried and evacuated before measuring, one has to consider the influence of this treatment on the material.

1.5. Inverse size exclusion chromatography and scanning electron microscopy

In addition to N_2 physisorption and mercury intrusion porosimetry pore size distributions can also be determined with inverse size exclusion chromatography[47], where a standard of sample molecules of different molecular mass and size is used. Due to a calibration curve determined with the standard sample the pore size distribution can be obtained.

A very good tool to examine the morphology of monolithic material is scanning electron microscopy (SEM). However, the average SEM does not have a resolution high enough to determine the pore size distribution visually. Yet, the microscopic pictures only give a good indication of the homogeneity of the monolithic structure. A good example is shown by Tanaka et at.[48] For the sake of completeness laser scanning confocal microscopy is mentioned. With this technique one can depict a three-dimensional figure of the monolithic structure.[49]

1.6. Different monolithic stationary phases

Depending on the separation problem, different functionalizations of the monolith are advantageous. The most common stationary phase used is reversed phase. The alkyl chains implemented are either C_8 or C_{18}.[50-53] Furthermore, the functionalization can either be

obtained in a one-step synthesis or via a two-step method. Both approaches are explained in detail in the chapter *Results and Discussion*.

In addition to reversed phase chromatography, chiral separations are applied in many fields of expertise like pharmaceutical and food industry. A good example for a chiral selector is γ – cyclodextrine, which after activation can be bonded to the silica backbone via an alkoxysilane linkage. A detailed overview is given by Lämmerhofer et al.[54] Furthermore, proteins attached to the silica monolith can be employed to overcome difficult separation problems. Zheng et al. summarize various possible proteins as chiral selectors bound to a monolithic backbone.[55]

Furthermore, the mixed mode stationary phases should be mentioned. In general, mixed mode functionalizations contain reversed phase and weak anion exchange functionalities like amino or thiol groups.[56,57]

2. Chromatography

The monolithic materials extensively described in the preceding chapter are used in different types of chromatography. Therefore, the basic theory will be summarized in this chapter and some main aspects are going to be explained in detail.

2.1. Theory and basics

The separation mechanism of chromatography is based on the concept of distribution of analytes – molecules that are needed to be analyzed or separated – between a stationary and a mobile phase. In liquid chromatography, the compounds are dissolved in the liquid mobile phase and due to different interactions with the solid stationary phase, one species is travelling faster than the other along the column. The slower one is retained more on the stationary phase. Therefore, this type of mechanism is also called adsorption equilibrium. The molecular interactions of the molecules and the two phases are based on three different forces: the ionic interactions, which are used in ion exchange chromatography; polar interactions, which are induced by dipols and dispersive interactions, which result from charge fluctuations and are underlying the separation in reversed phase chromatography.[58]

To define the obtained chromatograms and important parameters, Figure 2.1 shows an example chromatogram. Obviously, when the substances are injected into the column, this

point in time is the injection point. As the mobile phase is travelling faster than the solute molecules, the analytes, this small peak can be seen at the detector very early in the chromatogram. This is the dead point, the volume of the mobile phase till that point is the so-called dead volume, V_0. The retention volume, V_r, is the volume passed through the column between the injection point and the peak maximum. The corresponding amount of time is the retention time, t_r. The corrected retention volume, V'_r, is the retention volume reduced by the dead volume. The corrected retention time, t'_r, is the retention time reduced by the time, t_0, which is the time the dead volume needed to pass through the column. To summarize these important values, Table 2.1 gives an overview of the parameters given in Figure 2.1.

Table 2.1: Important parameters of a chromatogram

Parameter	Signification
V_0	dead volume
t_0	dead time
V_r	retention volume
t_r	retention time
V_r'	corrected retention volume
t_r'	corrected retention time

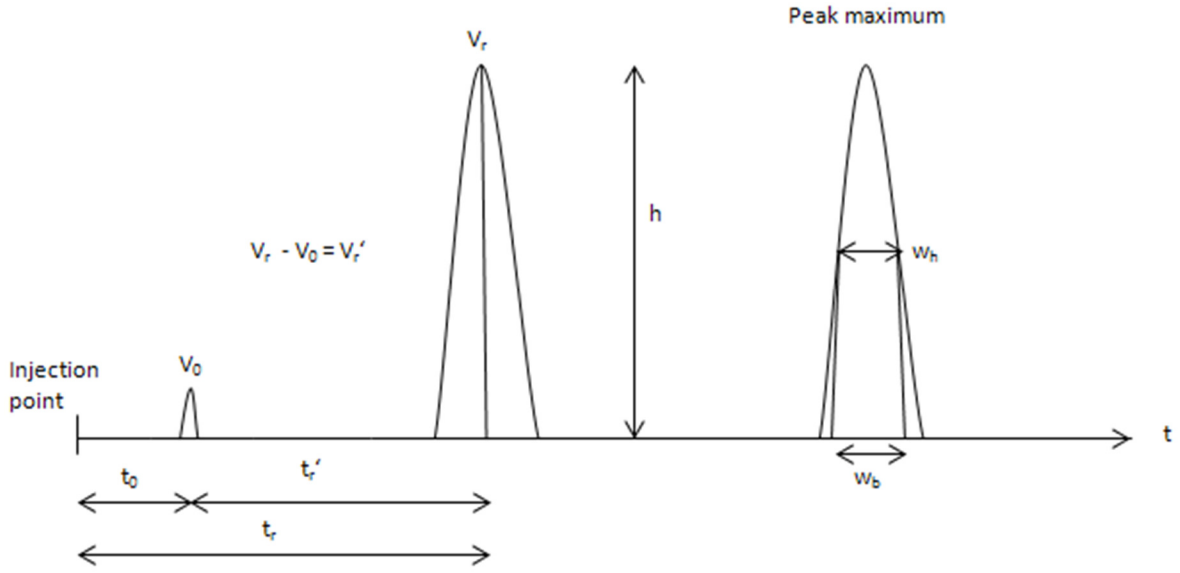

Figure 2.1: Example chromatogram to explain important parameters, adapted from[58]

For chromatographic theory, the width of the peak at 0.6505 times the height of the peak is important, because it is equivalent to two standard deviations, 2σ, of the Gauss distribution. The peak width at half of the peak height is important when the area of the peak is of interest.

These are the basic parameters given by the chromatogram. To be able to make statements about the separation, there are two theories that can be applied: the plate theory and the rate theory. Details are given in the following chapter.

2.2. The plate theory

The plate theory was developed by Martin and Synge[59] in the 1940s. The theory assumes that the solute is always in equilibrium with the mobile and the stationary phase. To be more precise, the column is divided into a number of plates or cells, where the solute is considered to spend the amount of time it needs to be in equilibrium with the phases. The smaller the plate heights the more efficient is the column. Therefore, the number of plates of a column is called the separation efficiency of the column. The distribution between the stationary and the mobile phase is correlated with the distribution coefficient K

$$c_s = Kc_m \qquad (8)$$

where c_s is the concentration of the solute in the stationary phase and c_m is the concentration of the solute in the mobile phase, respectively.

Furthermore, the retention volume can be calculated with the volume of the stationary phase, V_s, and the mobile phase, V_m,

$$V_r = V_m + KV_s \qquad (9)$$

and additionally, the adjusted retention volume, V'_r, is calculated via

$$V'_r = V_r - V_0 \qquad (10)\ .$$

Considering that V_0 is equivalent to V_m, when there are no additional ways besides the column for the mobile phase like tubes or something similar, we can conclude that

$$V'_r = KV_s \qquad (11)\ .$$

Another important parameter is the capacity ratio, k'. It is given by

$$k' = \frac{KV_s}{V_m} \qquad (12)$$

and can be measured directly from the chromatogram. It is convenient because in contrast to the retention volumina, k' is independent from the flow rate of the mobile phase.
In respect to the retention times, k' can also be expressed as

$$k' = \frac{t_r - t_0}{t_0} \qquad (13)\ .$$

The selectivity α gives an indication how well two adjacent peaks of two different solutes, A and B, are separated. It is given by

$$\alpha_{A/B} = \frac{V'_{r(A)}}{V'_{r(B)}} = \frac{K_{(A)}V_s}{K_{(B)}V_s} = \frac{K_{(A)}}{K_{(B)}} \qquad (14)\ .$$

The selectivity is the ratio of the distribution coefficients of the two solutes and is independent on column parameters, respectively.
The resolution, R_s, does also show the separation between two adjacent peaks, but includes the forms of the peaks. R_s is given by

$$R_s = 2 * \frac{t_{r(B)} - t_{r(B)}}{w_{b(A)} + w_{b(B)}} \qquad (15)\ .$$

Resolution can also be expressed in column parameters:

$$R_s = \frac{\sqrt{N}}{4} * (\alpha - 1) * \frac{k'}{k'+1} \qquad (16)\ .$$

2.2.1. Peak asymmetry

The major factors of peak asymmetry are non-linear adsorption isotherms. Before one can go into detail on that, one has to discuss adsorption isotherms first.
In general, six adsorption isotherms are known (see also Figure 1.1). Here, only the most important ones are mentioned. An adsorption isotherm describes the equilibrium of the

adsorption of a substance on a surface in dependence of the concentration in the bulk phase. The most common ones are the linear, the Freundlich and the Langmuir isotherm.[60]
The linear isotherm is described by Henry's adsorption isotherm equation

$$\Gamma = K_H P \qquad (17)$$

where Γ is the adsorption function, K_H is the Henry constant and P is the partial pressure of the adsorptive gas; for solutions, the concentration is used instead of the partial pressure.
The Freundlich isotherm equation describes the case of heterogeneous surfaces, where regions of high adsorption affinity and of low adsorption affinity are present. This type of isotherm is described by

$$\Gamma = K_F P^q \qquad (18)$$

where K_F and q are constants. The Freundlich isotherm is curved concave to the abscissa.
The Langmuir adsorption isotherm equation is given as

$$\Theta = \frac{K_L p}{1 + K_L p} \qquad (19)\ .$$

In this case Θ is the surface coverage, p is the gas pressure and K_L is the Langmuir constant. The Langmuir isotherm is characterized by the saturation of the adsorbent surface. As already mentioned in the previous chapter, the saturation can also appear in a microporous material. The Langmuir isotherm commonly results from adsorption in liquid systems.
In cases of non-linear adsorption isotherms, peak tailing or fronting can occur, see Figure 2.2.

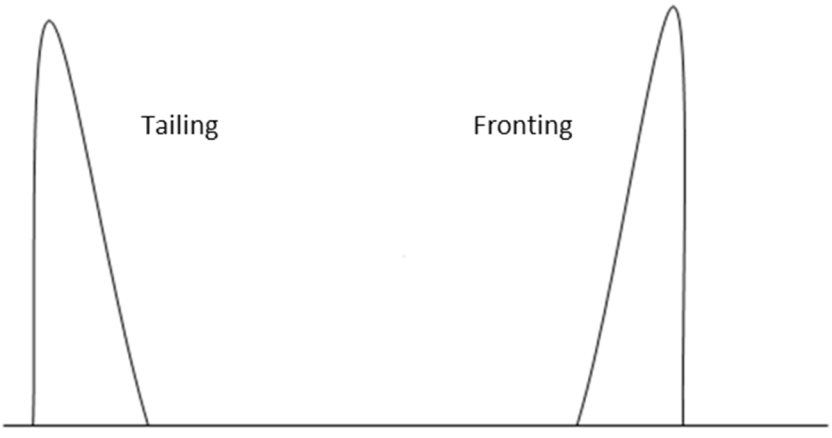

Figure 2.2: Peak asymmetry, adapted from[58]

Tailing usually occurs due to sample overload. In this case, a too large mass of sample is injected into the column. The interactions between the solute molecules and the stationary phase will increase, which leads to a higher K and a convex isotherm. Fronting is rather unusual in liquid chromatography, but when it occurs it is due to poorly packed columns.[61] Here, the isotherm formed is concave. Peak asymmetry has a great influence on column efficiency.

2.2.2. Column efficiency

To define the efficiency of a column, the different solute peaks have to be examined in respect to each other. Therefore, the peak widths are going to play an important role. To be more precise, because the peak has a Gaussian form, the points of inflection correspond to twice the standard deviation. In conclusion the variance of the peak is inversely proportional to the number of theoretical plates and it follows that the narrower the peak the higher the number of theoretical plates and the higher the column efficiency.

As the band broadening is also a function of time, the equation of the number of the theoretical steps in a column is

$$N = \left(\frac{t_r}{\sigma} \right)^2 \qquad (20) .$$

When we introduce the correlation of the standard deviation $\sigma = 4\ w_b$, where w_b is the width of the peak at the base, we can rearrange equation (20) and it follows that

$$N = 16 \left(\frac{t_r}{w_b} \right)^2 \qquad (21) .$$

When applied, it is often more practical to measure the peak at half height w_h, and this corresponds to 2.35σ.[62]

Again, we can adjust equation (20) to

$$N = 5.54 \left(\frac{t_r}{w_h} \right)^2 \qquad (22) .$$

To obtain the effective column efficiency, the retention time has to be exchanged with the adjusted retention time. As the efficiency of a column is influenced by band broadening of the peaks, which again is induced by dispersion, this is worth a closer look. Van Deemter proposed a theory, which will be topic in the next section.

2.3. The Van Deemter equation and the rate theory

The basic idea of Van Deemter et al. was to find a velocity of the mobile phase travelling through the column where the dispersion of the molecules is a minimum.[63] The authors combined the effects, which contribute to band broadening into three different factors: A, eddy diffusion, B, longitudinal diffusion and C, mass transfer resistance. The resulting equation for the plate height H at a given velocity u is

$$H = A + \frac{B}{u} + Cu \qquad (23)\ .$$

The eddy diffusion term, A, is defined as

$$A = \lambda d_P \qquad (24)$$

where d_P is the mean diameter of the particles of the stationary phase and λ is a factor which includes the packing uniformity and the particle size range of the stationary phase. Basically, the eddy diffusion describes the different ways a molecule might take along the column. Due to the tightly packed bed molecules are forced around the particles and therefore move different distances in the same unit length of the column. As the eddy diffusion is only depending on the properties of the stationary phase, small particles and high uniformity of the packed bed will lead to a decrease of that amount of dispersion, which is caused by eddy diffusion.

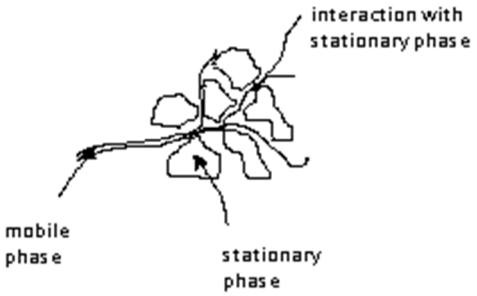

Figure 2.3: Different ways of mobile phase through the stationary phase, adapted from[62]

B, the longitudinal diffusion, considers the diffusion due to the movement of particles in a liquid phase, a scheme is shown in Figure 2.4. It describes the diffusion along the axis of the column parallel to the movement of the mobile phase. Therefore, the longitudinal diffusion is given by

$$B = 2\gamma D_M \qquad (25)$$

where γ is a constant considering the hindrance factor of the stationary phase packing and D_M is the diffusion coefficient of the solutes in the mobile phase. As the longitudinal diffusion is time dependent, the term is more important at low mobile phase velocities.

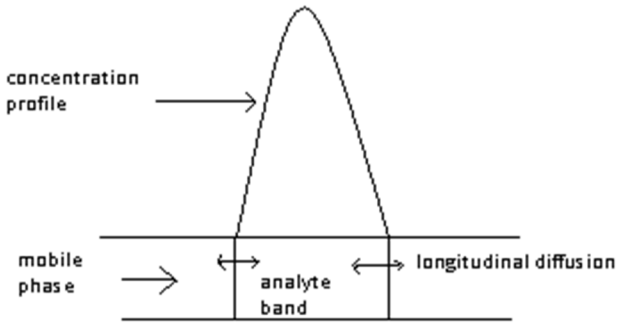

Figure 2.4: Diffusion of molecules as mobile phase moves along, adapted from[62]

The mass transfer resistance term, C, pays respect to the fact that molecules have different time spans to interact with the stationary phase. If we consider the distribution of the molecules along the radial axis of the column, there are several, which are near to the stationary phase and can enter it immediately and several molecules, which are not close

and are therefore transported further down to a spot where they can come in contact with the stationary phase. The same happens inside the stationary phase. The C term is the addition of the contribution in the stationary and in the mobile phase.

$$C = C_S + C_M = \frac{d_f^2}{D_S} + \frac{d_p^2}{D_M} \quad (26)$$

D_S and D_M are the diffusion coefficients of the solute in the stationary and in the mobile phase, whereas d_f and d_p are the thickness of the film on the stationary phase and the particle diameter.

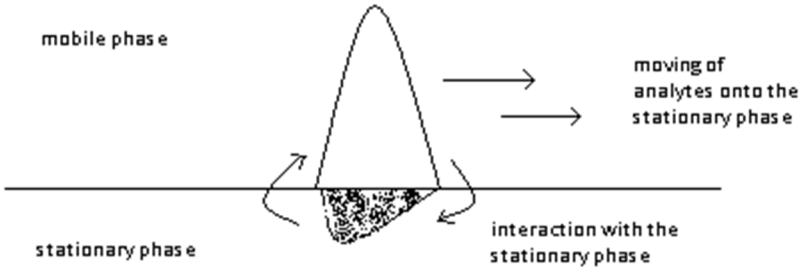

Figure 2.5: Interaction of solute with the stationary phase in the mobile phase, adapted from[62]

All these contributions to solute dispersion can be summarized in a plot, called Van Deemter plot and shown in Figure 2.6, with the plate height, H, as the ordinate and the velocity u as the abscissa. The minimum of the resulting curve shows the lowest plate height and therefore gives the optimum velocity. To sum up the dependencies of the Van Deemter equation, one can see clearly that A is independent of the mean velocity, B is inversely proportional and C is directly proportional to u.

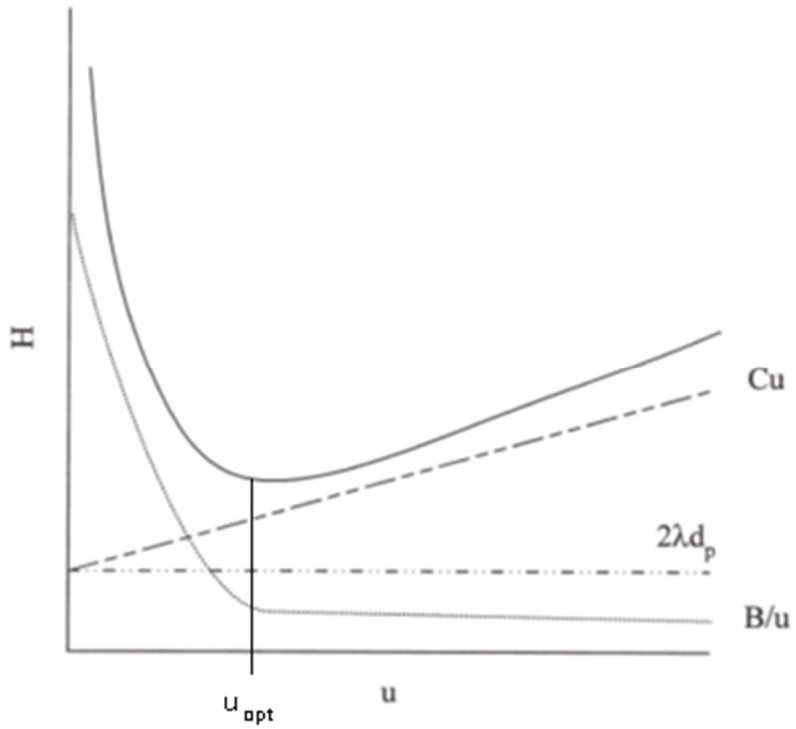

Figure 2.6: A (···-), B (···) and C (–--–) term resulting in the Van Deemter plot, taken from [64]

The Van Deemter equation was one of the first theories of the rate theory approaches. In the times of Van Deemter, not all effects of dispersion were perfectly understood. Therefore, several other colleagues of the authors developed extensions of the equation. Here, only the most important ones are going to be mentioned.

2.3.1. The Giddings equation

J. C. Giddings did not agree with Van Deemter, because it appeared to him as in irregularity that there is a finite contribution to dispersion at the limit of zero mean velocity.[65]

Therefore, he introduced an equation (equation (27)), where it appears that the Van Deemter equation is a particular form.

$$H = \frac{A}{1+\frac{E}{u}} + \frac{B}{u} + Cu \qquad (27)$$

It is clear that when the Giddings term E << u, equation (27) turns into the Van Deemter equation. On the other hand, when E >> u, the first term tends towards zero and meets the requirements Giddings intended to fulfill with this approach. Furthermore, Giddings introduced the concept of a reduced step height or velocity. More details on this will be given in the following section.

2.3.2. The Knox equation

The reduced plate height and the reduced velocity were introduced by Giddings in 1964 to be able to compare columns packed with particles of a different diameter.[66]

The reduced plate height, h is defined as

$$h = \frac{H}{d_p} \qquad (28)$$

whereas the reduced velocity is given by

$$v = \frac{ud_p}{D_M} \qquad (29)\ .$$

D_m is the diffusion coefficient in the mobile phase and d_p is the diameter of the particle. The equation derived by Knox et al.[67] is

$$h = av^{\frac{1}{3}} + \frac{b}{v} + cv \qquad (30)\ .$$

In this case, the parameters a, b and c are not derived theoretically, but are determined by fitting to an experimental curve. Therefore, the Knox equation has its limits concerning column design.

For completeness, the Golay equation is mentioned. The Golay equation is valid for open tubular columns and therefore, the A term for eddy diffusion can by neglected.[68] In open tubular columns, the mobile phase velocity is directly proportional to the diffusivity of the solute and inversely proportional to the diameter of the column.

2.4. Application of chromatography

Having discussed the basic theory of chromatography, the next step to take is the debate about application possibilities. The project presented is a combination of preparative

chromatography and the introduction of electrophoresis. First the basics of these principles are going to be explained, before the realization into one device will be addressed.

2.4.1. Electrophoresis

The basic principle of electrophoresis is the migration of ionic components in an electrolyte solution under the application of voltage.[69] Electrophoresis is the umbrella term for several separation techniques using an electric field to move the mobile phase through a column or something similar. Techniques used frequently are zone gel electrophoresis and capillary electrophoresis. A further development of the latter one is capillary electrochromatography, CEC.

The mobile phase and the analytes are moved through the system by application of a voltage. The main parameters and conjunctions between them are shown in the following.

The velocity, v, of every particle is proportional to the applied electric field, E, and a constant.

$$v = \mu E \qquad (31)$$

The constant, μ, is called electrophoretic mobility and is defined as

$$\mu = \frac{q}{6\pi\eta r_H} \qquad (32)$$

where q is the charge of the analyte, η is the viscosity of the solution and r_H is the hydrodynamic radius of the analyte. The basic mechanism, which transports the bulk or mobile phase through the column, is called the electroosmotic flow, EOF. The electroosmotic flow, u_{eo}, is defined by the Smoluchowski equation[70]

$$u_{eo} = \frac{\varepsilon_r \varepsilon_0 \xi E}{\eta} \qquad (33)$$

where ε_r is the dielectric constant of the solution, ε_0 is the permittivity of vacuum and ξ is the zeta-potential, which will be explained in the following.

The EOF originates from different layers of ions in a system. In capillary electrochromatography, the capillary walls are usually covered with silanol groups (due to the fused silica glass nature of the capillaries). Counter ions, in this case cations, build up on

the walls and form a fixed layer, which is also called Stern layer. Moving further away from the walls, another layer, the diffuse layer, is evolving.[14] The potential difference formed between the fixed layer and the bulk, which is the potential drop in the diffuse layer, is called the ξ-potential. The thickness of the double layer is δ. The distance between two adjacent double layers, i.e. the pore diameter in packed columns, has to be 10 to 40 times larger than δ to avoid overlapping of the double layers, which can lead to a decrease in EOF.[71] However, in capillary electrochromatography, the overlap is no problem, because a concentration of 1 mM salt in water gives a double layer thickness of 10 nm.[72] The zeta-potential is inversely proportional to the square root of the molar concentration of the buffer solution.

When an electric field is applied, the solvated cations move towards the cathode and drag the solvent molecules with them. Figure 2.7 shows how the electroosmotic flow is build up in a capillary for capillary electrochromatography.

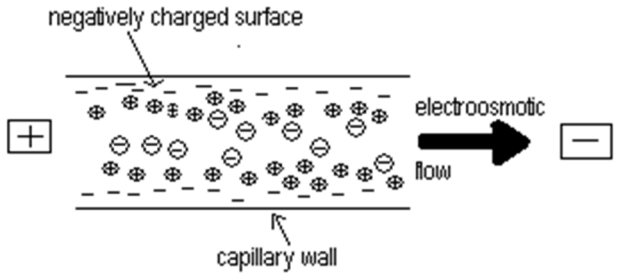

Figure 2.7: Scheme of electroosmotic flow, adapted from[14]

The main advantage of the electroosmitc flow is that it forms a flat flow profile. In contrast to a pressure-driven system, where the flow profile is parabolic, the backpressure does not play an important role. Therefore, one can use smaller particles in electrochromatography. When smaller particles are used, the eddy diffusion and the mass transfer resistance term of the Van Deemter equation decrease.[73] Figure 2.8 shows a scheme of electroosmotic flow profile.

Figure 2.8: Difference between pressure-driven and electroosmotic flow, adapted from[14]

This different flow profiles have been measured using an ultraviolet laser pulse by uncaging a fluorescent dye. This dye was illuminated with a pulse of visible light and could be photographed by a camera.[74]

Clearly, the materials used in CEC should be able to support electroosmotic flow. Therefore, in contrast to HPLC, the capillaries packed with silica materials are not end-capped, i.e. the silanol groups are not all reacted with a functional group. Additionally, the pH-value of the system influences the ionization of the silanol groups, which again has an impact on the EOF. Therefore, buffer solutions instead of pure water are used.

There are several factors, such as the mobile phase composition and the electric field strength that have to be considered to be able to achieve an efficient separation.[75-77] The addition of an organic modifier is contradictory in the literature – the vast majority agrees on an increase of the EOF when the amount of acetonitrile used as an organic modifier is increased.[78] When methanol is used, the electrophoretic mobility runs through a minimum at 60 w% methanol.[14]

Another aspect, which has to be paid attention to, is Joule heating, which arises inevitably when an electric current passes through a conductor. The increased temperature influences the electrical conductivity and the viscosity of the fluid which further has an impact on the electroosmotic flow profile due to a radial temperature gradient.[79] To avoid extensive Joule heating, low voltages, low column temperatures and narrow internal diameters should be used.[80] Additionally, low buffer concentrations support high EOF velocities, but their buffer capacity can quickly be depleted. Therefore, a compromise concentration of the buffer ions at 5 to 50 mM is advised.

In contrast one can stabilize or reverse the EOF, depending on the separation intended. Sodium dodecyl sulfate, SDS, is usually used as a surfactant, but when applied in CEC, it acts

as a surface modifier. The increase in EOF was assigned to the positively charged tails interacting with the stationary phase leaving the negatively charged heads of the SDS on the surface.[72] Another surfactant, cetyltrimehtylammonium bromide, CTAB, can reverse the EOF. To achieve an appropriate mobile phase velocity, the polarity of the power supply has to be reversed as well.[81]

In general, CEC is applied in separation problem containing neutral substances. Commonly, reversed phase stationary phases are used. Acidic analytes are not easily separated because they tend to move against the EOF towards the anode. However, they can be separated when injected in their neutral form and an adapted stationary phase, i.e. with sulfonic and alkyl functional groups[80] is used. With some modifications and trade-offs to the velocity of the EOF the separation in their ionized form is also possible.[82] Basic compounds show severe peak tailing on reversed phase stationary phases due to strong interactions of the bases with the ionized silanol groups. This problem can be overcome with the addition of triethylamine, which competes for the ionized silanol groups on the stationary phase.[72]

In conclusion it can be said that capillary electrochromatography has a wide range of application possibilities. However, only few nanoliters per hour can be put through an analytical device, therefore, other approaches for preparative tasks had to be found.

2.5. Preparative chromatography

Whereas capillary electrochromatography is used for an analytical purpose, preparative chromatography is a purification process. Therefore, the first priority of preparative chromatography might not be the resolution, but the through-put.[83] However, the term preparative is covering a wide range of sample weight; the preparative scale starts at several g/h through-put but can go up to a kg/h size.[84] The first intuitive approach to obtain more sample amount is an up-scale of the analytical devices. This attempt is usually done in industry on an empirical base. Columns with a diameter larger than 10 mm are used, but are packed with the same particles as in analytical chromatography. Rathore et al described, how to undertake this task.[85] Another way towards preparative chromatography with already existing columns is sample overload. This is the possibility to process high sample loads without acquiring new equipment. There are two ways of sample overload, the volume and the mass sample overload. Both can be very effective, if separation parameters are controlled carefully.[59]

2.5.1. Planar chromatography

Another technique for preparative chromatography is thin layer chromatography, TLC. The device is built of a thin adsorbent layer, for preparative scales more than 0.5 mm, which is strapped to a firm back, usually made of glass. Common sorbent layers are made from silica gels, cellulose or aluminum oxide. In contrast to conventional TLC, in preparative TLC the sample is placed in a band at the bottom of the layer in an amount as high as possible. The development is the same process as in analytical TLC, though the separation takes longer due to the sample amount. To improve resolution, the development can be carried out several times.[86] The advantage of this instrumentation is the in-time detection possibility, i.e. there are no long ways of the components to the detector and the separation happens simultaneously. The major disadvantage of TLC is that one cannot influence the velocity of the mobile phase, which is only achieved by the capillary forces.[87] When the separation is not carried out at the optimum velocity, the efficiency is not the highest possible. Therefore, other improved systems were developed. First, new adsorbent layers with smaller particles were introduced. The technique of the separation was the same as for TLC, but with the new plates, called high performance thin layer chromatography, HPTLC, less volume of the mobile phase was needed and resolution could be increased.[88]

Another approach is the possibility to control the flow through the system by force. To be able to induce forced flow, one has to seal the planar device. The flow can be forced through the device either by an electrical field, called planar electrochromatography (PEC), or by pressure, called overpressured layer chromatography (OPLC).

In the pressurized modes, high pressures and long development times have to be used to obtain reasonable plate efficiencies. The pressures applied range between 10-25 bars.[89] There are two basic development modes in OPLC: linear and circular separations in online and off-line mode. For the linear separation in online mode, impregnation is always necessary whereas for the circular separation in the off-line mode no preparation is needed.

The method discussed in the literature more frequently is planar electrochromatography. PEC can be divided into open planar electrochromatography, still called PEC and closed planar electrochromatography, PPEC. In open PEC, all three phases, namely solid, liquid and vapor phase are involved in the separation process. In recent years, many researchers published articles on different modes of operation.[87,90,91] The main disadvantage of open

PEC is the development of Joule heating that leads to mobile phase evaporation. If there is excessive solvent evaporation, dry spots can occur. However, only moderate evaporation of the mobile phase does help to improve efficiency due to focused separation bands. Another disadvantage is the flux of the mobile phase to the surface of the adsorbent layer, which leads to a poor reproducibility of the results.[92] To overcome this undesired effect, pressurized planar electrochromatography was developed. The closed system of PPEC is assured by the elimination of the vapor phase through a foil pressed to adsorbent layer. In the literature, there are different ways described, how the foil can be pressed to the adsorbent layer.[93-96] The adsorbent layer can be placed in the chamber horizontally or vertically and the pressure can be applied with a hydraulic press or with the force of gravity. Although the work done promises very interesting results, the authors mentioned agree that there is still need to further develop PEC and PPEC. A detailed review what has been done so far is given by Joseph Sherma.[97]

2.5.2. Continuous modes of chromatography

There are several ways how to operate chromatography in a continuous way. The most prominent ones are true moving bed, TMB, and simulated moving bed, SMB, chromatography, which has more significance in practice. In true moving bed chromatography, the solid phase is trickled from the top of the column, whereas the solvent phase is pumped in from the bottom of the column upwards, i.e. counter-current. The feed is induced constantly at the middle of the column into the liquid phase. The phases are collected at the point contrary to their inlet point and stripped of the feed components. The solvent and the stationary phase are recycled and moved back into the column.[98] Although the counter-current mode of operation should lead to high efficiencies due to the reduction of mass transfer resistance[99], in practice there are many difficulties with the realization of TMB, because no constant flow profile and no homogeneous packing can be achieved. This results in low separation efficiencies.[100] Therefore, some adaptions in the operation mode led to simulated moving bed chromatography. Here, the stationary phase is not moved for real, but its movement is simulated by changing the inlet and outlet ports of the system. The liquid phase is flushed through several shorter columns filled with stationary phase that are interconnected. Depending on the system, there can be six to 12 columns, which are

connected in series and with valves placed in between to open and close them when needed.[101] Figure 2.9 shows a scheme of the SMB process.

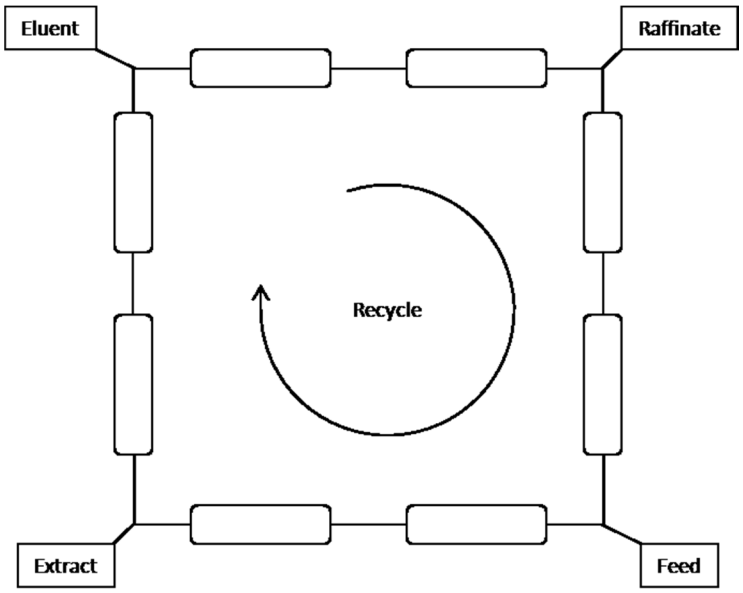

Figure 2.9: Scheme of the simulated moving bed process, adapted from[102]

Several pumps are installed to move the recycling flow through the system, inject feed and fresh solvent and withdraw the raffinate and extract flows. The design and control of the SMB process is complex, therefore the operation is supported by mathematical modeling.[103] Developed in the 1960s, SMB technology was mainly used for separation of sugar and xylene isomers; in the 1990s, the process was brought towards purification of fine chemicals and pharmaceuticals, especially enantiomers.[104] Although SMB has significant advantages over elution chromatography, i.e. lower solvent consumption, there is still room for process improvement.[103]

A true continuous mode of operation is annular chromatography. The first annular apparatus was built by Martin in the 1950s.[105] In contrast to the SMB method, it can separate more than two fractions. Two glass cylinders with a gap in between, where the stationary phase is filled into, are assembled in that way that the feed and the solvent is continuously injected into the top part. The cylinders are rotating at a fixed speed and the analytes can be collected in fractions at the bottom. Due to their distribution, the components form helical bands and separate along the rotating cylindrical stationary phase.[106] If the system is in a

steady state, the analytes always leave the annulus at the same angle.[107] The relationship between time and the angle of the outlet flow can be described as[108]

$$t = \frac{\Theta}{\omega} \qquad (34)$$

where t is the time, Θ is the angular coordinate and ω is the angular velocity. A scheme of an annular chromatographic device is shown in Figure 2.10.

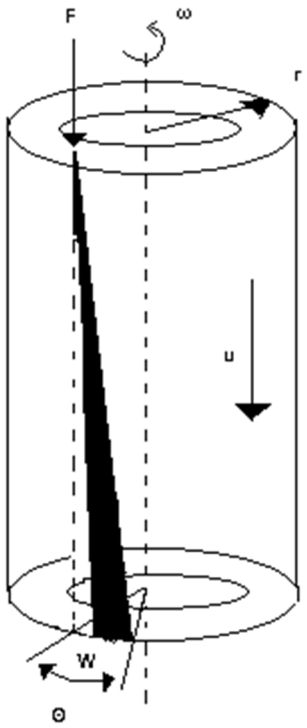

Figure 2.10: Drawing of annular chromatography with r = radius, u = velocity of the mobile phase, F stands for feed, ω is the rotation rate, W is the band width and Θ is the displacement of the band to the feed point[109]

Since the first development, many versions of the annular chromatography device have been constructed.[109] The first commercially available type of continuous annular chromatography was sold by Prior Separation Technology GmbH (Götzis, Austria) under the name P-CAC in 1999.[110] Since then, more and more applications for different separation problems have been published. A good overview is given by Frank Hilbring.[106] Complementary to the experimental set-ups, the research area of process simulation is growing rapidly. Several approaches based on mass balance equations to optimize the separation process were published recently.[111-113]

Another mode of operation was introduced by Hans-Jörg Bart[iii] and is the goal of this work. Here, the cylinders with the implemented stationary phase are fixed and the feed inlet at the top of the device is rotated around the gap. Furthermore, two electrodes are built into the system to be able to apply voltage similar to capillary electrochromatography. This new concept is called Continuous Annular Electrochromatography, CAEC. A scheme of the apparatus is shown in Figure 2.11.

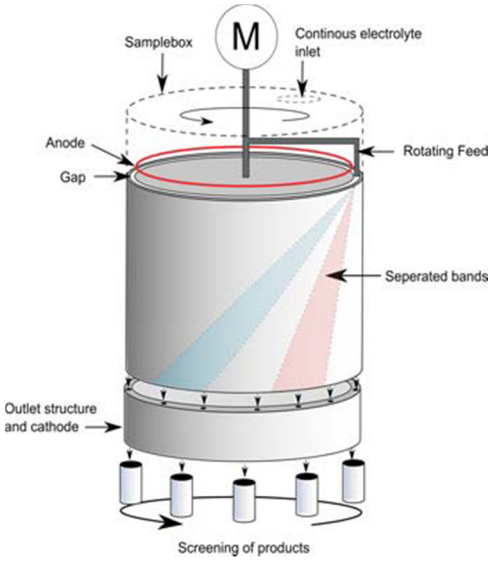

Figure 2.11: Drawing of CAEC device[iii]

This work is dedicated to develop the appropriate stationary phase for this CAEC device. More details are given in the following chapters.

[iii] www.caec-eu.de/

B) PRACTICAL WORK

3. Chemistry development

Based on the advantages mentioned in the *Introduction* (Part A), silica-based monoliths with different functional groups were developed. A lot of work was put into the decision, which functionalization should be assigned with the highest significance, so experiments were carried out to introduce cyano-, amino-, thiol-, reversed phase (C_8 and C_{18}) and normal phase functionalization. A detailed description of the set of experiments to facilitate the decision is described elsewhere.[114] The main chemicals used for the preparation of functionalized monoliths are given in Table 3.1.

Table 3.1: Chemicals and their function for the preparation of silica-based monoliths

Compound	Abbreviation	Function
tetraethoxysilane	TEOS	silica backbone normal phase (NP)
triethoxy(octyl)silane	C_8-TEOS	reversed phase (RP)
3-aminopropyltriethoxysilane	APTES	catalyst, amino groups
3-cyanopropyltriethoxysilane	CPTES	cyano functionalization
3-mercaptopropyltrimethoxysilane	MPTMS	thiol functionalization

Due to the results of the previous experiments[114], the decision was made to pursue the approaches to synthesize normal phase, reversed phase and amino functionalized silica-based monoliths. In the following sections, the syntheses of these materials are explained and discussed in detail.

3.1. Normal phase monolith

As the silica backbone only has hydroxyl groups on the surface, this stationary phase is very polar and can be used to separate polar substances.[115] Furthermore, the amount of ionizable components– compared to a reversed phase stationary phase – is increased, which can lead to an increase in electroosmotic flow. Although normal phase monoliths are not very

common in industry, it can be beneficial to provide normal phase monoliths for specific separation problems, like purine and pyrimidine derivates.[116] The starting chemicals for the synthesis of our NP materials are shown in Table 3.2.

Table 3.2: Chemicals for normal phase monolith, amounts given for our preparation approach

Compound	Abbreviation	Equivalent	Function
tetraethoxysilane	TEOS	1	silica backbone
diethylamine	DEA	0.5	catalyst
cetyltrimethylammonium bromide	CTAB	0.04	porogen
water	H_2O	7.4	solvent
ethanol	EtOH	6	solvent

The material tended to crack and shrink after drying, so the recipe of the monolithic precursor mixture had to be improved. In the literature there are many advises how to avoid this problem.[117-119] In our case, we decided to add a drying control chemical agent, dimethylformamide. The exact amounts can be looked up in the chapter *Experimental*. To ensure high porosity of the material, the surfactant – also called porogen – CTAB was added to the precursor mixture. Further information on the topic is given later in this chapter. The precursor mixtures discussed in the next chapters already include these additional chemicals.

3.2. Amino groups functionalized monolith

This monolithic material is actually a mixed mode weak anion exchange monolithic because amino groups and alkyl chains are introduced. The concept is based on a method reported by Ding et al.[120] A detailed overview of the components used is given in Table 3.3.

Table 3.3: Compounds for the amino functionalized monolith, amounts given for our preparation approach

Compound	Abbreviation	Equivalent	Function
tetraethoxysilane	TEOS	1	silica backbone
triethoxy(octyl)silane	C_8-TEOS	1.4	reversed phase mode
3-aminopropyltriethoxysilane	APTES	0.5	catalyst, amino groups
cetyltrimethylammonium bromide	CTAB	0.04	porogen
dimethylformamide	DMF	1.3	drying control chemical agent
water	H_2O	3.5	solvent
ethanol	EtOH	6	solvent

Amino functionalized materials can be used to separate biomolecules and proteins.[121-123] Furthermore, active pharmaceutical ingredients can be purified.[124]

3.3. Reversed phase monolith in a two-step approach

As the normal phase silica monolith has a hydrophilic surface, spiked with OH groups, the possibility of functionalization is obvious. Several suggestions are mentioned in literature.[125-127] We used the following approach: after preparation of the silica backbone as mentioned in the previous chapter, the monolith is washed and a solution with a chlorated alkylsilane depending on the desired functionalization is prepared. The monolith is flushed with the solution for several minutes or even left submerged overnight. After functionalization, the monolith has to be washed again and conditioned with mobile phase before use. The advantage of this proceeding is the possibility of adaption of different functional groups. However, the functionalizing chemical is rather aggressive, as it is highly reactive due to the chloride and corrodes metallic surfaces. In our case, it was not an appropriate way of preparing a reversed phase monolith. Synthesis is described in detail in the section *Experimental*.

3.4. Reversed phase monolith in an one-step approach

Reversed phase stationary phases are the most common materials used in chromatography and capillary electrochromatography. Small chemically synthesized molecules as well as

large biomolecules can be separated. Depending on the mobile phase, almost every separation problem can be adapted.

To facilitate the preparation of a reversed phase stationary phase, a one-step octyl-group functionalized monolith was prepared. The exact precursor amounts are shown in Table 3.4.

Table 3.4: Compounds of reversed phase monolith, amounts given for our approach

Compound	Abbreviation	Equiv.	Function
tetraethoxysilane	TEOS	1	silica backbone
triethoxy(octyl)silane	C_8-TEOS	0.4	reversed phase mode
diethylamine	DEA	0.5	catalyst
cetyltrimethylammonium bromide	CTAB	0.04	porogen
hydrochloric acid, 0.5 N	HCl	0.3	solvent, catalyst
water	H_2O	1.4	solvent
methanol	MeOH	11	solvent

As this monolith appeared to us as the most promising one, this preparation was pursued further. In the beginning, the monolithic mixture was only filled into capillaries for capillary electrochromatography. For this purpose, the addition of DMF was sufficient as a cracking prevention. However, as the molds were upscaled and the amount of material increased, the prepared stationary phase was not as mechanically stable. Another approach had to be found. We decided to add silica particles to support the monolithic structure. This kind of material is called particle-loaded monolith.[128]

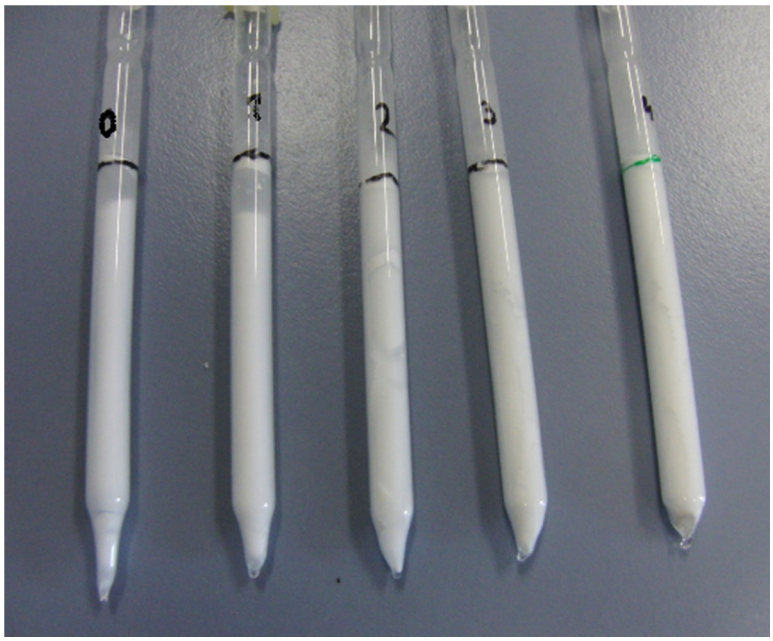

Figure 3.1: Comparison of monolithic precursor mixtures with different weight percentages of silica particles: 0: 0 mg, 1: 5 mg (0.4 w%), 2: 10 mg (0.8 w%), 3: 20 mg (1.6 w%), 4: 30 mg (2.4 w%) silica particles.

Figure 3.1 shows the decrease of shrinkage when adding silica particles. Another advantage of this amendment is the possibility to either increase the functional groups – e.g. to add C_8-functionalized particles to the reversed phase precursor mixture or add another functionalization for a more complex separation problem. Another modification of our monolith synthesis was the omittance of the drying step after aging due to the severe shrinking even with additional particles. Figure 3.2 shows the results after drying.

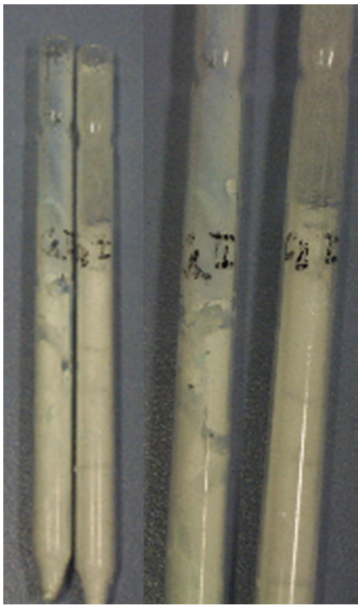

Figure 3.2: Monolithic material after drying at 100°C

This aspect was only important for major applications. The capillaries could be dried at 40°C. After adjustment of the stability by addition of silica particles, the porosity of the monolith decreased, which is also part of the discussion in the chapter *Characterization*. Reasons for that could be the uptake of space by the particles as well as the filling of the pores of the particles by monolithic material. However, one of the major tasks was a high through-put of macromolecules so again different amounts of CTAB were added to adjust the pore size. Exact values are given in the chapter *Characterization*. A pleasant side effect was that due to the particles no DMF was needed as a drying control chemical agent. The last modifications are further explained in the following.

3.5. Addition of particles

To decrease costs and to work sustainably, silica particles were prepared in situ. Therefore, different types of monoliths were synthesized. After polymerization, the monolith was washed and grinded mechanically into particles.

Three different kinds of particles were prepared:

- TEOS particles
- TMOS particles
- Stöber particles.

A more detailed description is given in the chapter *Experimental*. Unfortunately, the addition of "home-made" particles did not give the expected effect and caused instant polymerization of the precursor mixture. Furthermore, the particles were not porous, so the internal surface was even more decreased. To obtain always the same porosity and size distribution, the decision was made to use commercial silica particles of the size of 5 µm in diameter.[iv]

3.6. Addition of porogen

As already mentioned, a porogen or surfactant is an essential ingredient for the precursor mixture to control pore size and pore volume. In our case, cetyltrimethylammonium bromide, CTAB, is used (see Figure 3.3).

[iv] Polygosil®, Macherey-Nagel GmbH & Co KG, Düren, Germany

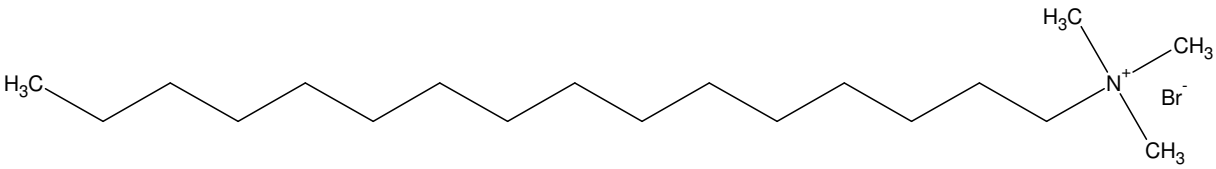

Figure 3.3: Molecular structure of CTAB

The figure shows that the compound is positively charged and for this reason it can be used in excess to influence the electroosmotic flow. Another porogen that is often used is sodium dodecyl sulfate, SDS, which is anionic (see Figure 3.4).

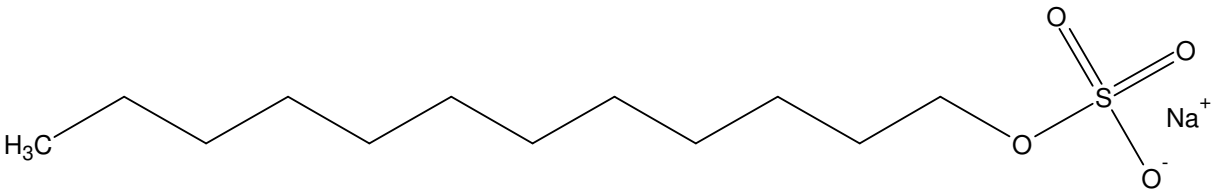

Figure 3.4: Molecular structure of sodium dodecyl sulfate

The amount of porogen added can be adapted depending on the desired through-put. Furthermore, the specific surface area can be increased, and therefore, more possibilities for adsorption processes are accessible. A detailed study will be shown in the chapter *Characterization*.

3.7. Summary of the main aspects in chemistry development

Besides the modifications mentioned, the influences of different parameters were investigated. An overview is given in Table 3.5.

Table 3.5: Influence of the single components

Component	Resulting influence	Details
Amount of catalyst	Polymerization time	Important for implementation in different molds
Temperature of precursor mixture	Polymerization time	Important for implementation in different molds
Mixing	Distribution of particles, homogeneity of monolith	Influence on high homogeneity
Filling procedure	Distribution of particles, homogeneity of monolith	Influence on high homogeneity
Air-tight sealing	Heterogeneity	Cracks and voids due to dryness

Figure 3.5 shows the influence of the amount of catalyst added as an example. The left pipette was filled with a precursor mixture, where not enough catalyst was added. The material was more gel than monolith, the polymerization took too long. In the right pipette, the appropriate amount of catalyst was added. The monolith had the desired properties of porosity and specific surface area.

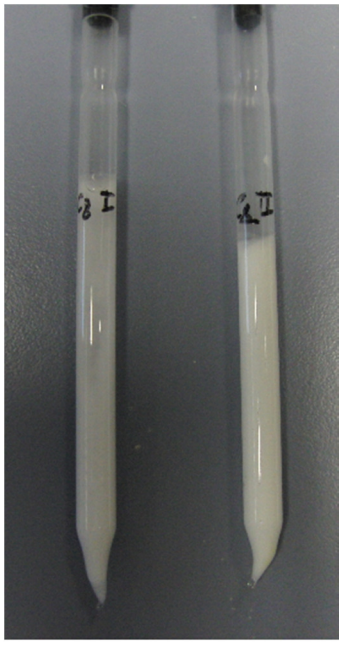

Figure 3.5: Difference in amount of catalyst added

4. EXCURSUS

4.1. Tetramethoxy silicate approaches

An alternative to our method, namely to prepare a TEOS based monolith, is to use tetramethoxy silicate, TMOS, as a precursor in a two-step approach.[22,31,48,129,130] Three different recipes were used to see, if these kinds of monoliths can be used for an up-scale application. In Figure 4.1 monoliths according to Allen et al., [1][131], Tanaka et al., [3][132] and Tanaka et al., [4][31] are shown.

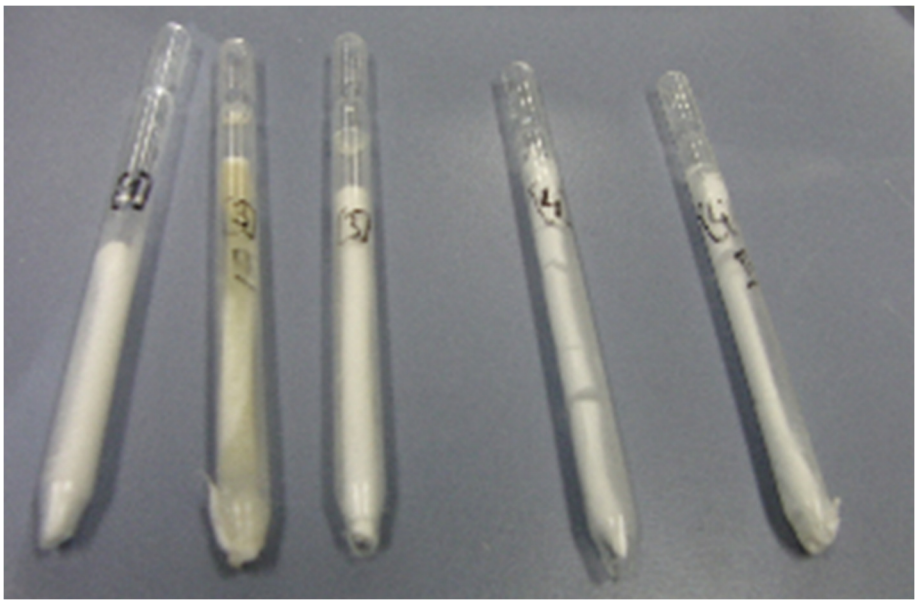

Figure 4.1: Samples of different TMOS monolith preparations

All monoliths, normal phase and functionalized in a second step, sample [3] II (second from the left) and [4] II (first from the right), shrunk significantly and are not adequate for our experiments. These findings are also reported in the literature.[117] Furthermore, the influence of the porogen on the texture was investigated. In the picture below, Figure 4.2, different amounts of the porogen polyethylene glycol, PEG, in a TMOS precursor mixture were investigated. The more porogen was added, the more the monolith shrunk. A reason for that is the increased instability of the system. Detailed recipes can be looked up in the section *Experimental*.

Figure 4.2: Different amounts of porogen PEG added to the TMOS precursor mixture

4.2. Organic monoliths

To cover all possibilities common in modern CEC, organic polymer monoliths were taken into consideration. In contrast to inorganic monolithic structures, monoliths based on organic precursors have not found an application at industrial scale yet. However, in analytical devices, polymer-based monolithic capillaries can achieve impressive results.[7,133,134] Our approach was based on work done by Schmid et al.[135] The basic monomers used are piperazine diacrylamide, PAA, and methacrylamide, MAA. The preparation is described elaborately in the section *Experimental*. The material was again filled into capillaries for CEC, pipettes and the planar test cell, which can be seen in Figure 4.3. However, for our purpose the basic monolith was not suitable due to no apparent porosity. A second step of adding TEOS particles to increase the flow through-put did not lead to the desired advance. Therefore, after a couple of additional experiments without any improvements, this approach was not followed further.

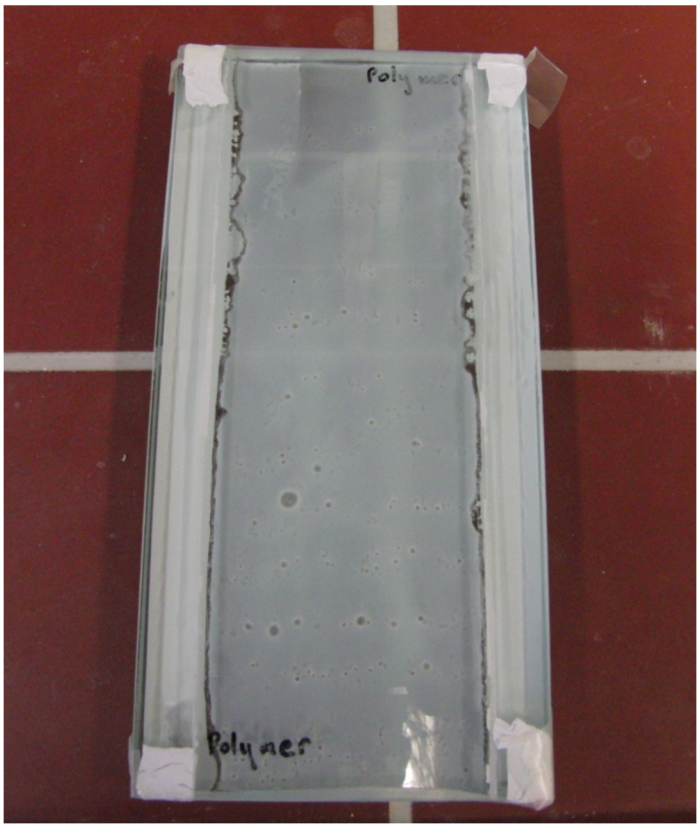

Figure 4.3: Polymer monolith in planar glass plates

5. Material characterization

As mentioned in the previous chapters, different functional groups bond to the monolithic backbone can be useful for different separation problems. To ensure the molecule structure, several analysis methods were examined.

The monolithic materials with different functionalizations were characterized with FTIR spectroscopy and RAMAN spectroscopy.[114] The most important spectra are shown in Figure 5.1. The samples show intense peaks at 2950 cm^{-1} which correspond to the stretching vibration of the alkyl groups[13], amino groups are shown at 1656 and 1553 cm^{-1}.

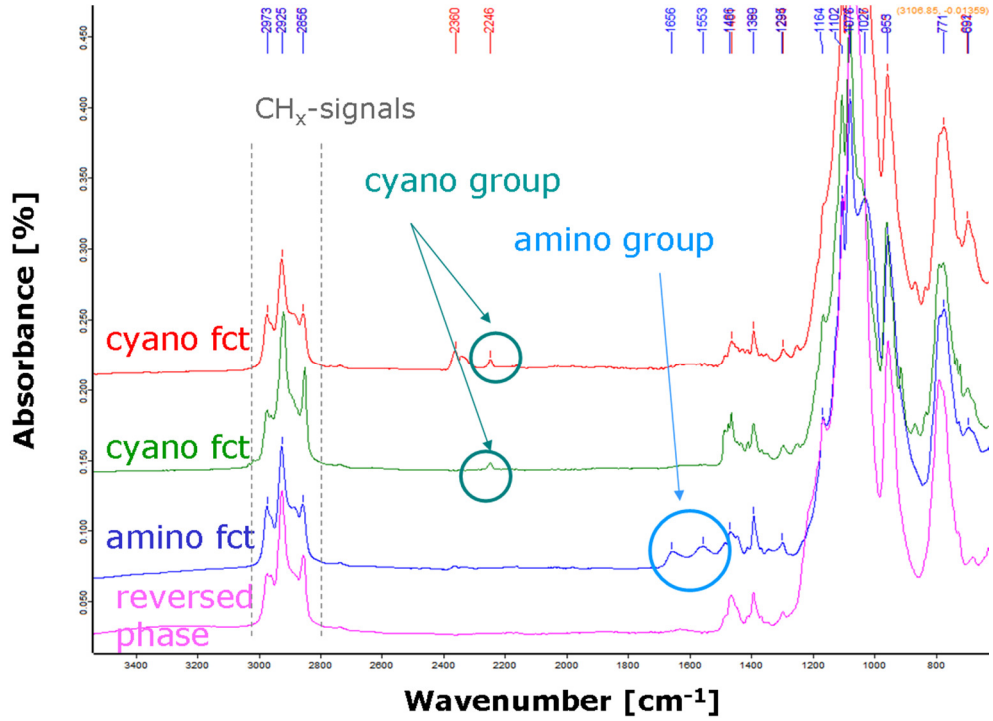

Figure 5.1: FTIR spectra of the functionalized stationary phases

Furthermore, spectra of different compositions of the monolith were taken. It was investigated if different particles, namely C_8-functionalized particles and non-functionalized particles do have an impact on the IR spectra. The resulting spectrum is shown in Figure 5.2.

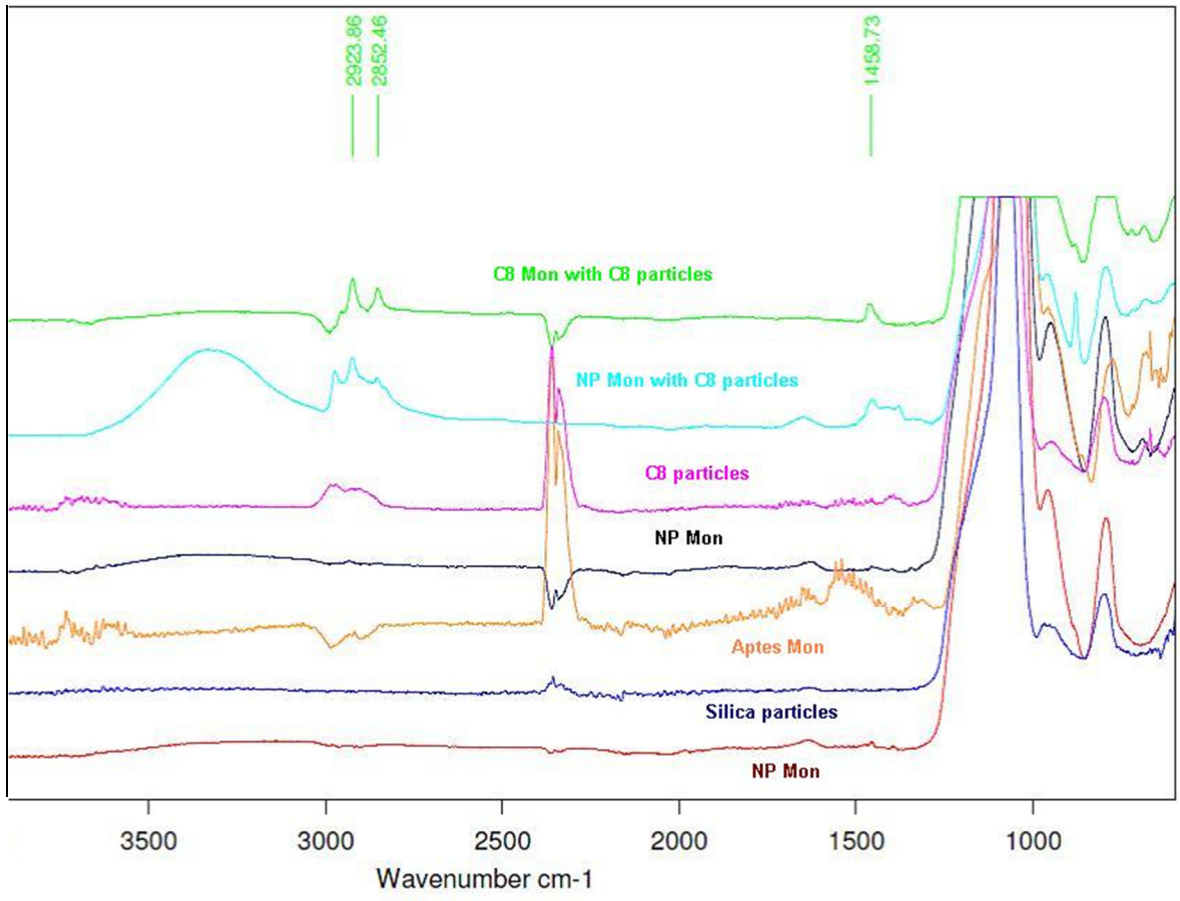

Figure 5.2: Comparison of different C_8-monoliths

The increase in the amount of functional groups – adding C_8-particles to the C_8-monolith does not show any effect in the IR spectrum. However, the signs of the alkyl chains are clearly visible at 2800 – 3000 cm^{-1}. Additionally, the peak of the amino group at 1553 cm^{1} is visible and for the NP Monolith with C_8-particles a broad peak is shown between 3000 and 3500, which indicates that the monolith was not yet totally dry at the moment of measurement.

5.1. Elemental analysis

To be able to calculate the amount of functional groups on the surface, elemental analysis was performed. The results showed 15.2% C for the RP material, and 22.8% C as well as 5.2% N for the amino-functionalized RP material, indicating 1.6 mmol/g C_8-groups on the RP material and 4 mmol/g amino groups on the amino functionalized material. When taking into account the results of the BET surface measurement (see later in this chapter), these

values indicate a loading of 3.8 µmol/m^2 C_8-groups for the reversed phase and 13 µmol/m^2 amino groups on the amino functionalized material. A commercially available monolith, namely Chromolith® by Merck, functionalized with C_{18} groups for HPLC has a surface loading of 3.6 µmol/m^2.[v]

5.2. Microscope examination

Monolithic materials have a certain kind of vermicular structure, which is very typical and often documented in the literature.[33,39,136] The easiest way to ensure the homogeneity of the material as well as the distribution of through pores is the examination through a microscope. Several pictures were taken with a Scanning Electron Microscope (SEM) to have a closer look at the structure.

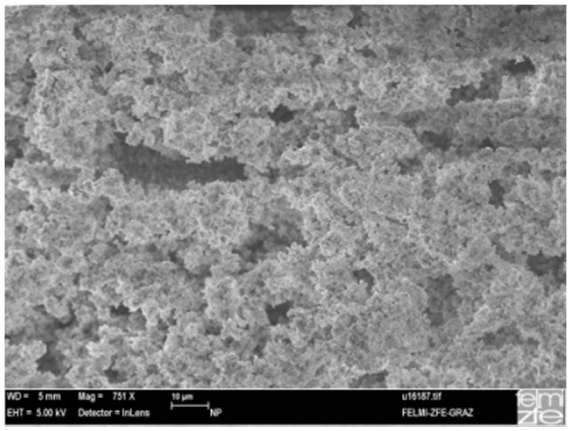

Figure 5.3: Normal phase monolithic structure I

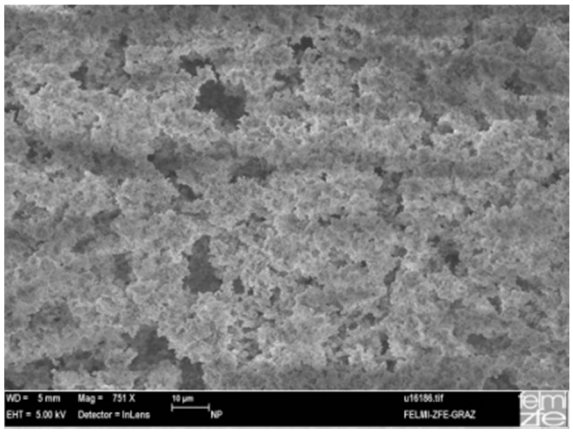

Figure 5.4: Normal phase monolithic structure II

In Figure 5.3 and Figure 5.4 one can see the branched structure characteristic for monoliths. The through-pores are in magnitude 100 to 1000 times larger than the mesopores, which is in agreement with the literature.[137] Furthermore, it can be seen that the monolith does not have significant cracks or holes.

The influence of the porogen amount, which can enlarge or decrease the diameter of the pores, was also of high interest and could be investigated with the SEM. The pictures series of Figure 5.5, Figure 5.6 and Figure 5.7 shows three different amounts of porogen added. It is clearly visible that in the second picture, the through-pores are enlarged and in the third picture these pores are demagnified again. These results are consistent with the results

[v] Please compare: www.merck-chemicals.com/analytical-hplc pp. 176

obtained from the surface measurements (given later in this chapter), which indicate that a too large amount of porogen destabilizes the structure due to too large gaps. Therefore, the inner structure collapses and the whole monolith becomes denser during aging. The through-pores become smaller. The material shown in the SEM pictures were amino functionalized. Figure 5.8 is a detailed view of Figure 5.7.

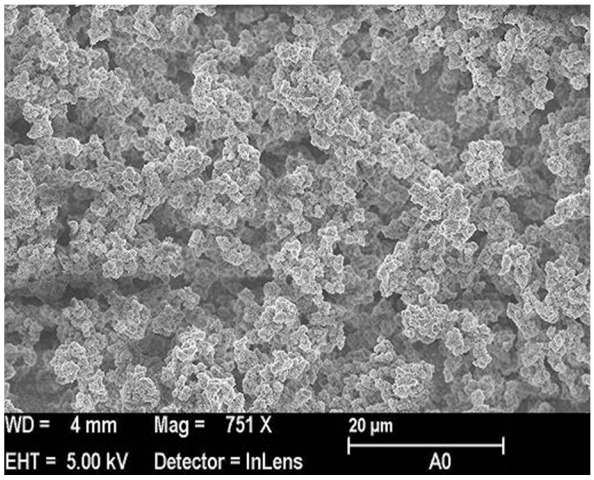

Figure 5.5: Monolithic material with no addition of porogen

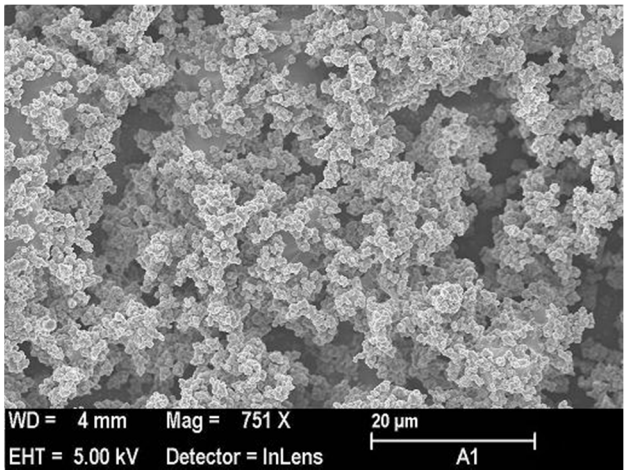

Figure 5.6: Monolithic material with addition of porogen

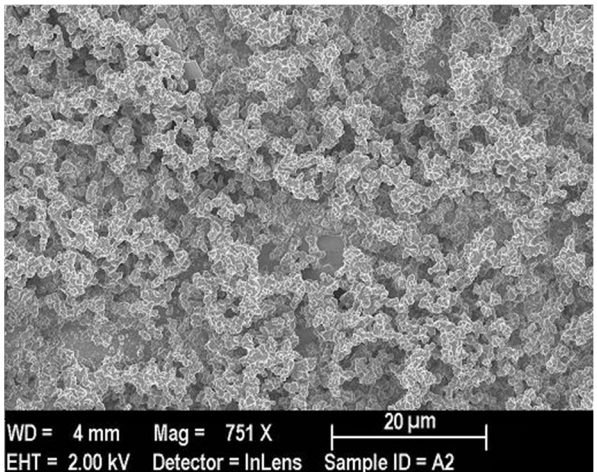

Figure 5.7: Monolithic material with 2x addition of porogen

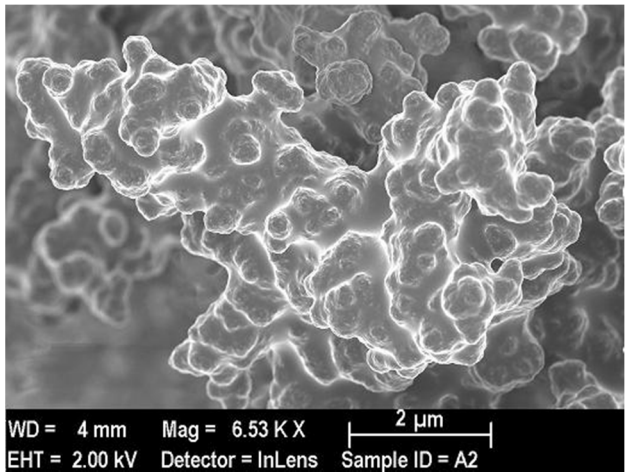

Figure 5.8: Monolithic structure, magnified view

Furthermore, the SEM pictures of a filled capillary could show the filling level and the homogeneity of the material in the fused silica capillary used for capillary electrochromatography. Figure 5.9 shows that the material fills the capillary completely and no voids, i.e. between monolith and wall, or cracks can be observed.

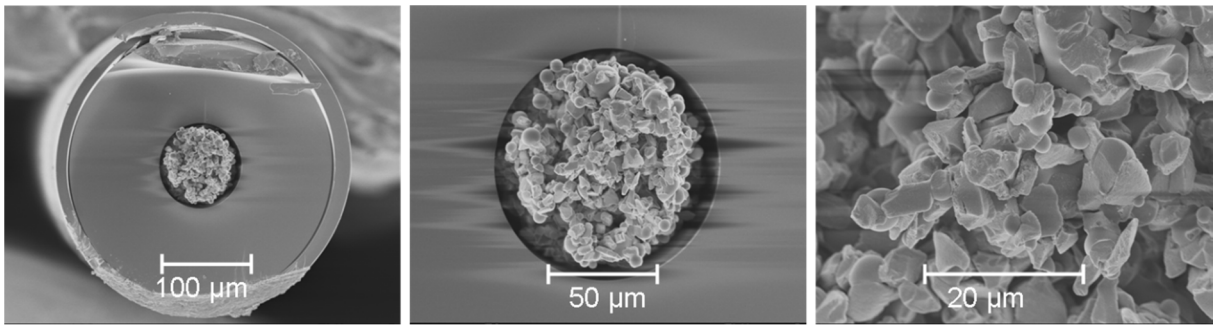

Figure 5.9: SEM pictures of a capillary filled with monolithic material

Optic, i.e. microscopic examination on micrometer scale is a good tool to gain knowledge about the physical condition of the monolithic structure. A picture of a filled capillary is shown in Figure 5.10. The measured and calculated values are presented in the next chapter.

Figure 5.10: Microscope picture of a filled capillary

5.3. Surface and porosity measurements

To characterize the material and to be able to calculate the through-put in the annular geometry, nitrogen physisorption and mercury porosimetry experiments were performed. The density was determined with a helium pycnometer. Furthermore, the results were also resorted to calculate the surface coverage, details are given in the previous chapter.

As already mentioned in the *Introduction*, two methods are needed to measure the mesopores on one hand and the through-pores on the other.[138] Amino-functionalized materials were only investigated with nitrogen physisoprtion, because no upscale was intended.

5.4. Density

The most accurate way to determine densities of newly prepared materials is helium pycnometry. However, to be more precise, the measured quantity is the volume; the density is calculated via the mass/volume ratio. Closed pores are included in the measurement. A detailed description of the different kinds of porosity is given in the *Introduction*. The results of the measurements are given in Table 5.1.

Table 5.1: Density values of the monoliths measured by He-pycnometry

Sample	X_{mean} [cm^3/g]	σ^2
C_8 + particles	1.55	0.12
C_8 + particles + CTAB	1.30	0.08
C_8-recycled + CTAB	1.37	0.36
TMOS	1.65	0.11
C_{18}	1.47	0.45

One can clearly see that the addition of porogen, in this case CTAB, decreases the density due to increased porosity. The other values should show the contrast between materials. The standard density for silica materials is 2.33 cm^3/g.[139]

5.5. Surface and pore volume measurements

The specific surface area and pore volume as well as pore diameter were analyzed by the ASAP 2010. With the physisorption of nitrogen on surfaces and in pores of the material, the specific surface area can be calculated with the BET theory. Detailed explanations can be looked up in the chapter *Introduction*. A huge amount of experiences were carried out to have comparable results. The most important values are summarized in the following table.

Table 5.2: Surface properties of monolithic samples

Sample	BET [m^2/g]	Volume [cm^3/g]	Diameter [Å]
NP2	127.25	0.2182	66.89
PG Particles	302.48	0.8576	113.40
TMOS Monolith	309.39	0.3653	47.23
Amino 3	22.31	0.0226	45.73
C8_C81	153.52	0.1578	38.23
C8-TEOS Mon	71.31	0.0745	41.81
C8 + PG rec	47.18	0.0955	80.93
C8+27mg CTAB	167.59	0.1822	43.49
NP1+CTAB	193.12	0.2107	45.45

Table 5.2 gives an overview of the materials used; a detailed sample description is given in the chapter *Experimental*. However, one has to keep in mind that all the samples need to be dried before the measurement. Therefore, the high specific surface area of the TMOS monolith, which is well documented in the literature, is connected to a massive shrinkage of the material. Recycling in this case stands for a material, which was prepared as a monolith before pounded to particles again. After washing, the particles were used as stabilizer. The specific surface area of these materials is significantly smaller than of the monoliths prepared with Polygosil® particles. A reason for that can be more filled pores or residues in the materials used twice. Figure 5.11 shows the typical hysteresis of nitrogen adsorption/desorption of monolithic materials. This type of hysteresis corresponds to a type IV isotherm. The detailed explanation and literature can be looked up in the chapter *Introduction*.

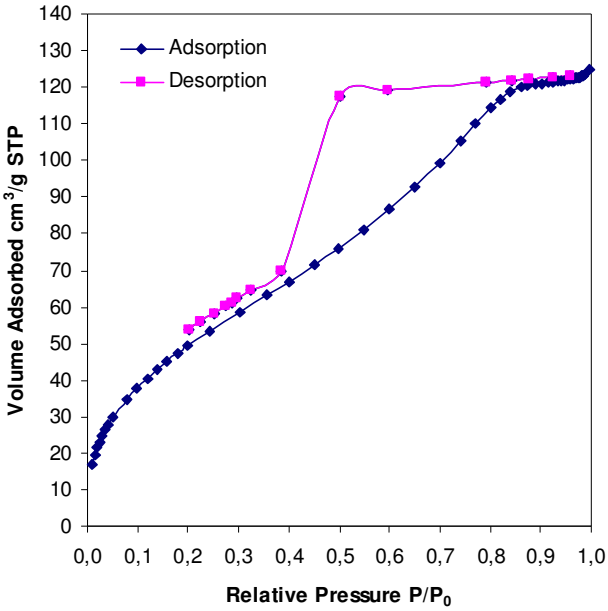

Figure 5.11: Isotherm plot of the BET analysis of the manufactured C_8-stationary phase.

5.6. Particle size measurement

The Polygosil® silica particles were measured with a HELOS instrument to reassure the mean diameter of the particles. The results show a volume mean diameter, VMD, of 5.53 µm, see Figure 5.12.

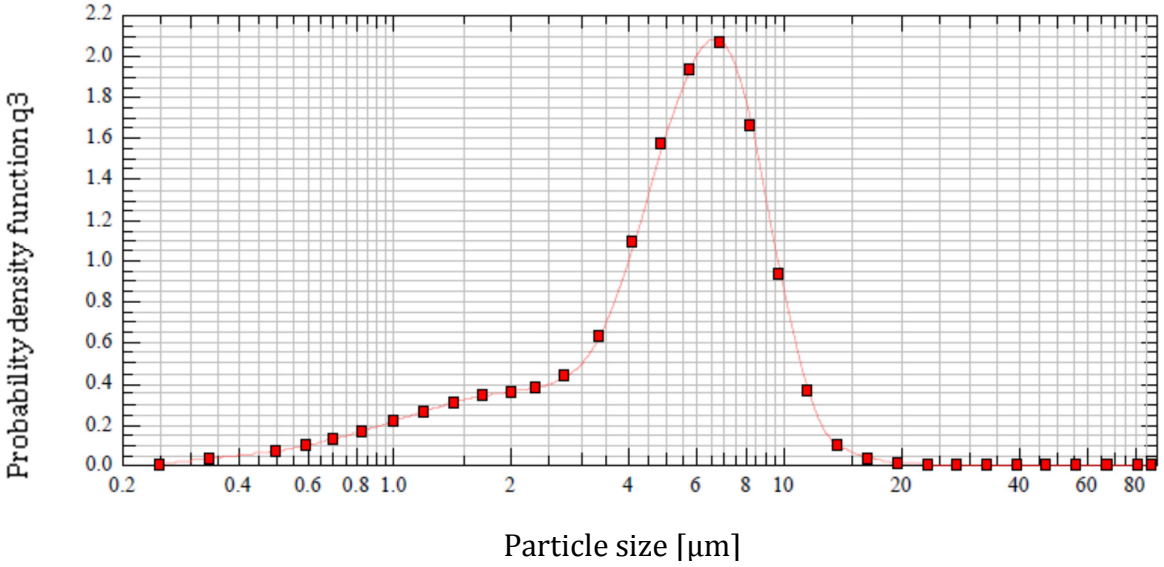

Figure 5.12: HELOS measurement of PG particles

In comparison, the in place synthesized normal phase silica particles were tested. The VMD was 35.81 µm. However, the Q3 function was bimodal, i.e. the curve had two maxima, one at 5 µm and one at 50 µm, see Figure 5.13. Through sieving the desired class can be obtained. Unfortunately, the nitrogen physisorption showed that with the in-house production the specific surface area was significantly lower than with the Polygosil® particles. Due to that fact only commercial silica particles were used.

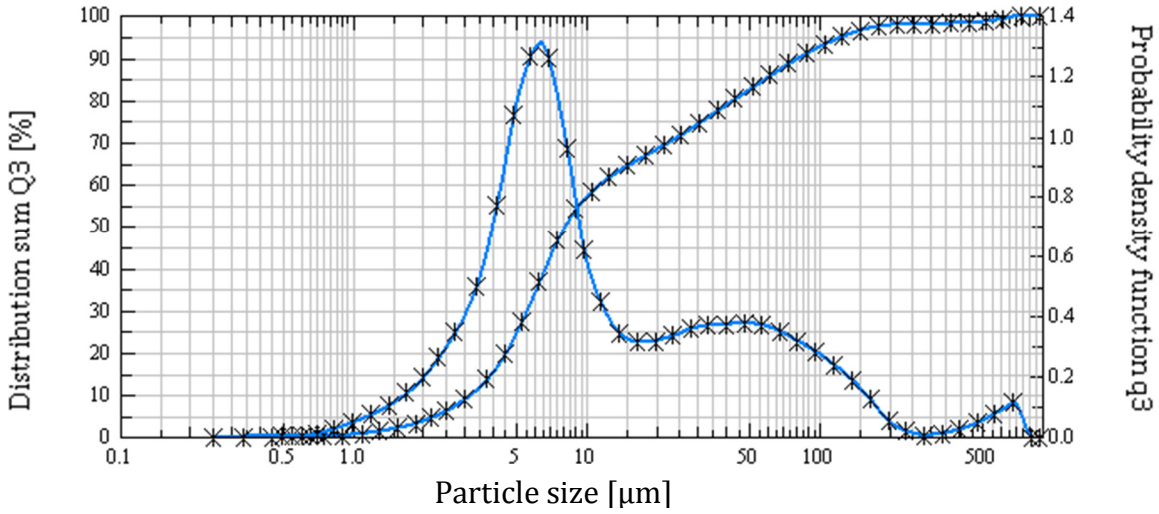

Figure 5.13: Particle size measurements of recycled silica particles

5.7. Porosity measurements with mercury intrusion

As mentioned in the *Introduction*, the pore size distribution of monoliths is in general bimodal. Therefore, supplementary experiments were carried out. Details on mercury intrusion porosity can be looked up in the *Introduction*. The samples were sent to two different companies for comparison. The monolithic rods are shown in Figure 5.14.

Figure 5.14: Samples for mercury intrusion porosity

To have an insight into mercury intrusion, the diagrams of the different measurements are shown in the following section.

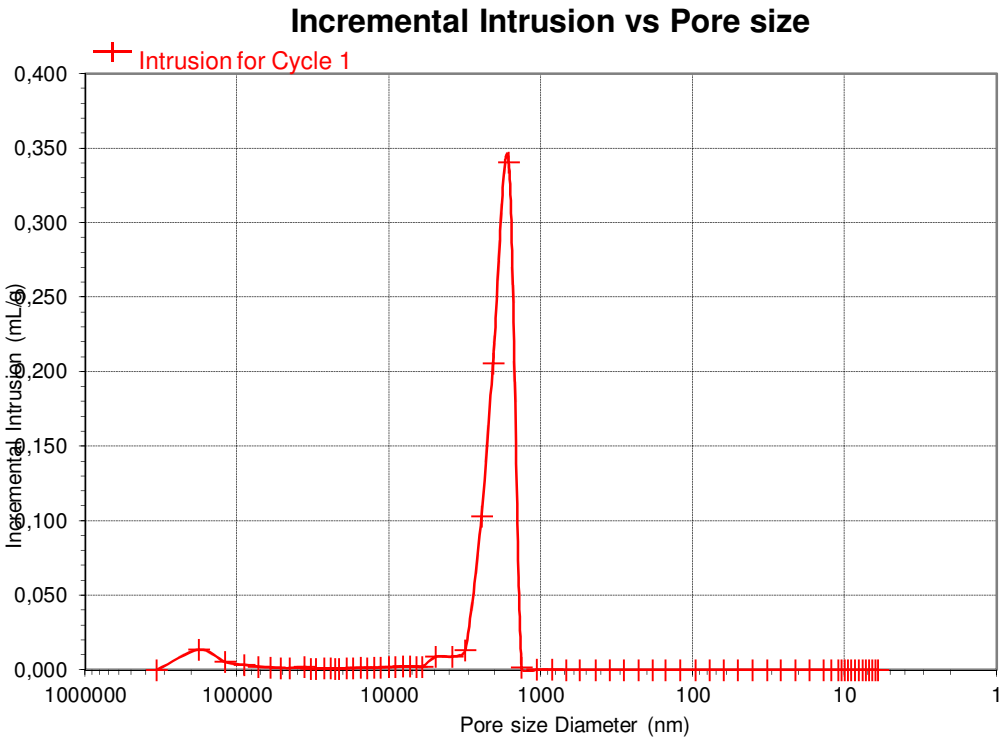

Figure 5.15: Diagram of mercury intrusion – incremental cycle[vi]

Figure 5.15 shows the first cycle of the mercury intrusion measurement, where during one increment, which is related to the diameter of the pores, a certain amount of mercury is forced into the system. Another diagram, see Figure 5.16, shows the addition of mercury volume in every incremental step and thereby the cumulative intrusion volume.

[vi] Measurements carried out at CERAM Frauenthal GmbH

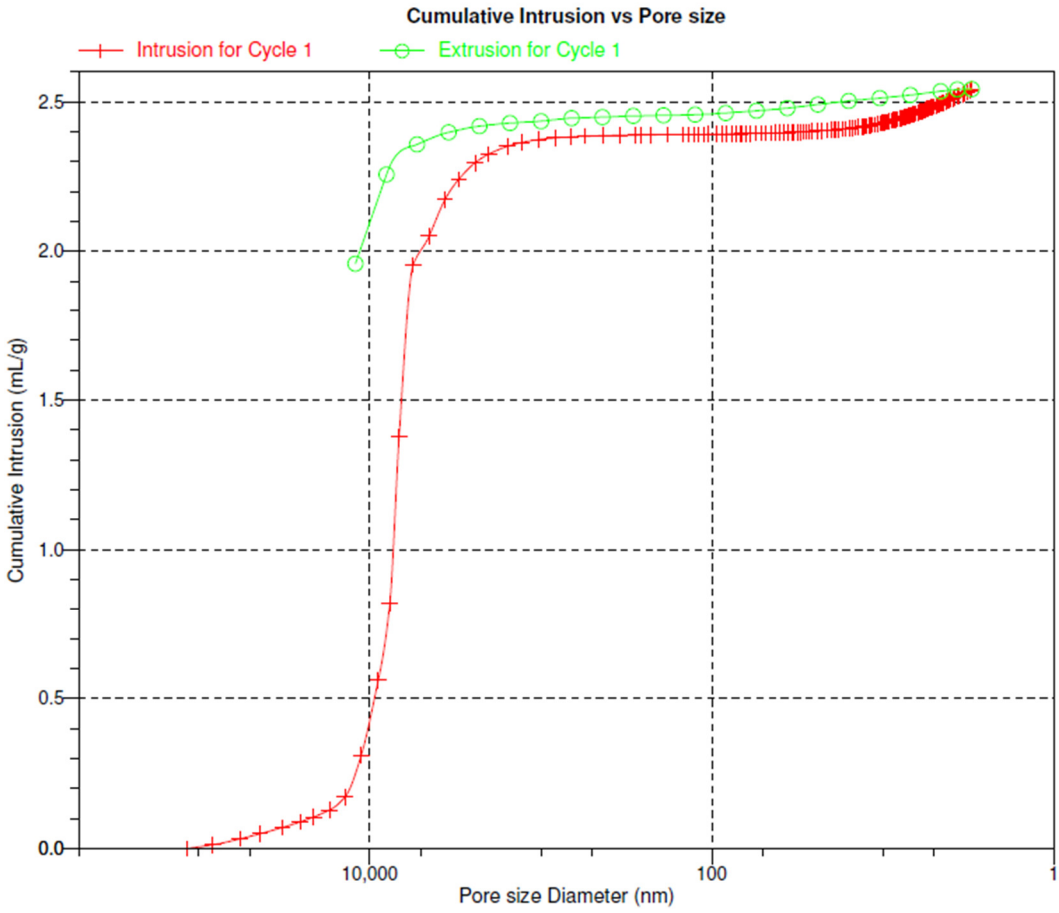

Figure 5.16: Diagram of mercury intrusion – cumulative view[vii]

The porosity can be determined with the following equation[139]:

$$P[\%] = \frac{100 \cdot tpv}{tpv + \frac{1}{\rho}} \qquad (35)$$

where, tpv is the total pore volume and ρ is the density of the material. In the following table an overview of porosities of several different materials is given. Looking at Table 5.3, the total pore volumes differ from the previous experiments. This is due to the fact that the pore structure is bimodal; therefore, the larger through-pores cannot be captured with nitrogen physisorption. Mercury intrusion on the contrary is able to render true values for porosity calculation. Results are also given in Table 5.3.

[vii] Measurements carried out at Micromeritics Instruments Cooperation

Table 5.3: Porosity properties of monolithic materials

	Density [cm^3/g]	Total pore volume [cm^3/g]	Porosity [%]
C8_1	1.55	0.9133	58.60
NP fct	1.55	1.6573	71.98
TMOS_1	1.65	1.2152	66.72
27mg CTAB	1.30	2.5426	76.77
47mg CTAB	1.30	3.7936	83.14

Thus it can be seen, porosities higher than 80% can be reached due to the addition of the porogen CTAB.

6. Implementation

As the goal of the project is the implementation of the stationary phase into an annulus with a diameter of 9 cm and a gap of 1 mm, the amount of the material is comparatively large compared to the common application, namely capillaries for capillary electrochromatography. Many of the experiments described in this thesis were examined with respect to an upscale. However, there had to be some testing along a broad range of magnitude to cover any application possible. The basic development is described in previous work.[114] These experiments lay the ground for the decision that the focus is laid on normal and reversed phase materials. Besides the upscale in the planar geometry and the annulus, the development of capillaries was still of interest due to the simple procedure and the possibility to check the separation efficiency for several test systems in an easy way.

6.1. Activation

Independent of the mold in which the monolith should be implemented into, the inner glass walls had to be activated to ensure a covalent binding of the monolith to the outer cover. Therefore, the capillaries, glass plates and cylinders had to be flushed with HCl 1M for half an hour, than washed with water till the washing fluid was neutral again. Then the glass had to be washed with NaOH 1M for half an hour, again washed with water till the effluent is neutral, then MeOH was used to remove all water residues and as last step everything was dried with nitrogen.

6.2. Capillaries

In literature, the easiest way described to prepare a capillary for capillary electrochromatography (CEC) is to push the precursor mixture into the capillaries with a syringe.[140-143] Figure 6.1 shows a scheme of our filling approach.

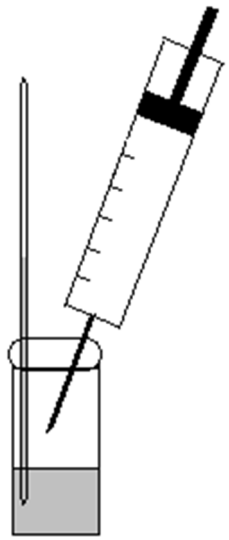

Figure 6.1: Filling procedure for capillaries

The capillary was filled till a length of 25 cm of a total length of 40 cm and the ends were sealed with rubber stoppers. The capillary was left for polymerization at 40°C overnight if not mentioned elsewise.

As the results were not as reproducible as expected, different ways of filling were examined. To obtain a more homogeneous filling, HPLC pumps were used.[144,145] The exact description of the procedure is described in a previous work.[146] Furthermore, the precursor mixture was pushed into the capillary by applying a constant gas flow of nitrogen via a vial and by applying vacuum over the capillary.[128] The different filling procedures, except using a HPLC pump as a filling aid, did not have a significant impact on the performance of the capillaries shown in the chapter *Results and Discussion*.

Another try was with help from colleagues of the Institute of Pharmaceutical Chemistry.[viii] This approach is based on pushing the precursor mixture directly from the syringe into the

[viii] Department of Pharmaceutical Chemistry, Institute of Pharmaceutical Sciences, Graz, Austria

capillary via a connecting piece. However, despite of countless tries, the monolithic precursor mixture seems to be too viscous to be pushed through in the small time frame between adding the catalyst and polymerization. Thus, this approach was not successful. Therefore, the results shown in the adjacent chapter are all obtained with the capillaries either filled by a syringe or a HPLC pump. The capillaries filled with the help of a HPLC pump showed higher separation efficiencies than capillaries filled with a syringe.

6.2.1. The capillary filling procedure in detail

After preparing the precursor mixture as described in the *Experimental* chapter the catalyst is added. The filling of the capillary has to happen rather fast due to the quick polymerization of the mixture. The polymerization starts within 3 minutes after adding the catalyst. The capillary and a syringe were introduced into the septum of the vial, and the liquid was forced into the capillary via physical pressure. In that way, the liquid level could be stopped within a certain range. The capillary was sealed with silicone stoppers and left for polymerization overnight. To see if the monolithic packing was homogeneous and without voids or cracks an optical examination using the microscope was performed. Furthermore, the pressure resistance of the capillaries were again tested with a HPLC pump. The capillaries could withstand a pressure of at least 50 bars.

6.3. Planar test cell

The dimensions of the planar prototype were 10 cm x 20 cm. Two glass plates had to be assembled in the filling frame, one 4 mm and the other one 1 mm thick. The filling frame was designed and manufactured by the Institut für Mikrotechnik Mainz GmbH. The guideline in the beginning was to leave a 0.3 mm gap between those glass plates. Due to this small gap width, the assembling was not an easy issue. The gap was ensured with a PEEK inlet of the same thickness. After getting to know the handling, the filling worked well in the provided filling frame.

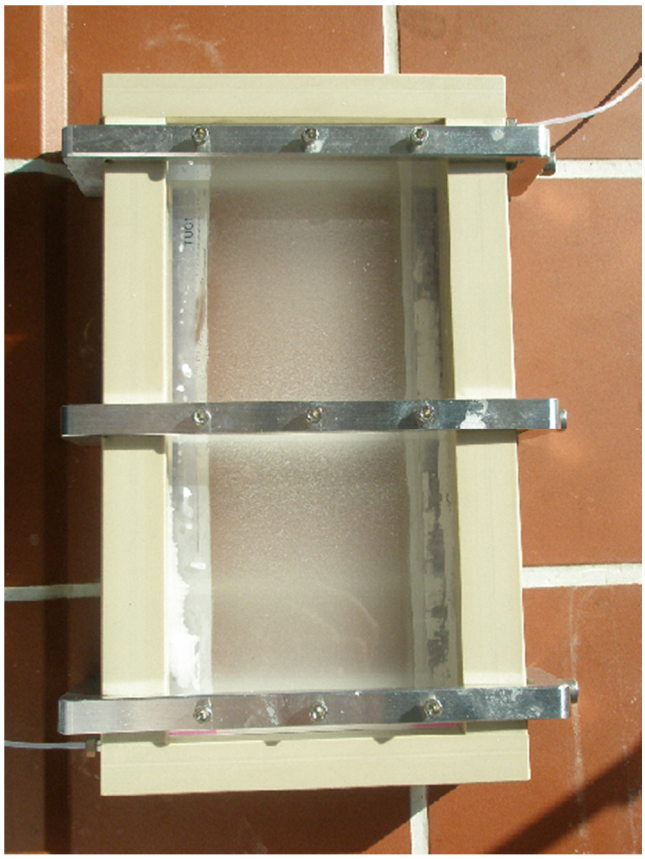

Figure 6.2: Filling frame for the planar test cell with 0.3 mm gap

In Figure 6.2 the filling of the monolith is homogeneous, but this approach is still without any particles added. Therefore, the substance of the monolith appears transparent. After the consortium decided to increase the gap to 1 mm due to stability issues of the annular geometry, the synthesis had to be adjusted. The silica particles were added and the filling frame had to be extended.

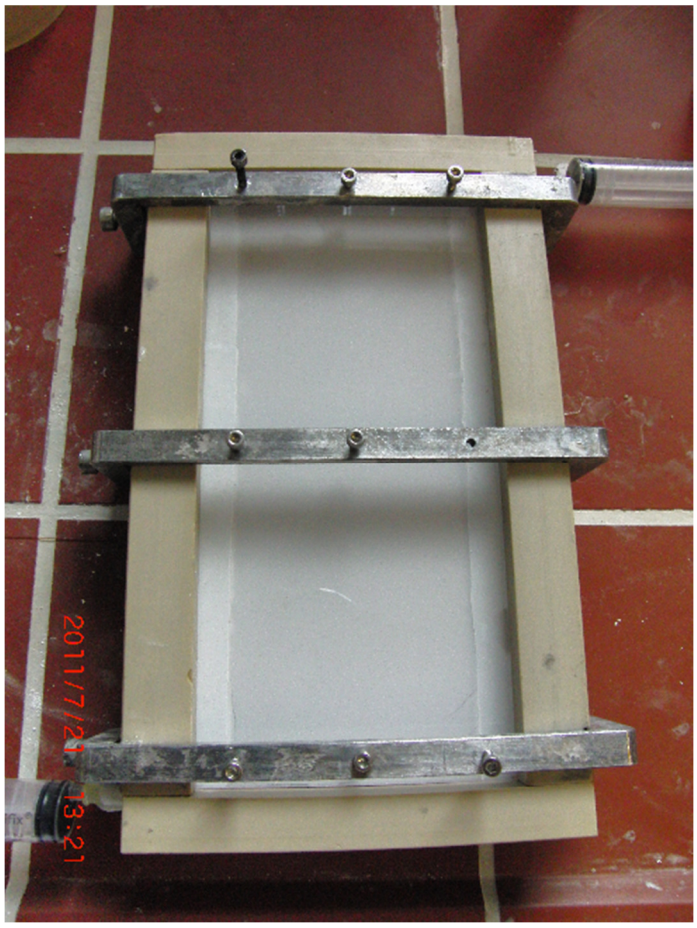

Figure 6.3: Planar test cell filled with monolith in 1 mm gap

Figure 6.3 shows the planar test cell filled with monolithic stationary phase supported by particles in the 1 mm gap. The planar monolith was dismounted from the filling frame and implemented into the planar device. The arrangement is shown in Figure 6.4. All results presented in the next chapter are obtained with this experimental set-up.

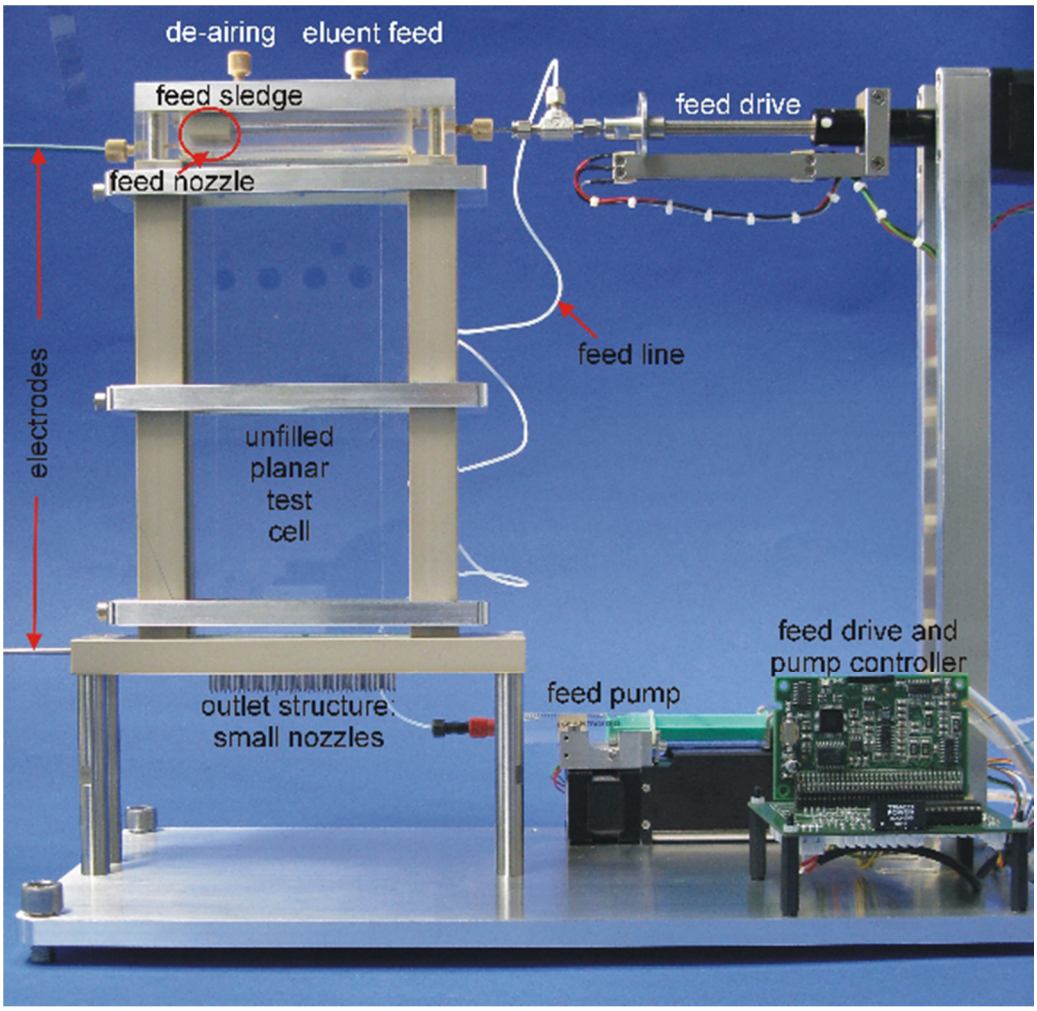

Figure 6.4: Test cell implemented into the planar device[ix]

6.4. Annular prototype

The final part of the project was the preparation of the monolith in the annular geometry. At first, a filling frame for a 0.3 mm gap was produced and successfully filled with monolithic material. As the decision was made to change over to the 1 mm gap no further adaptions had to be done in our case. A standard filling procedure is given in the following. A filled annulus is shown in Figure 6.5.

[ix] Designed and manufactured by the Institut für Mikrotechnik Mainz GmbH

Figure 6.5: Annulus filled with monolithic stationary phase[x]

In the following the standardized filling procedure for the annular geometry is disposed:

- Activation: flushing with HCl 1M for 30 min, washing with water, flushing with NaOH 1M for 30 min, washing with water and MeOH, drying.
- The precursor mixture and Polygosil® particles are stirred at 60°C for 1 h. After cooling to room temperature, diethylamine is added.
- The solution is quickly filled into 2 60 ml syringes. These are put into a syringe pump and the cylinders are filled from bottom to top.
- The monolith is left for polymerization for 48 h.
- After this amount of time the monolith can be transferred into the adapted filling frame and washed with MeOH.

[x] Designed and manufactured by the Institut für Mikrotechnik Mainz GmbH

To avoid cracks and dry-outs due to transportation or storage, the monolith should be prepared in place. After a washing period, the annular geometry can be mounted into the operating system shown in Figure 6.6.

Figure 6.6: Annular prototype with full equipment ready to be operated[xi]

7. Results and discussion

As mentioned in the *Introduction* main goal of the experimental work was to find the most suitable stationary phase for the annular geometry. Besides the challenges of the main requirements like separation efficiency and separation selectivity one major task was the possibility to use the stationary phase in different scales. As the project stretches out into a variety of chromatographic applications and separation problems, it was rather important to define an adaptable but stable basis.

[xi] Set-up implemented by the Institut für Mikrotechnik Mainz GmbH and Microinnova

To be in accordance with the materials mainly used in chromatography the first attempt was to make a reversed phase stationary phase. As mentioned before (see *Introduction*), the decision was made to use monolithic materials. Considering the intention to upscale the stationary phase, inorganic monolithic materials, i.e. based on silanes, were chosen. The basic recipe rooted in the suggestions of Ding et al.[120] and Yan et al.[143] The first article mentioned is dealing with a reversed phase chromatographic stationary phase in combination with a weak anion exchange ligand. The other one presents a material that is strictly octyl-chain functionalized. Both experimental set-ups were slightly modified for our purpose. The preparation procedure is described in detail in the chapter *Experimental*. As the characterization of the material is focus of the previous chapter, this part should deal with the discussion of the development of the monoliths as well as the experimental testing and separation results in the different molds.

7.1. Monolithic stationary phase

As introduced in the previous chapters, many syntheses of silica-based stationary phases were tested in the beginning. In addition to amino and cyano group functionalizations of the silica backbone, the most promising one was the octyl-chain functionalized, also called reversed phase silica stationary phase. The material was improved due to addition of porous silica particles and could easily be implemented into different gap and diameter sizes. No shrinkage occurred and homogeneously filled devices could be tested. Considering the specific surface area and the porosity, the values were lower than comparable examples from the literature. However, these were only used in capillary electrochromatography, whereas the materials presented here could be used for 1 mm gaps. The lower specific surface area compared to the previous samples can be attributed to the filling of the pores of the porous silica particles. In contrast to that the high porosity achieved with the additional porogen ensures a high through-put and for this application this is the most important property. The detailed values are listed in Table 7.1.

Table 7.1: Properties of the C_8-functionalized monolith

	Density [cm^3/g]	BET Surface Area [m^2/g]	Porosity [%]	Average Pore Volume [cm^3/g]	C_8-group Coverage [$\mu mol/m^2$]
C_8-monolithic material	1.30	156	83	3.80	3.8

To observe the shrinkage of the material it was filled into bottom-closed Pasteur pipettes. A detailed description can be found in chapter *Characterization*. The addition of silica particles stabilized the material in all scales and increased the stability of the monoliths.

7.2. Test systems

The genuine intention of developing monolithic materials for chromatographic separations was to be able to separate complex separation problems. These monolithic materials can be the solution for the huge amount of new synthesized or extracted active pharmaceutical ingredients, APIs, in biopharmaceutical industry. To have an easy accessible and well documented test system in the beginning a simple mixture of analytes was used, namely thiourea, naphthalene and anthracene. The molecular structures of these compounds are shown in Figure 7.1.

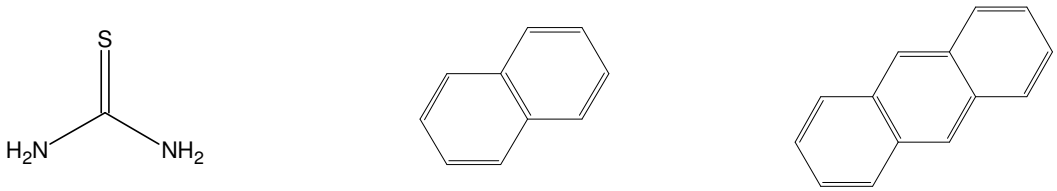

Thiourea Naphthalene Anthracene

Figure 7.1: Molecular structures of the standard test system thiourea, naphthalene and anthracene

To test a more sophisticated system, a mixture of polycyclic aromatic hydrocarbons, PAHs[143], was chosen. Furthermore, six different alkylbenzenes[143] and a phenol mixture were used as analytes.[143] The molecular structures of all compounds are shown in the following figures.

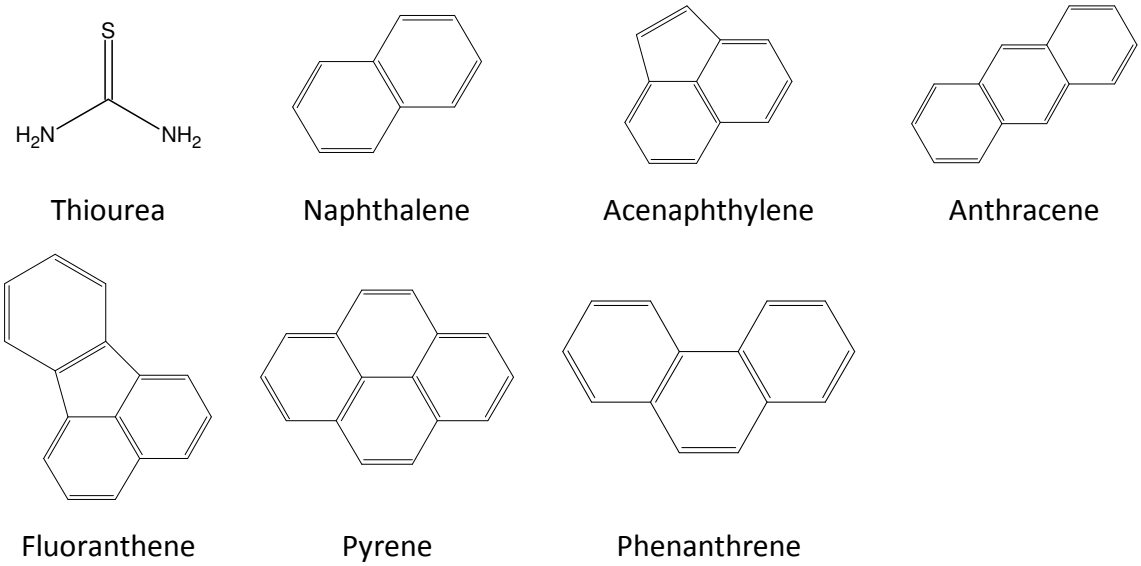

Figure 7.2: Molecular structures of thiourea and six PAHs

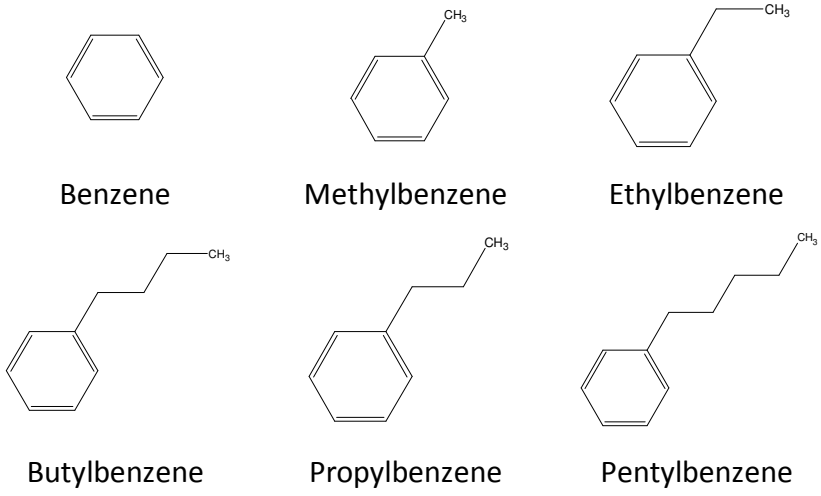

Figure 7.3: Molecular structures of alkylbenzenes

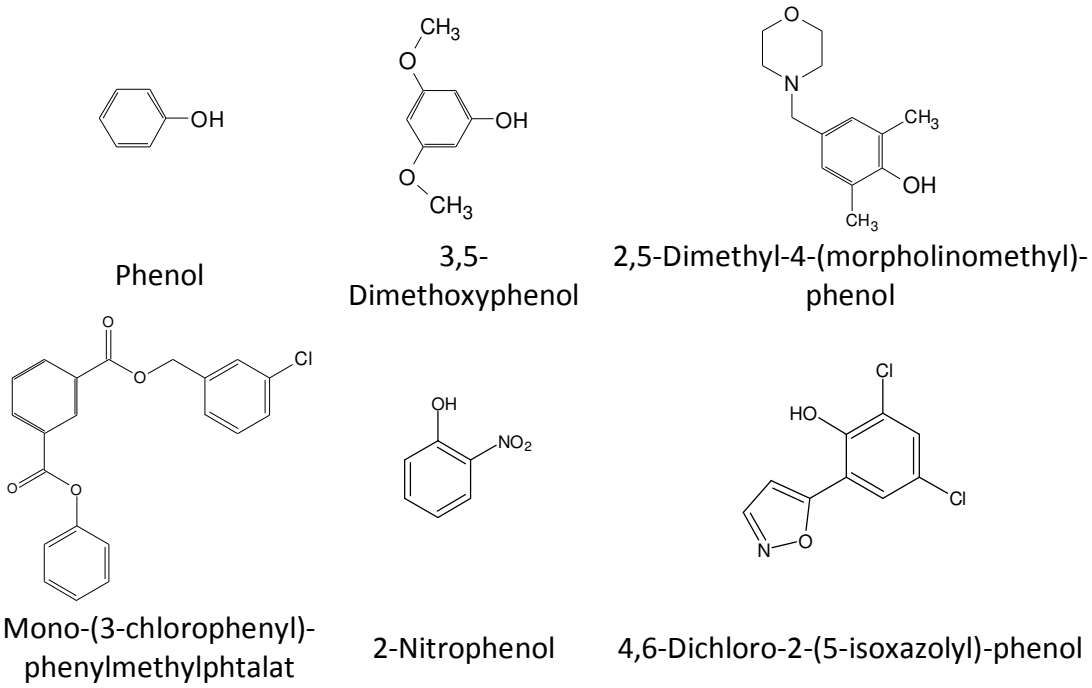

Figure 7.4: Molecular structures of phenols

All these mixtures are often used in literature to serve as standards in order to have comparable results between different stationary phases. Additionally, the composition and pH-value of the mobile phase have to be adjusted. All considerations concerning these subjects are expressed in the specific chapters.

7.3. Mobile phase development

The choice of mobile phase depends not only on the stationary phase but also on the separation problem. The separation efficiency is depending greatly on the mobile phase. To achieve good results, one needs to run through several experiment series to find the right mobile phase composition. In this special situation a common mobile phase composition was chosen. The usual mixtures contain acetonitrile, ACN, and a tris(hydroxymethyl)-aminomethane, TRIS, buffer. Unfortunately, parts of the prototype were corroded by these solvents, so alternatives had to be found. The choice was citrate buffer, citric acid-1-hydrate in bidistilled water mixed with water in different volume ratios. The properties of the different mobile phases are shown in Table 7.2.

Table 7.2: Different mobile phases and their properties

Mobile Phase Components	Ratio	Conductivity [µS/cm]	ph-Value
TRIS (50mM) : methanol	1:4	356	8.0
Citrate (25mM) : methanol	1:4	113	4.7
Citrate (25mM) : methanol	1:9	66	5.1
Citrate (25mM) : methanol	1:19	34	5.3
Citrate (25mM) : methanol	1:29	29	5.4

To visualize the influence of the mobile phase on the retention times, the different solvent compositions were tested with a capillary electrochromatography device. The stationary phase used was an octyl-functionalized silica-based stationary phase, prepared in a 100 µm i.d. fused-silica capillary. Details can be looked up in the chapter *Experimental*.

The influence of the solvents of the mobile phase and the ratio thereof is shown in Figure 7.5. The comparison is made with the retention times of the unretained marker thiourea, the detailed values are given in Table 7.3.

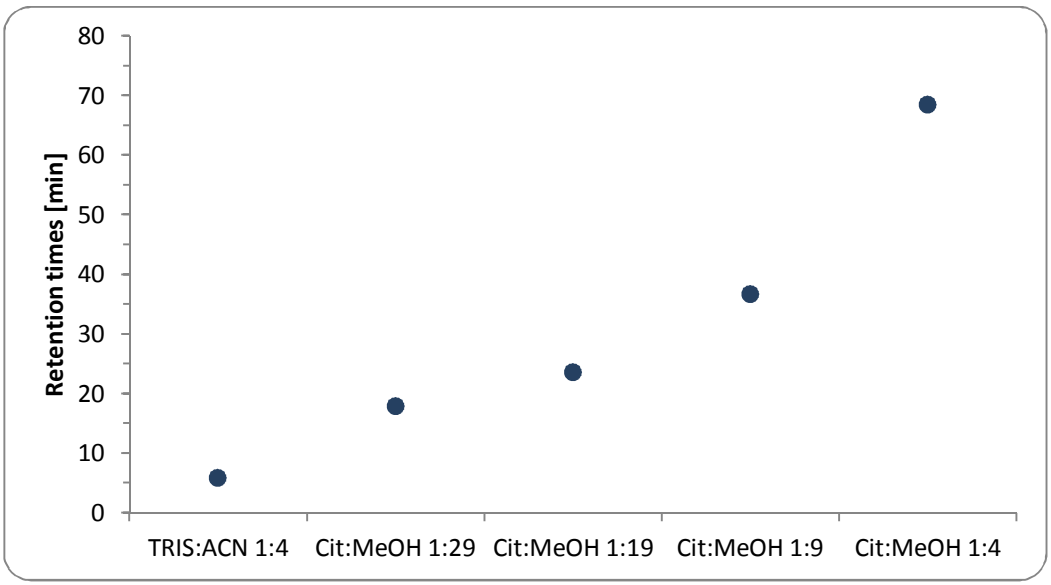

Figure 7.5: Retention times of unretained marker (thiourea) at 20 kV as a function of mobile phase composition[xii]

[xii] Measurements carried out by R. Laskowski at TU Kaiserslautern.

Table 7.3: Retention times of unretained marker (thiourea) at 20 kV with different mobile phase compositions

Mobile phase composition	Retention time [min]
TRIS:ACN 1:4	5.81
Cit:MeOH 1:29	17.86
Cit:MeOH 1:19	23.56
Cit:MeOH 1:9	36.72
Cit:MeOH 1:4	68.43

Considering these results and the fact that ACN cannot be used in the annular device, the mobile phase of choice was Cit:MeOH=1:29. However, depending on the device and the separation problems, different mobile phases were used. The mobile phase chosen will be listed with every electrochromatogram. The following two figures (Figure 7.6, Figure 7.7) are presented to illustrate the significant difference in retention time the mentioned mobile phases can provoke. The peak of the unretained marker is with the mobile phase Cit:MeOH=1:29 eluted after 17.6 min. whereas with TRIS:ACN=1:4 thiourea is eluted after 5.8 min.

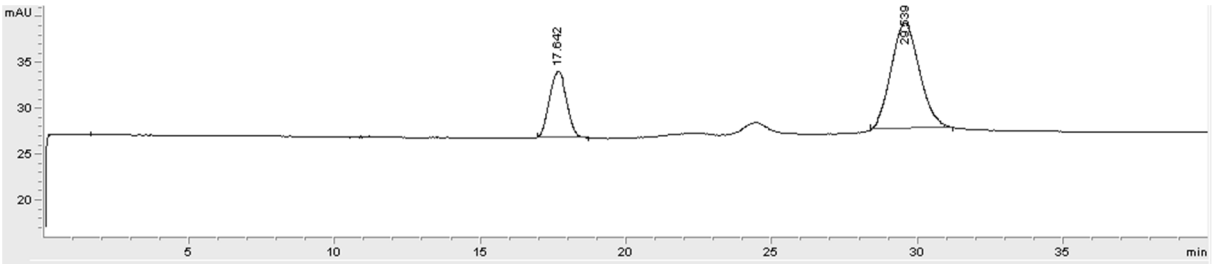

Figure 7.6: Separation of thiourea, naphthalene and anthracene with Cit:MeOH=1:29, 20 kV

Again, Figure 7.6 and Figure 7.7 show electrochromatograms obtained with a C_8-functionalized silica-bases monolithic capillary including porous silica particles.

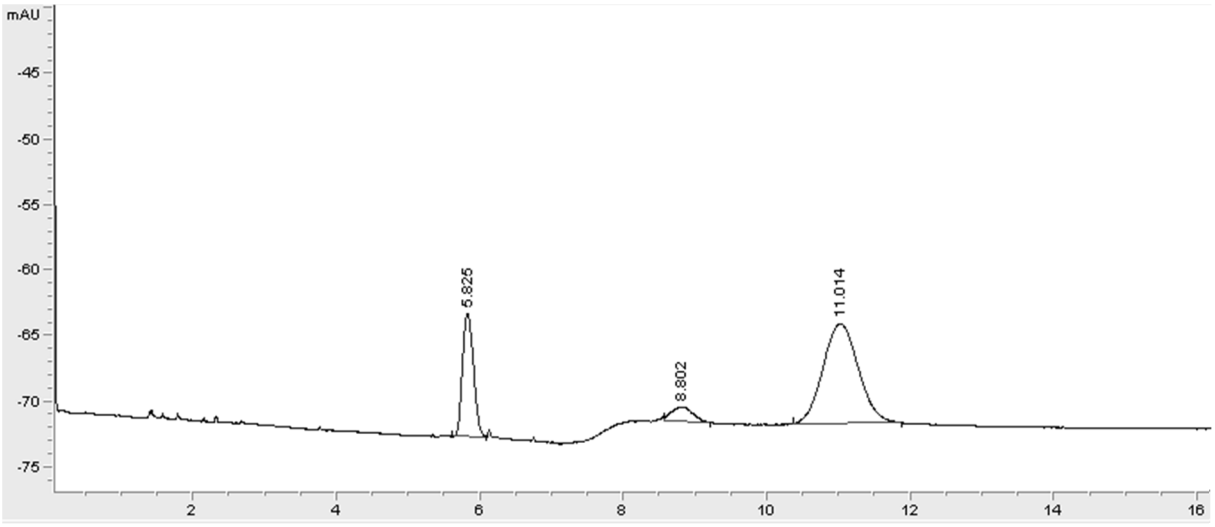

Figure 7.7: Separation of thiourea, naphthalene and anthracene with TRIS:ACN=1:4, 20kV

7.4. Influence of voltage

Not only the mobile phase composition, but also the applied voltage has an influence on the separation time and selectivity. Figure 7.8 shows the dependence of retention time on applied voltage.

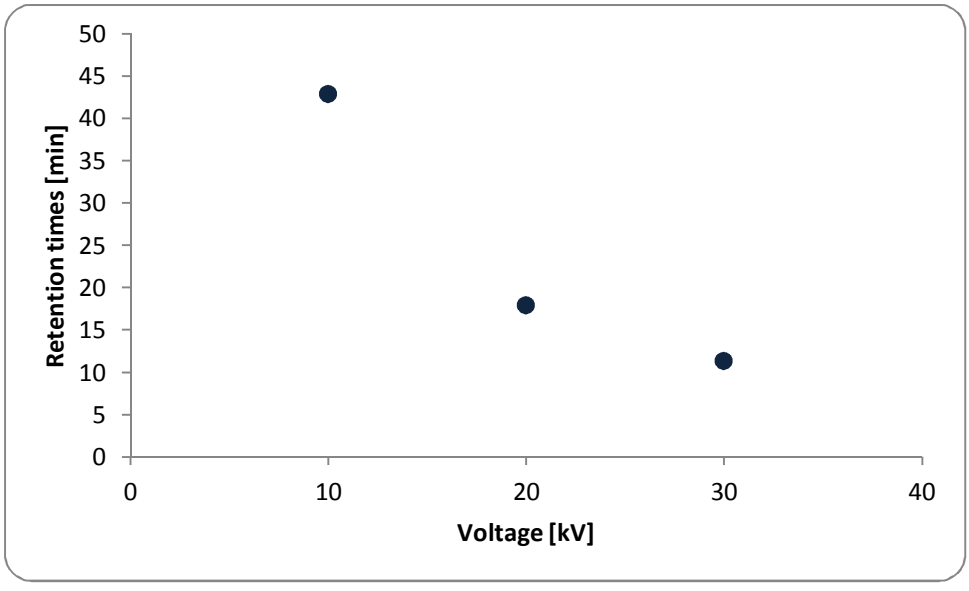

Figure 7.8: Influence of applied voltage on retention times of thiourea, mobile phase Cit:MeOH=1:29

The results shown in Figure 7.8 that a higher voltage applied could bring a faster separation. In case of the capillaries this is true due to the small amount of analyte and mobile phase

volume. However, in case of the upscaled devices, problems with higher voltages occurred. This will be explained in detail later on. The following electrochromatograms (Figure 7.9, Figure 7.10 and Figure 7.11) show the separation of thiourea, naphthalene and anthracene at different applied voltages. The stationary phase used is a C_8-functionalized silica-based monolithic column including silica particles and the mobile phase used in every run is MeOH:ACN=1:4.

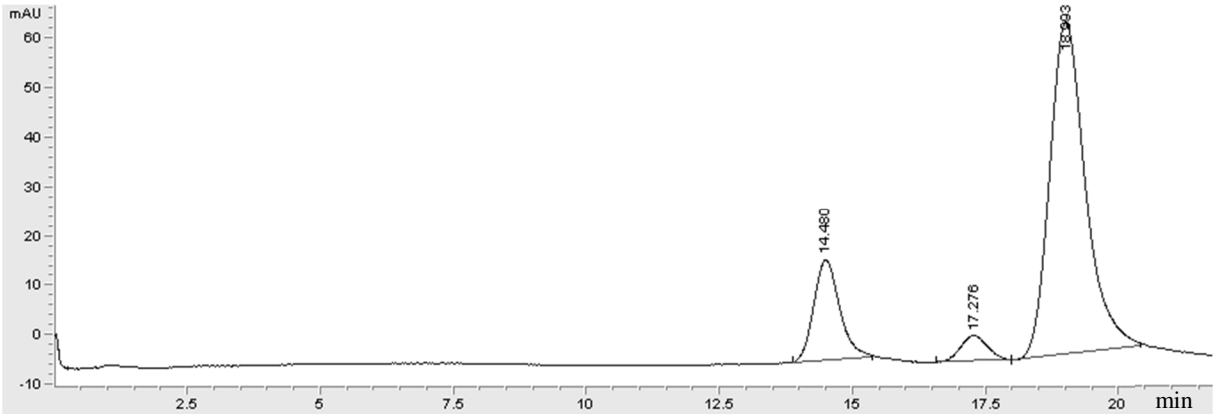

Figure 7.9: Separation of thiourea, naphthalene and anthracene at 10 kV, mobile phase MeOH:ACN=1:4

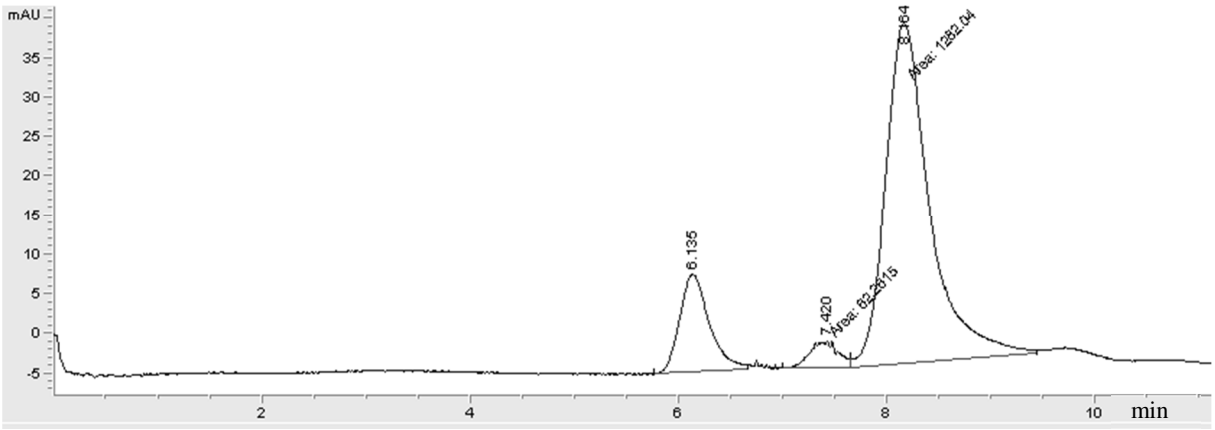

Figure 7.10: Separation of thiourea, naphthalene and anthracene at 20 kV, mobile phase MeOH:ACN=1:4

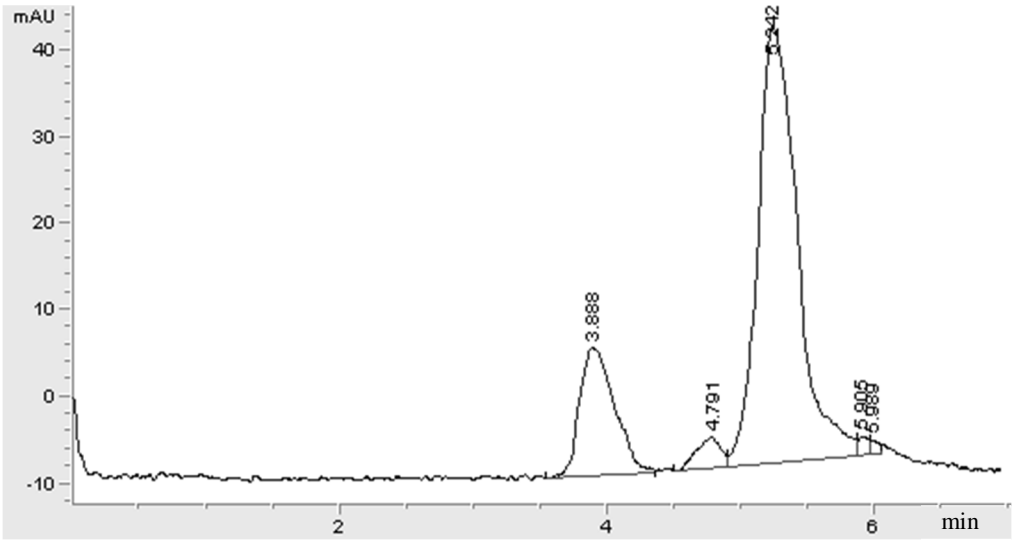

Figure 7.11: Separation of thiourea, naphthalene and anthracene at 30 kV, mobile phase MeOH:ACN=1:4

This example should show how a higher voltage can decrease the time of a separation. However, Table 7.4 shows how retention time and resolution decrease with increasing voltage.

Table 7.4: Influence of voltage on electrochromatographic parameters

	10 kV	**20 kV**	**30 kV**
Retention times [min]			
Naphthalene	17.28	7.42	4.79
Anthracene	18.99	8.16	5.24
Plates [1/m]			
Naphthalene	21 600	10 024	10 404
Anthracene	16 628	8 788	6 476
Resolution			
Naphthalene:Anthracene	1.62	1.15	1.01

Therefore, for any separation problem, an optimized voltage has to be found.

7.5. Capillaries

Capillaries for capillary electrochromatography filled with monolithic materials are already established in industry. Research areas are dealing with this topic since the late 1980s.[6] Therefore, a lot of material and literature is present for silica-based monolithic materials. However, to compare the results of the capillaries, the planar test cell and the annular geometry, reversed phase monolith in 100 µm diameter capillaries were prepared. These capillaries were tested with different standard systems to investigate their separation efficiency. The measurements were carried out at two partner institutes, as our institute does not have a CEC device. Therefore, operator and institute are mentioned in the foot notes.

In the beginning, only the simple standard test system was used, i.e. thiourea, anthracene, naphthalene to study the separation efficiency of the stationary phase. One can see from the development of the electrochromatograms that the handling of the material and the filling of the capillaries improved. We discovered furthermore that the fillings worked more precisely with an HPLC pump than with a syringe. Some examples of differently filled C_8-functionlalized stationary phases are taken from previous works.[146]

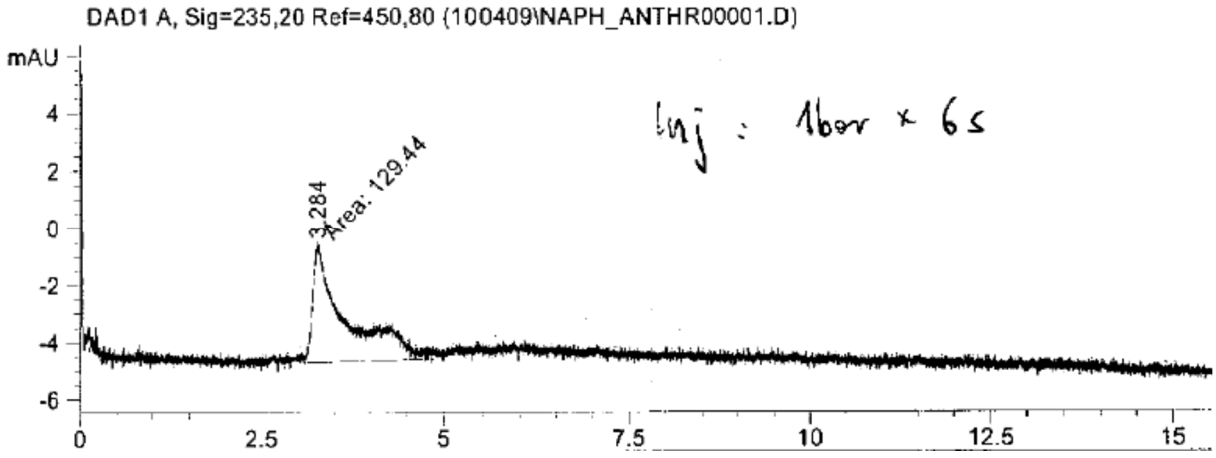

Figure 7.12: Electrochromatogram with two adjacent peaks of naphthalene and anthracene, mobile phase: TRIS(50mM):ACN=1:4, voltage 22kV, stationary phase: C_8-silica-based monolith [xiii]

Figure 7.12 shows the first attempt to separate naphthalene and anthracene. Obviously, no satisfying separation of the components could be achieved.

[xiii] Measurement carried out by S. Mohr, Karl-Franzens-Universität Graz 2010

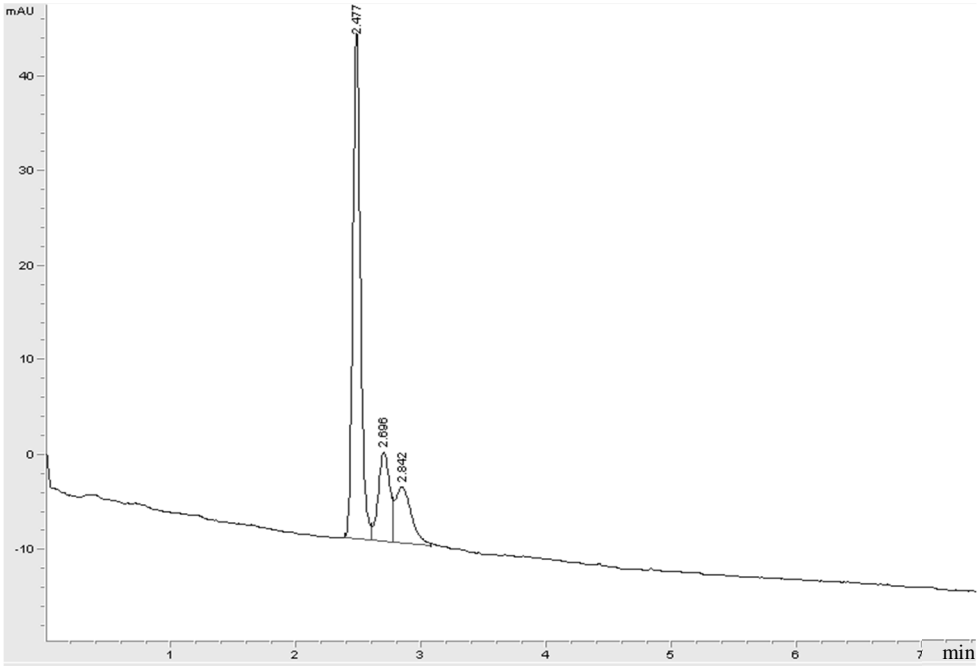

Figure 7.13: Electrochromatogram of thiourea, naphthalene and anthracene, mobile phase TRIS(50mM):ACN=1:4, voltage 20 kV, stationary phase: C_8-silica-based monolith[xiv]

Figure 7.13 does not show a good separation between adjacent peaks, either. The reasons for these results are variations in the precursor mixtures. All recipes can be looked up in chapter *Experimental*. The main difference between the first and the following capillaries are certainly the omittance of the surfactant, in this case CTAB. The reason for the better separation without any porogen is the smaller size of the through-pores which help on the micrometer scale to separate the substances due to their interaction with the silica monolith. The pores formed by the phase separation are therefore absolutely sufficient for the transportation through the capillary. In contrast to that the planar test cell and the annular geometry need the larger through-pores to ensure a high through-put of material. In this way, the recipe of the precursor mixture for the capillaries varies slightly from the recipe for the larger devices.

[xiv] Measurements carried out by R. Laskowski at TU Kaiserslautern 2010

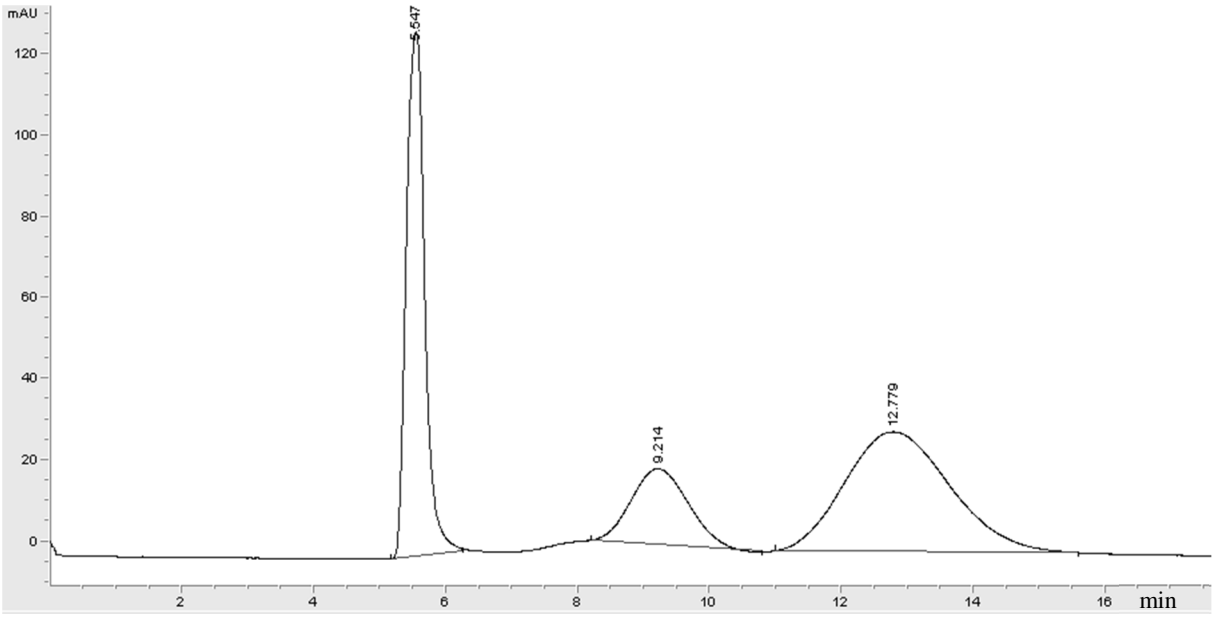

Figure 7.14: Electrochromatogram of thiourea, naphthalene and anthracene, mobile phase TRIS(50mM):ACN=1:4, voltage 20 kV[xv]

Table 7.5: Characteristics of electrochromatogram in Figure 7.14

	Retention time [min]	Resolution	Selectivity	Plates
Thiourea	5.55	-	-	2027
Naphthalene	9.21	3.48	1.66	525
Anthracene	12.78	1.56	1.39	297

The first good results were achieved with a C_8-functionalized silica-based monolithic capillary. The results are shown in and Table 7.5. To ensure reproducibility of the results, eight runs were performed. Figure 7.15 shows the mean value and the deviation of the measured retention times. One may notice the low plate numbers in Table 7.5 compared to commercially available columns. These are due to the broad peak shapes which may be caused by large through-pores.

[xv] Measurements carried out by R. Laskowski at TU Kaiserslautern 2010

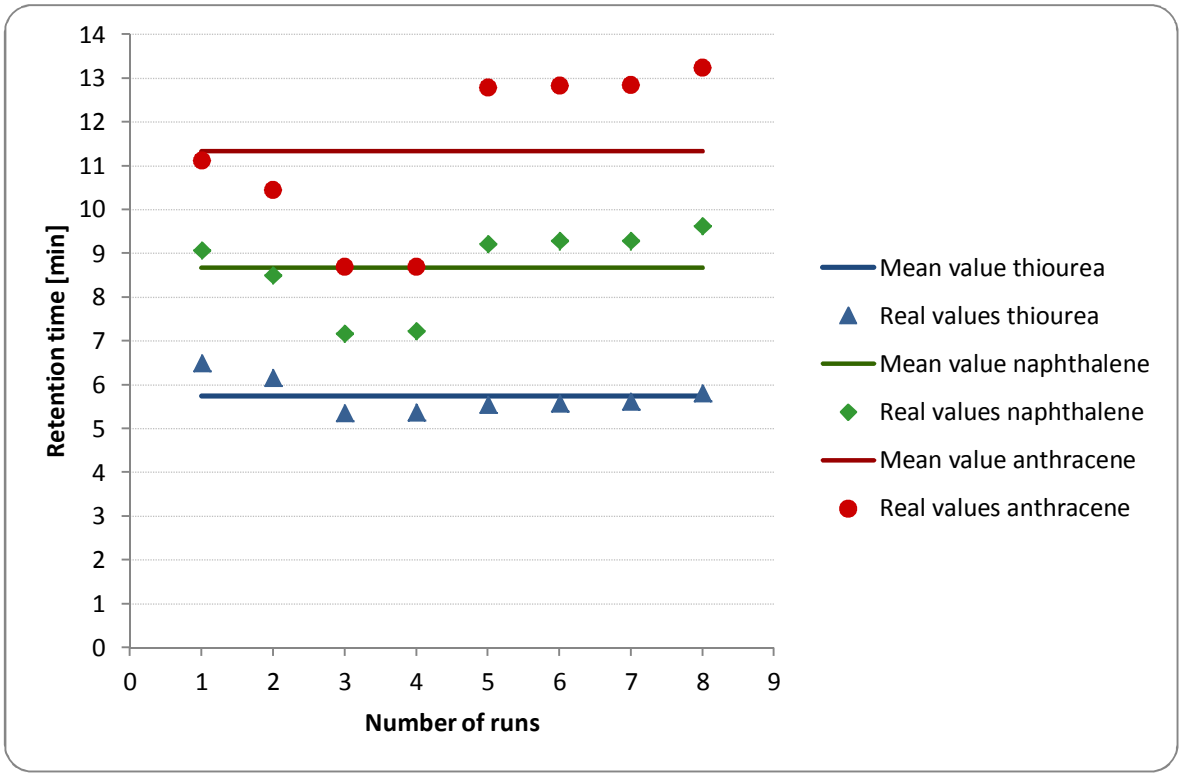

Figure 7.15: Comparison of the retention times of analytes in different runs

Figure 7.15 shows the results of one capillary with different runs. These results are inasmuch interesting as deviations differ from analyte to analyte. Especially, runs three and four show significant discrepancy to the mean value. Reason for this is the use of the capillary without any conditioning in the first four runs. The monolithic material has to be flushed with the mobile phase to obtain the same solvent everywhere and to guarantee homogeneous electroosmotic flow. The latter runs show nice conformity and prove therefore a well packed, homogeneous stationary phase. Therefore, the mean value and standard deviation is calculated from the last four runs. Results are given in Table 7.6.

Table 7.6: Mean value and RSD of four runs with TRIS:CAN = 1:4, V = 20 kV

	Mean value [min]	**RSD [%]**
Thiourea	5.64	3.0
Naphthalene	9.36	8.6
Anthracene	12.92	14.3

In addition to the reproducibility of the results in one capillary, the reproducibility from capillary to capillary is of interest. In Figure 7.16 the retention times of naphthalene and anthracene in five different capillaries are compared.

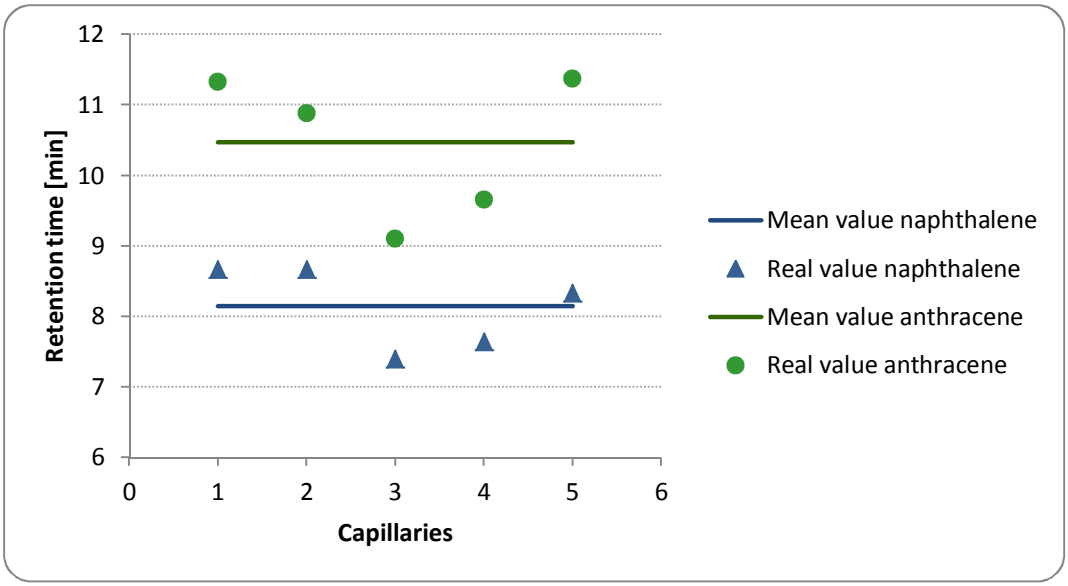

Figure 7.16: Comparison of retention times of naphthalene and anthracene in different capillaries

Table 7.7 shows the mean value and the relative standard deviation of the retention times of analytes in five different capillaries. The values are in reasonable agreement.

Table 7.7: Mean value and RSD of comparison of different capillaries

	Mean value [min]	**RSD [%]**
Naphthalene	8.14	7.2
Anthracene	10.47	9.8

7.5.1. Separation of PAHs

To look closer at the separation efficiency of the monolithic material, the test systems mentioned in the *Introduction* of this chapter were examined. Depending on the separation problem, different mobile phases were used. These are cited with the particular electrochromatograms. The results shown in this chapter are all obtained with a C_8-silica-based monolithic capillary including silica particles.

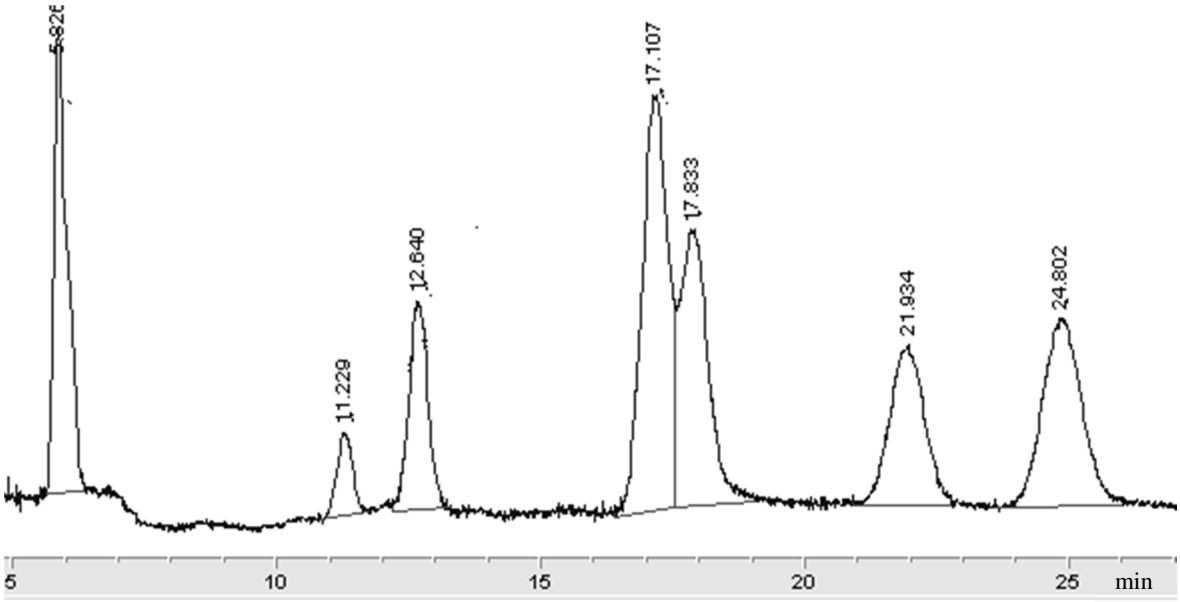

Figure 7.17: Separation of a PAHs mixture, mobile phase: ACN:MeOH=1:3 + 20% H_2O, voltage 20 kV[xvi]

To ensure reproducibility, results are given as an average of three runs. The sample concentration was 83 mg/l, the injection time was 6s at a voltage of 10 kV. Parameters are given in Table 7.8.

Table 7.8: Separation parameters of the PAHs mixture

Substances	Retention time [min]	Plates [1/m]	Resolution
Thiourea	6.25 ± 0.37	14880 ± 4170	-
Naphthalene	11.29 ± 0.06	38680 ± 10950	11.40 ± 0.72
Acenaphthylene	12.53 ± 0.09	35120 ± 10300	2.43 ± 0.11
Phenanthrene	16.45 ± 0.57	25630 ± 11240	5.58 ± 0.72
Anthracene	17.06 ± 0.67	27640 ± 7140	0.72 ± 0.06
Fluoranthene	20.62 ± 1.14	29400 ± 6380	3.92 ± 0.13
Pyrene	23.26 ± 1.34	31330 ± 8390	2.60 ± 0.29

[xvi] Measurements carried out by R. Laskowski at TU Kaiserslautern 2011

7.5.2. Separation of alkylbenzenes

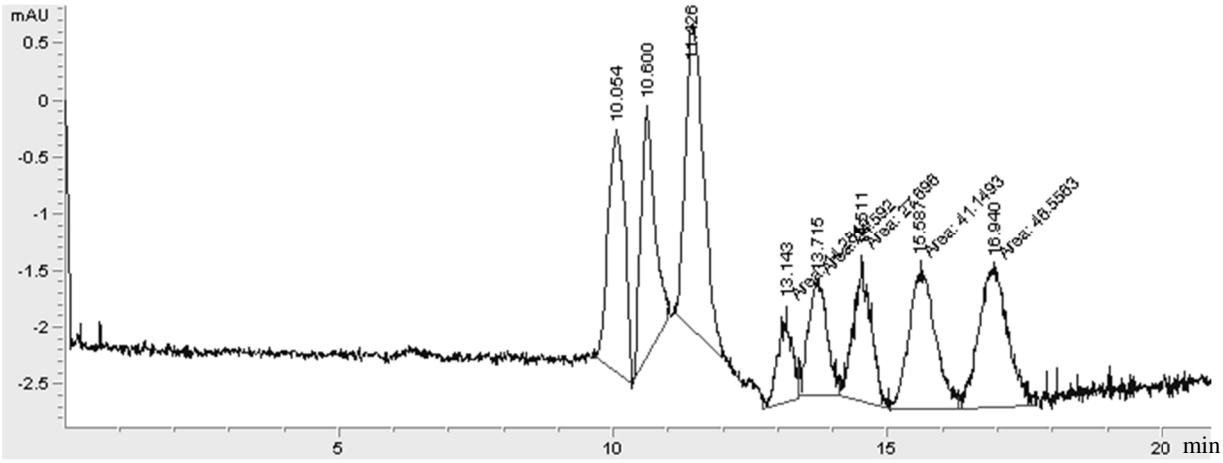

Figure 7.18: Separation of alkylbenzenes, mobile phase: Cit:ACN=1:9, voltage 20 kV[xvii]

Figure 7.18 shows the separation of six alkylbenzenes and the marker thiourea. In the electrochromatogram more peaks than substances are recorded. The first peak visible is an impurity in the analyte mixture. Injection was at 10 kV for 6s, sample concentration was 83 mg/l and data is given as an average of two runs. Resulting values are given in Table 7.9.

Table 7.9: Separation parameters of alkylbenzenes mixture

Substances	Retention time [min]	Plates [1/m]	Resolution
Thiourea	10.60 ± 0.01	25570 ± 7190	-
Benzene	11.41 ± 0.02	17200 ± 1250	1.33 ± 0.13
Methylbenzene	13.11 ± 0.04	37910 ± 2750	2.67 ± 0.56
Ethylbenzene	13.69 ± 0.03	22855 ± 2750	0.89 ± 0.18
Propylbenzene	14.47 ± 0.05	27250 ± 9380	1.10 ± 0.15
Butylbenzene	15.56 ± 0.04	19190 ± 6370	1.34 ± 0.21
Pentylbenzene	16.87 ± 0.10	17780 ± 3540	1.37 ± 0.23

[xvii] Measurements carried out by R. Laskowski at TU Kaiserslautern 2011

7.5.3. Separation of phenols

The phenol separation electrochromatogram was recorded at two different wavelengths, at 121 nm (Figure 7.19) and 235 nm (Figure 7.20), to display all analytes. Figure 7.19 shows phenol, mono-(3-chlorophenyl)phenylmethylphthalat, 3,5-dimethoxyphenol, 2,5-dimethyl-4-(morpholinomethyl)-phenol, 4,6-dichloro-2-(5-isoxazolyl)phenol and Figure 7.20 shows phenol, mono-(3-chlorophenyl)phenylmethylphthalat, 3,5-dimethoxyphenol, 2-nitrophenol and 2,5-dimethyl-4-(morpholinomethyl)-phenol. Sample concentrations were 100 mg/l and injection was at 10 kV for 3 s.

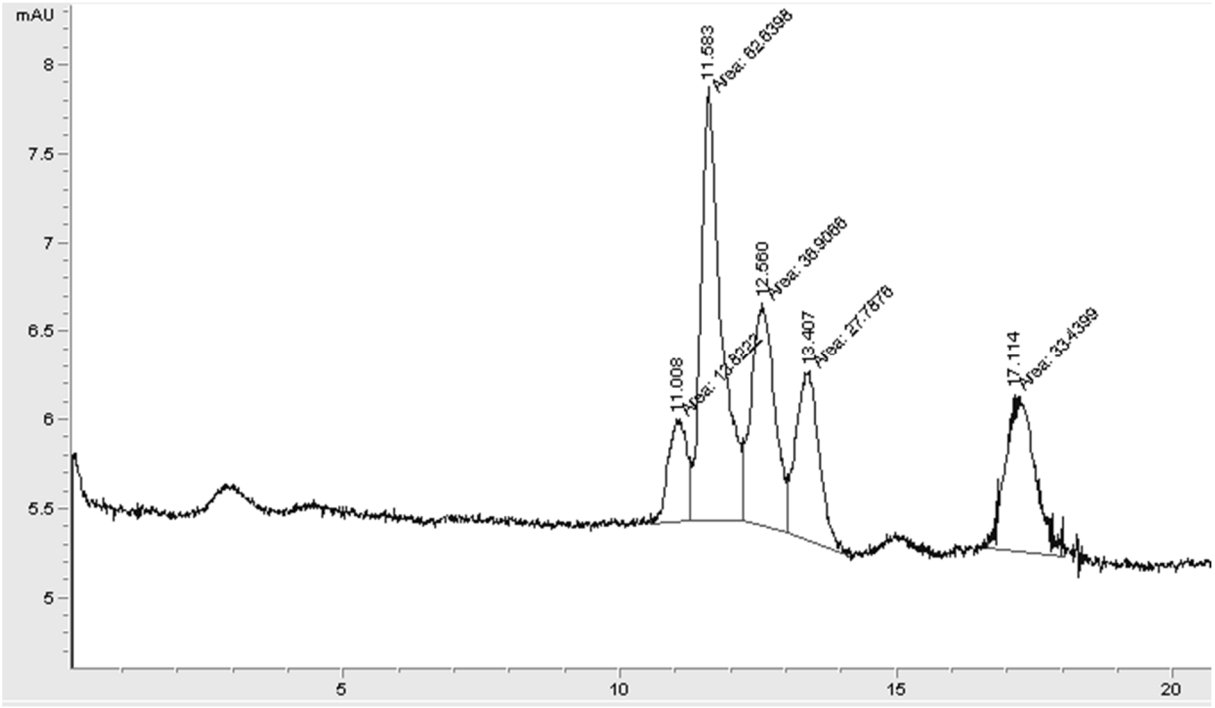

Figure 7.19: Separation of phenol mixture, mobile phase: Cit:ACN=1:9, voltage 20 kV[xviii]

[xviii] Measurements carried out by R. Laskowski at TU Kaiserslautern 2011

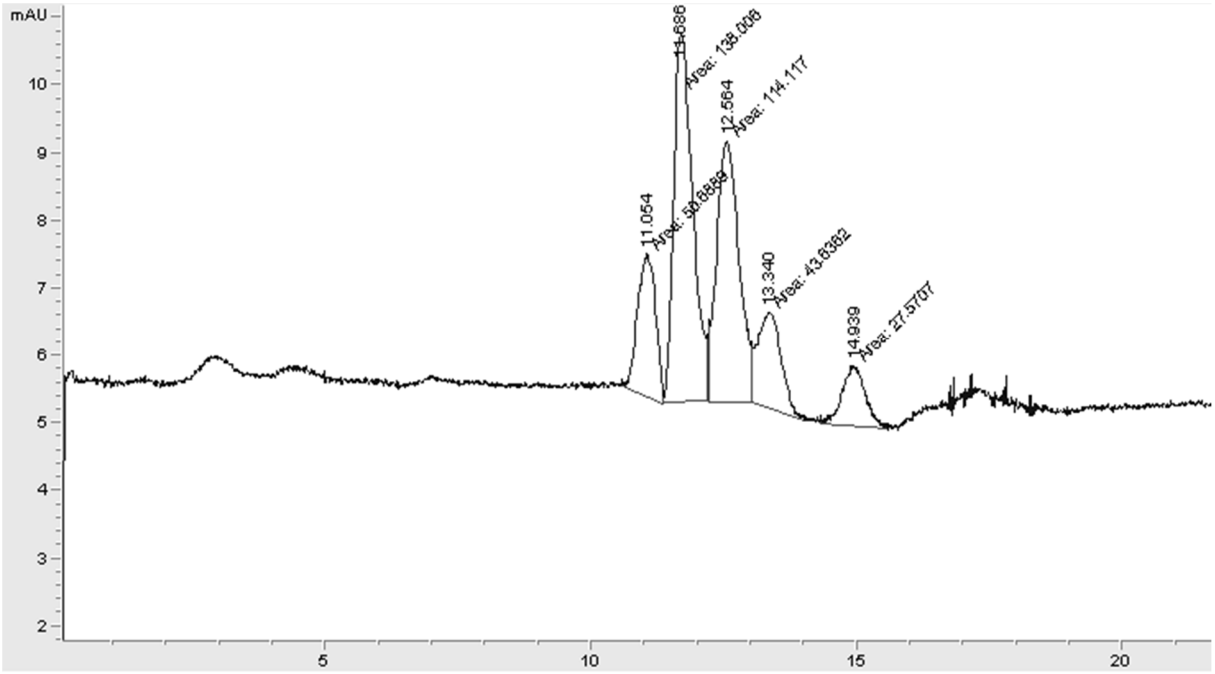

Figure 7.20: Separation of phenol mixture, mobile phase: Cit:ACN=1:9, voltage 20 kV[xix]

Table 7.10 combines the results of both electrochromatograms recorded.

Table 7.10: Separation parameters of phenol mixture

Substances	Retention time [min]	Plates [1/m]	Resolution
Phenol	10.82 ± 0.33	14470 ± 2700	-
3,5-Dimethoxyphenol	11.50 ± 0.26	16550 ± 4260	0.94 ± 0.01
2,5-Dimethyl-4-(morpholinomethyl)-phenol	12.32 ± 0.34	15180 ± 1040	1.09 ± 0.16
Mono-(3-chlorophenyl)-phenylmethylphtalat	13.14 ± 0.29	15220 ± 2550	0.98 ± 0.11
2-Nitrophenol	14.72 ± 0.31	31830 ± 11970	2.08 ± 0.29
4,6-Dichloro-2-(5-isoxazolyl)-phenol	16.93 ± 0.27	22130 ± 2030	4.58 ± 0.49

[xix] Measurements carried out by R. Laskowski at TU Kaiserslautern 2011

7.5.4. Comparison to C_8-C_8 capillaries

Another approach was to add C_8-functionalized particles to the silica precursor mixture. The idea was to increase the adsorption sides to improve the theoretical plate number and the selectivity. The recipe for this type of capillary can be looked up in the section *Experimental*. Figure 7.21 shows the obtained electrochromatogram.

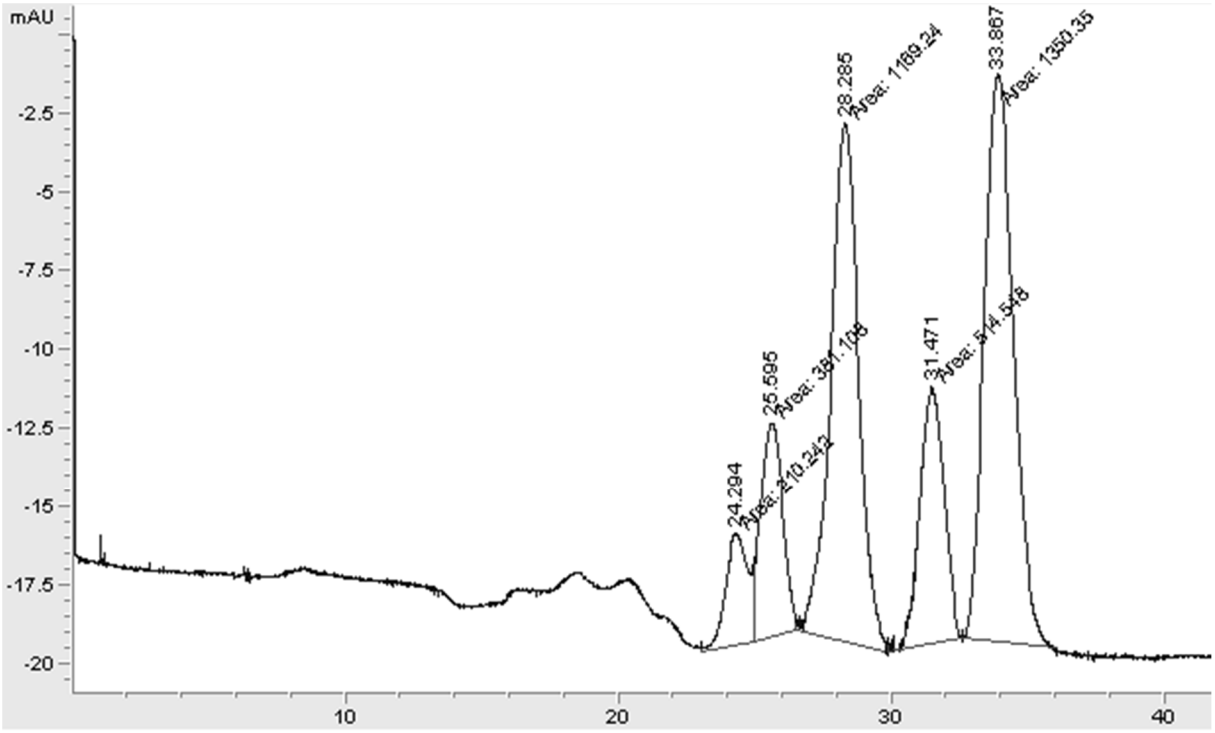

Figure 7.21: Separation of PAHs with a C_8-C_8 capillary, mobile phase: Cit:MeOH=1:29, voltage 20 kV[xx]

Figure 7.21 shows that the separation efficiency with the C_8-C_8 capillary is worse than with the non-functionalized particles. Phenanthrene and anthracene were not separated at all and the resolution of the other peaks is lower than with the earlier presented capillary. Reason for that can be the higher interaction forces and the higher hydrophobicity of the surface of the capillary. The detailed parameters are listed in Table 7.11.

[xx] Measurements carried out by R. Laskowski at TU Kaiserslautern 2011

Table 7.11: Separation parameters of PAHs in C_8-C_8 capillary

Substances	Retention time [min]	Plates [1/m]	Resolution
Naphthalene	24.35 ± 0.08	12150 ± 2610	-
Acenaphthylene	25.65 ± 0.08	16050 ± 210	1.05 ± 0.00
Phenanthrene+Anthracene	28.34 ± 0.08	16560 ± 240	1.11 ± 0.01
Fluoranthene	31.51 ± 0.06	19340 ± 2480	1.11 ± 0.00
Pyrene	33.85 ± 0.02	17840 ± 590	1.08 ± 0.01

7.5.5. Summary

The electrochromatograms of the more complex analyte mixtures, namely the PAHs mixture, the alkylbenzenes mixture and the phenol mixture, are presented in the preceding section. The results obtained with a C_8-functionalized stationary phase with non-functionalized silica particles show reasonable good separation of the different analytes and high theoretical plate numbers. The highest plate numbers could be achieved for the polycyclic aromatic hydrocarbons and the alkylbenzenes. In the first case, they range around 25 000 to 39 000, whereas in the second case theoretical plate numbers in the range of 15 000 to 25 000 were achieved. The phenol mixture could be separated with reasonable good resolutions and theoretical plate heights from 15 000 to 30 000. Yan et al presented the investigation of similar separation tasks with a C_8-functionalized hybrid monolithic column without the addition of particles.[143] All in all the development of a reversed phase silica-based monolith that can be used for simple and more complex separation tasks in capillaries for electrochromatography is presented. The stationary phase was synthesized in respect to the intended upscale. The results for the planar test cell and the annular geometry are presented in the following chapters.

In comparison to that a C_8-functionalized stationary phase with C_8-functionalized silica particles was prepared. The results in Figure 7.21 and Table 7.11 show that this stationary phase can separate the analytes except anthracene and phenanthrene. The theoretical plate number is similar to that achieved with the C_8-functionalized stationary phase including silica particles, whereas the resolution of the adjacent peaks is lower. Due to this reason, the C_8-C_8- functionalized stationary phase was not scaled up.

7.5.6. Separation in a commercially available Agilent capillary

To compare these results, the same mixtures as presented in the previous section were separated in a commercially available Agilent capillary. The electrochromatogram of the PAHs mixture is shown in Figure 7.22 and the results are listed in Table 7.12, the electrochromatogram of the alkylbenzene mixture is shown in Figure 7.23, with the results listed in Table 7.13 and the electrochromatogram of the phenol mixture is given in Figure 7.24.

Table 7.14 shows the parameters of the phenol mixture electrochromatogram.

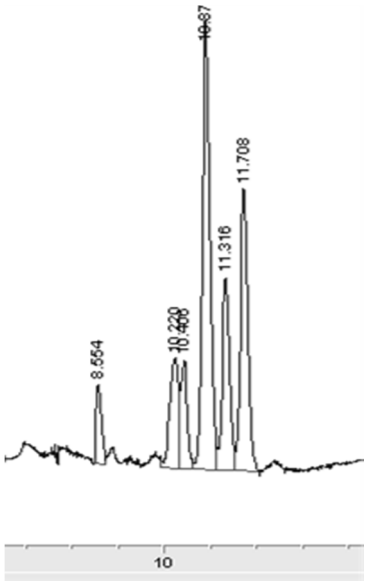

Figure 7.22: Electrochromatogram of the PAH test system (thiourea, naphthalene, acenaphthylene, phenanthrene, anthracene, fluoranthene and pyrene) using a Agilent C_8-capillary. Sample concentration: 83 mg/L; injection: 10 kV, 6 s; voltage: 20 kV; electrolyte: ACN:MeOH = 1:3 + 20% H_2O[xxi]

[xxi] Measurements carried out by R. Laskowski at TU Kaiserslautern 2011

Table 7.12: Retention times, theoretical plate numbers and resolutions of PAH mixture using a Agilent C_8-capillary. Sample concentration: 83 mg/L; injection: 10 kV, 6 s; voltage: 20 kV; electrolyte: ACN:MeOH = 1:3 + 20% H_2O. Data represents average values of 5 runs.

Substances	Retention time [min]	Plates [1/m]	Resolution
Thiourea	8.79 ± 0.38	95878 ± 7618	-
Naphthalene	10.53 ± 0.47	49303 ± 2837	5.72 ± 0.14
Acenaphthylene	10.73 ± 0.49	72311 ± 4147	0.59 ± 0.02
Phenanthrene + Anthracene	11.23 ± 0.52	74026 ± 1496	1.53 ± 0.02
Fluoranthene	11.69 ± 0.55	97646± 3476	1.46 ± 0.02
Pyrene	12.12 ± 0.57	96002 ± 2366	1.35 ± 0.04

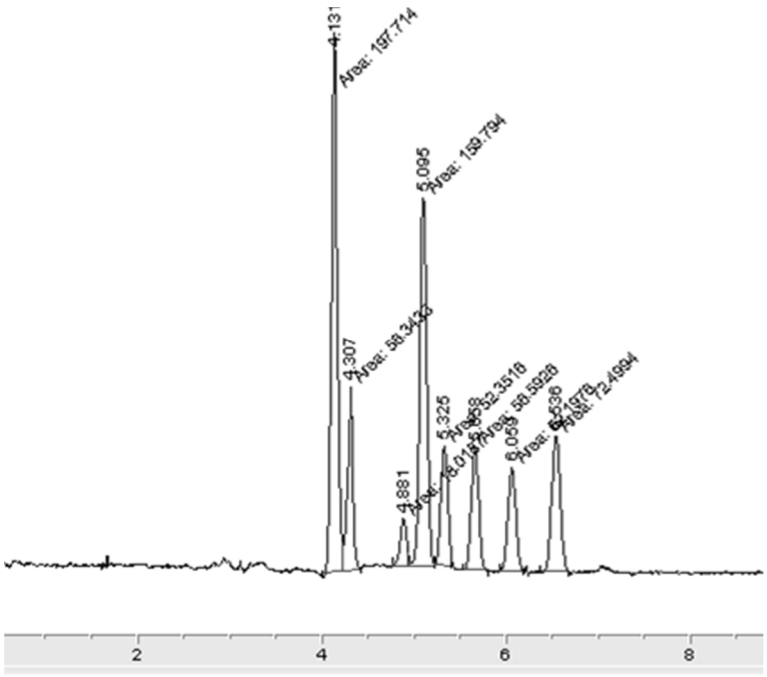

Figure 7.23: Electrochromatogram of the alkylbenzene test system (thiourea, benzene, methylbenzene, ethylbenzene, propylbenzene, butylbenzene, pentylbenzene) using a commercial Agilent capillary. Sample concentration: 83 mg/L; injection: 10 kV, 3 s; voltage: 20 kV; electrolyte: Cit:ACN 1:9.[xxii]

[xxii] Measurements carried out by R. Laskowski at TU Kaiserslautern 2011

Table 7.13: Retention times, theoretical plate numbers and resolutions of the alkylbenzene mixture using an Agilent C_8-capillary. Sample concentration: 83 mg/L; injection: 10 kV, 3 s; voltage: 20 kV; electrolyte: Cit:ACN 1:9. Data represents average values of 5 runs.

Substances	Retention time [min]	Plates [1/m]	Resolution
Thiourea	4.13 ± 0.03	293981 ± 36588	-
Benzene	4.32 ± 0.03	386272 ± 91181	1.61 ± 0.08
Unknown Impurities	4.90 ± 0.04	236902 ± 7639	4.24 ± 0.22
Methylbenzene	5.11 ± 0.03	321232 ± 9147	1.40 ± 0.07
Ethylbenzene	5.35 ± 0.04	312083 ± 6634	1.57 ± 0.01
Propylbenzene	5.68 ± 0.04	327229 ± 13028	2.15 ± 0.04
Butylbenzene	6.09 ± 0.04	329590 ± 28854	2.47 ± 0.08
Pentylbenzene	6.57 ± 0.05	347443 ±15739	2.79 ± 0.07

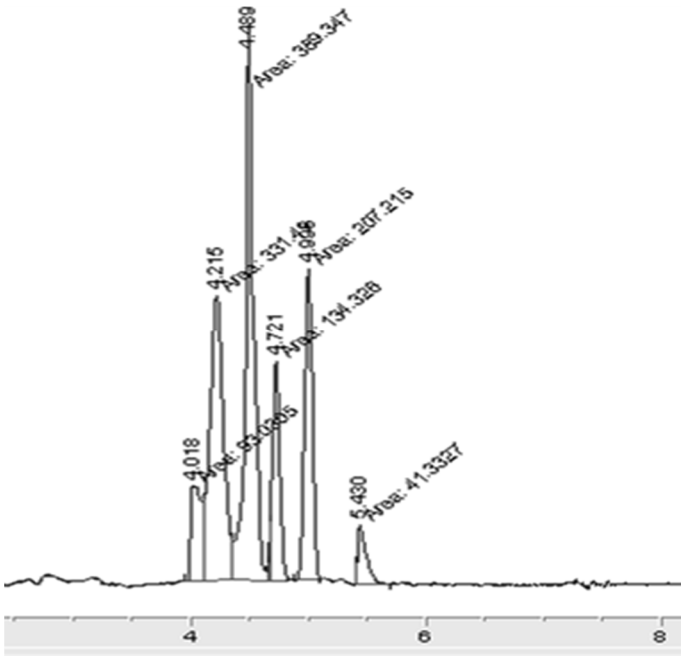

Figure 7.24: Electrochromatogram of the phenol test system (phenol, 3,5-dimethoxyphenol, 2,5-dimethyl-4-(morpholinomethyl)-phenol, mono-(3-chlorophenyl)phenylmethylphthalat, 2-nitrophenol, 4,6-dichloro-2-(5-isoxazolyl)phenol) using a C_8-Agilent capillary. Sample concentration: 100 mg/L; injection: 10 kV, 3 s; voltage: 20 kV; electrolyte: Cit:ACN = 1:9.[xxiii]

[xxiii] Measurements carried out by R. Laskowski at TU Kaiserslautern 2011

Table 7.14: Retention times, theoretical plate numbers and resolutions of the phenol mixture. using an Agilent C_8-capillary. Sample concentration: 100 mg/L; injection: 10 kV, 3 s; voltage: 20 kV; electrolyte: Cit:ACN = 1:9. Data represents average values of 6 runs.

Substances	Retention time [min]	Plates [1/m]	Resolution
Thiourea	4.01 ± 0.02	33706 ± 20502	-
Phenol	4.22 ± 0.04	27658 ± 4029	1.03 ± 0.15
3,5-Dimethoxyphenol + 2,5-Dimethyl-4-(morpholino-methyl)phenol	4.50 ± 0.04	157907 ± 9408	1.86 ± 0.10
Mono-(3-chlorophenyl)phenylmethyl phthalat	4.73 ± 0.04	101069 ± 2658	2.22 ± 0.05
2-Nitrophenol	5.01 ± 0.04	109243 ± 1675	2.30 ± 0.02
4,6-Dichloro-2-(5-isoxazolyl) phenol	5.43 ± 0.02	106691 ± 6691	3.32 ± 0.25

The electrochromatograms of the commercially available C_8-functionalized silica-based Agilent capillary show higher theoretical plate numbers and shorter retention times than the ones obtained with our C_8-functionalized silica-based monolithic capillary including silica particles. However, the resolutions for the PAHs mixture are better in the electrochromatogram obtained with our C_8-functionalized monolithic capillary due to the separation of anthracene and phenanthrene.

7.6. Planar test cell

To simplify the upscale from the capillary to the annular dimensions, a step in between was introduced and a planar test cell was built. The first approach to scale up monolithic material for chromatographic applications was already documented in the literature.[147] The planar test cell has the dimensions of 10 cm x 20 cm and the gap between the two glass plates was 0.3 mm and 1 mm, respectively. More details are given in the chapter *Implementation*. In this part the investigation of the volume flow and of the separation of the presented test systems in the two gap width of the planar device is going to be presented.

A good insight of the difference in through flow due to the different gap width is shown in Figure 7.25. The volume flow in the 1 mm gap is increased 3x compared to the 0.3 mm gap

and a through flow of more than 50 ml/h could be achieved. Furthermore, the trend increased volume flow with increased voltage is linear which is in good agreement with theory. The results of the separation are shown at the optimized voltage applied, given that higher voltages can induce increased Joule heating and bubble formation.

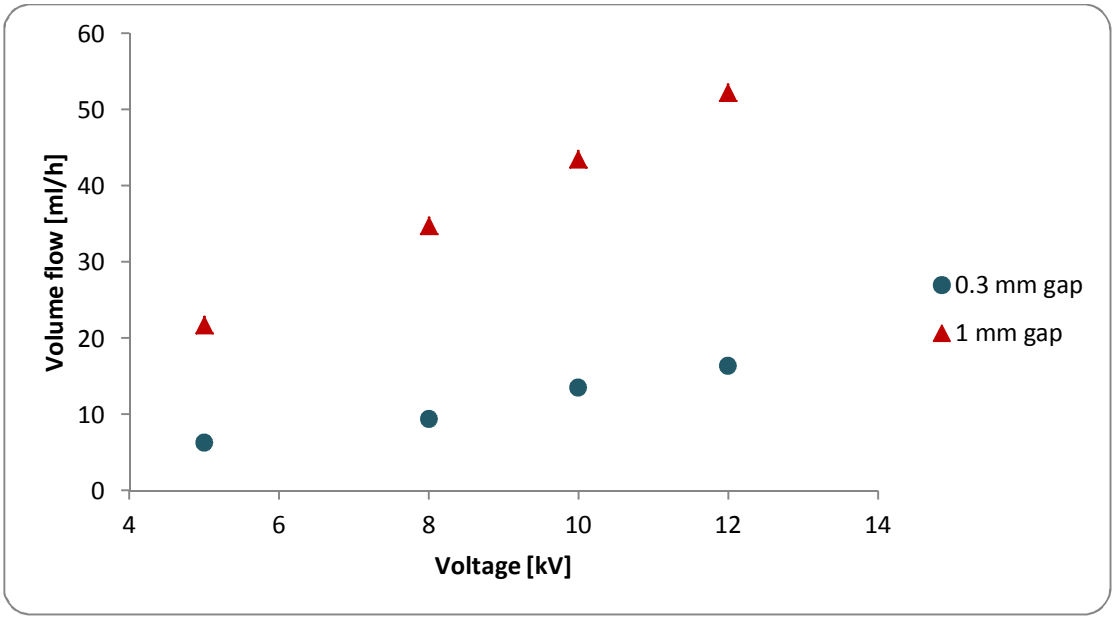

Figure 7.25: Comparison of the volume flow in the planar test cell with different gap widths, mobile phase Cit:MeOH=1:29

Detailed data can be looked up in the section *Experimental*.

7.6.1. Influence of the mobile phase on the volume flow

After the decision was made to use the 1 mm gap in further experiments, the influence of the mobile phase on the volume flow was validated. Figure 7.26 shows the results for the planar test cell with a 1 mm gap.

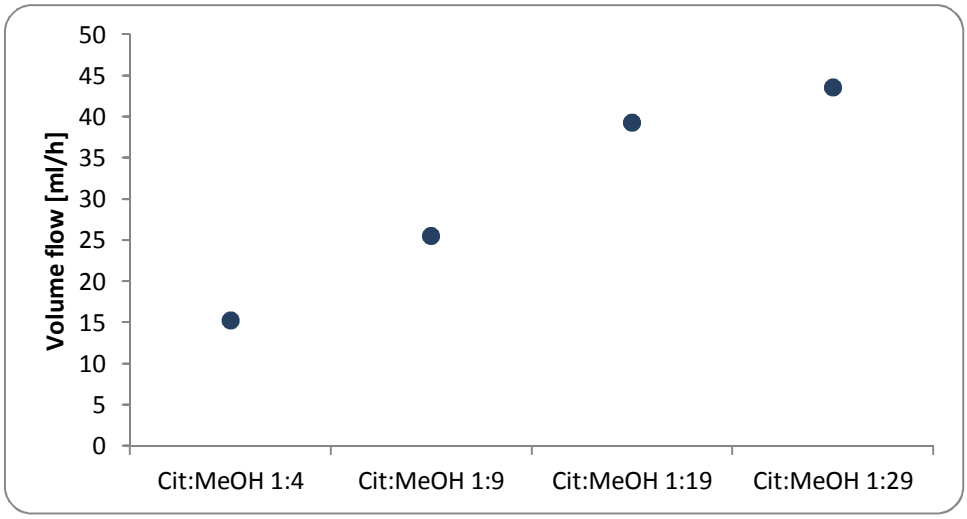

Figure 7.26: Influence of the mobile phase composition on the volume flow at 10 kV in the planar test cell with 1 mm gap.

The values are in good agreement with the results obtained in the capillaries, which also show a linear trend of higher volume flow when increasing the amount of methanol in the mobile phase composition, which is in line with the theory of the elctroosmotic flow, explained in the chapter *Introduction*. Therefore, the mobile phase composition used is Cit:MeOH = 1:29.

7.6.2. Separation in the planar test cell

The first separation experiments in the planar test cell were carried out with a dye mixture of brilliant green and methyl red in methanol. The molecular structures of these molecules are shown in Figure 7.27.

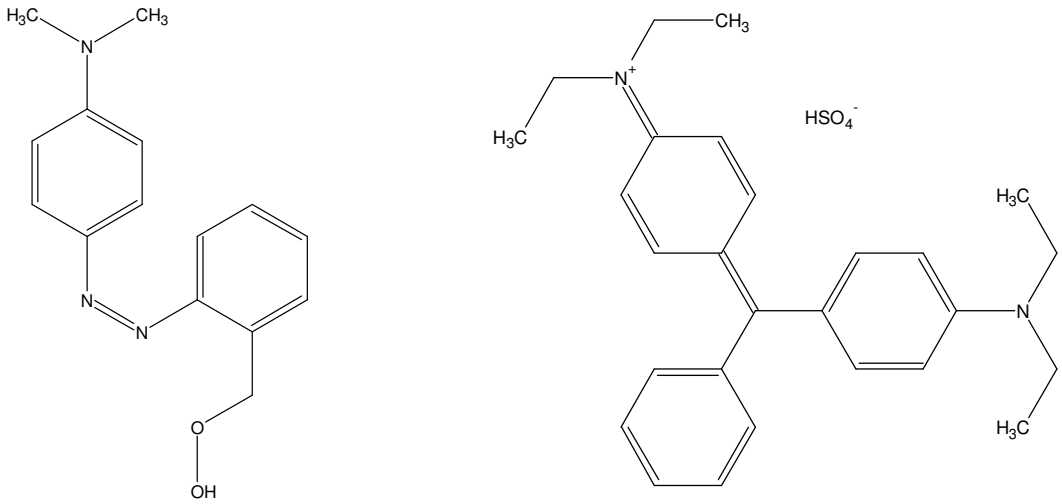

Methyl Red Brilliant Green

Figure 7.27: Molecular structures of methyl red and brilliant green

The first separation achieved is shown in Figure 7.28.

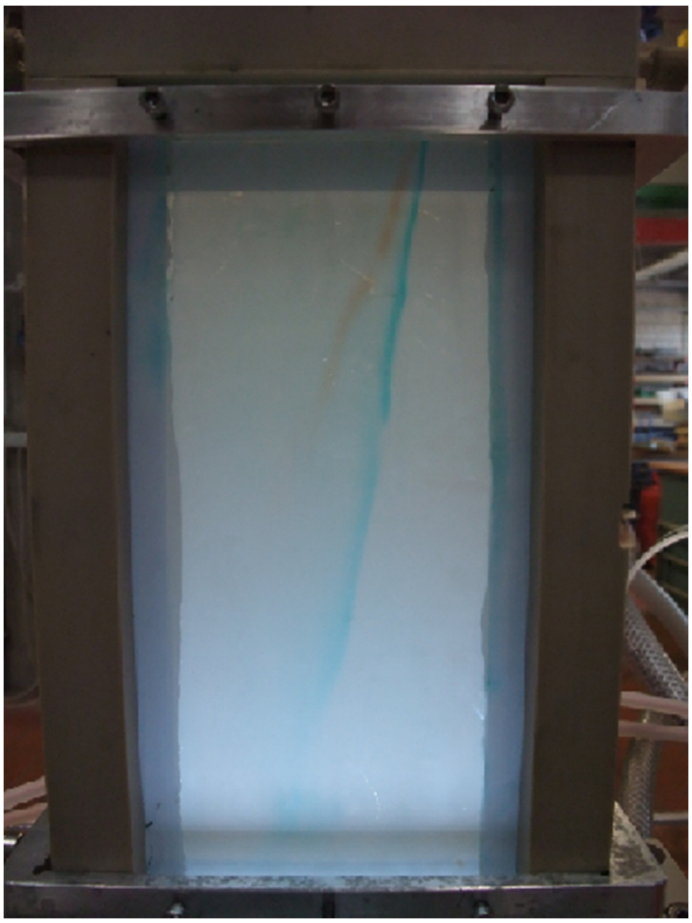

Figure 7.28: Separation of methyl red and brilliant green in the planar test cell

Examining Figure 7.28 one can clearly see how the planar test cell refers to the annular prototype. The separation process happens along the horizontal axis, which is the major advantage of the annular geometry. The separation bands are well visible and it is easy to envision these results in the annular geometry.

7.6.3. Separation in the 0.3 mm gap test cell

Having achieved this good separation, the next step was to obtain a well separated electrochromatogram of the simple test system thiourea, naphthalene and anthracene. The first experiments were carried out in the planar test cell with the 0.3 mm gap. The electrochromatogram is shown in Figure 7.29.

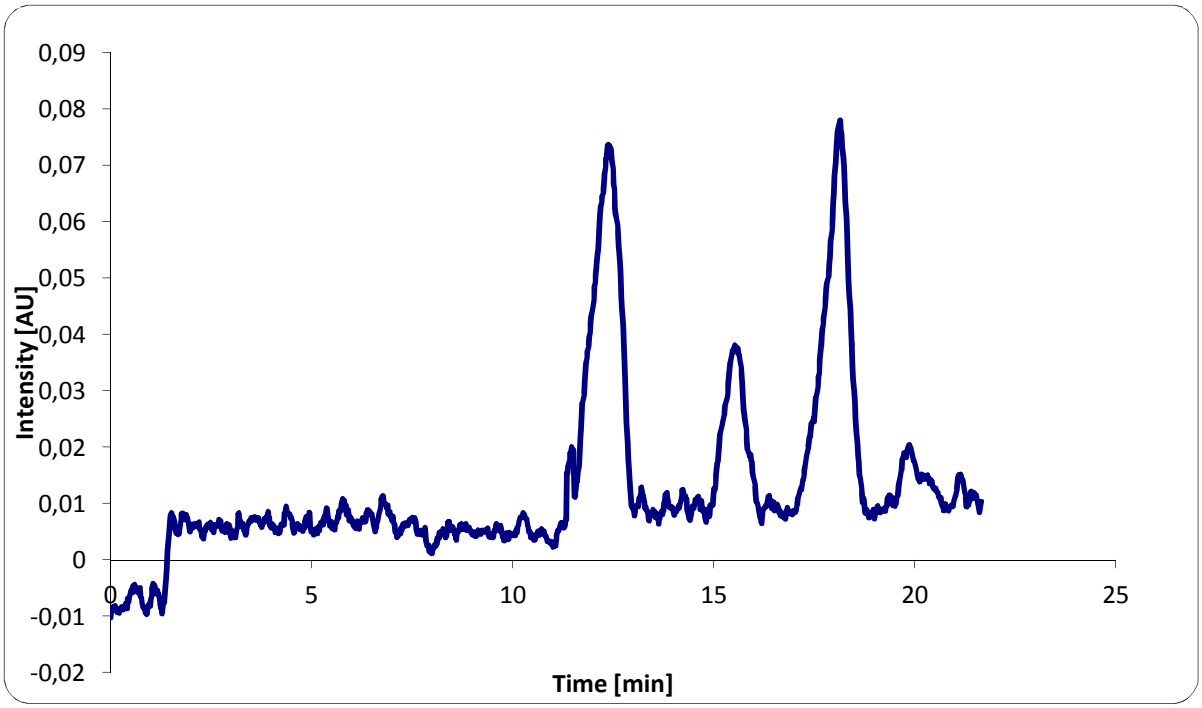

Figure 7.29: Separation of thiourea, naphthalene and anthracene in the 0.3 mm gap planar test cell, mobile phase: Cit:MeOH=1:29, voltage: 8 kV[xxiv]

The parameters of the separation are given in Table 7.15.

Considering the widening of the gap, and the associated diffusion in lateral direction, the theoretical plate number is in a good range. All peaks are well separated and in a Gaussian shape.

Table 7.15: Separation parameters of the simple test system in the planar test cell, 0.3 mm gap, 8 kV

Substances	Retention time [min]	Plates [1/m]	Resolution
Thiourea	12.38	5490	-
Naphthalene	15.53	12310	3.90
Anthracene	18.13	16180	3.49

To compare and verify the results, an electrochromatogram at a voltage of 9 kV was recorded. The electrochromatogram is shown in Figure 7.30 and separation values are given in Table 7.16.

[xxiv] Measurements carried out by R. Laskowski at TU Kaiserslautern 2011

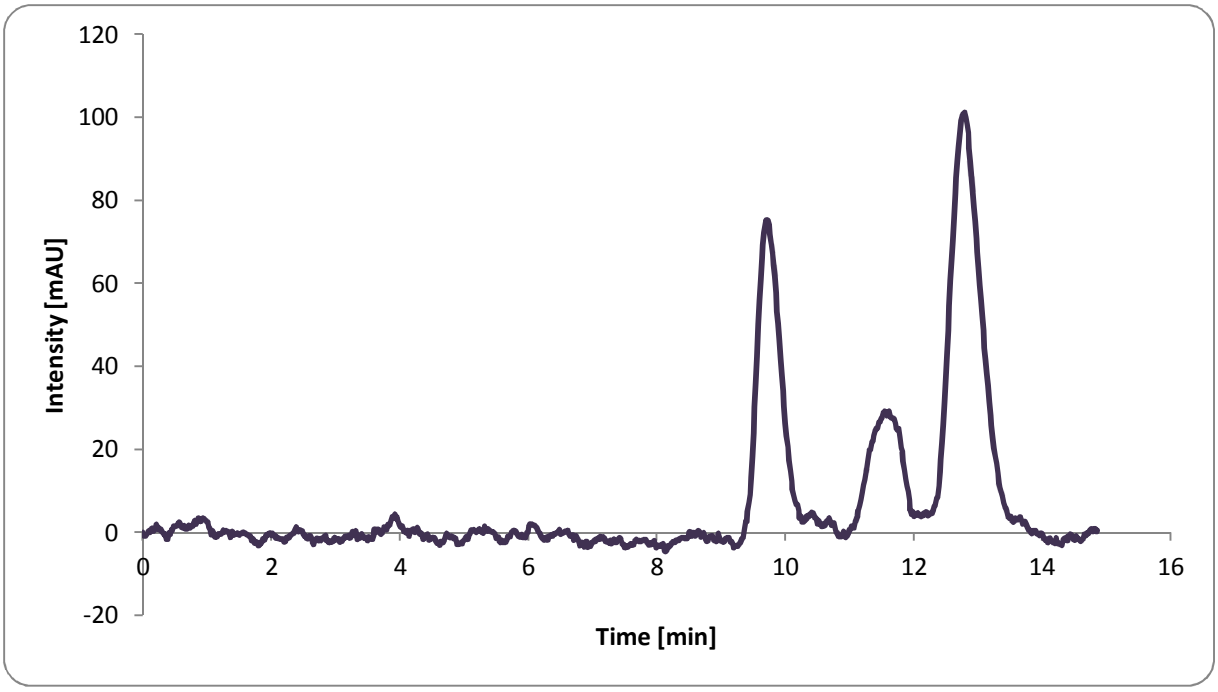

Figure 7.30: Separation of thiourea, naphthalene and anthracene in the 0.3 mm gap planar test cell, mobile phase: Cit:MeOH=1:29, voltage: 9 kV[xxv]

Table 7.16: Separation parameters of the simple test system in the planar test cell, 0.3 mm gap, 9 kV

Substances	Retention time [min]	Plates [1/m]	Resolution
Thiourea	9.71	10200	-
Naphthalene	11.62	17310	3.71
Anthracene	12.79	14690	2.10

The retention times are lower due to the higher voltage. The theoretical plate number is similar to the figures shown in Table 7.15. The separation of the analytes is still acceptable at higher voltages. However, the limitation of elevation of applied voltage lies in the formation of bubbles in the stationary phase.

7.6.4. Separation in the 1 mm gap test cell

As mentioned in the *Implementation* part, the scale-up happened in two steps, from the capillary to the bigger devices and from 0.3 mm to 1 mm gap width. Considering the dimensions, one has to take the lateral diffusion into account. The first results obtained fit perfectly in the assumption of broader peaks. Figure 7.31 shows the first

[xxv] Measurements carried out by R. Laskowski at TU Kaiserslautern 2011

electrochromatogram in the planar test cell with 1 mm gap. The peaks are not as nicely shaped as in the previous electrochromatograms, but the through-put was increased more than three fold. Also the feed flow could be increased from 0.003 to 0.01 ml/min. Table 7.17 summarizes the results of the electrochromatogram.

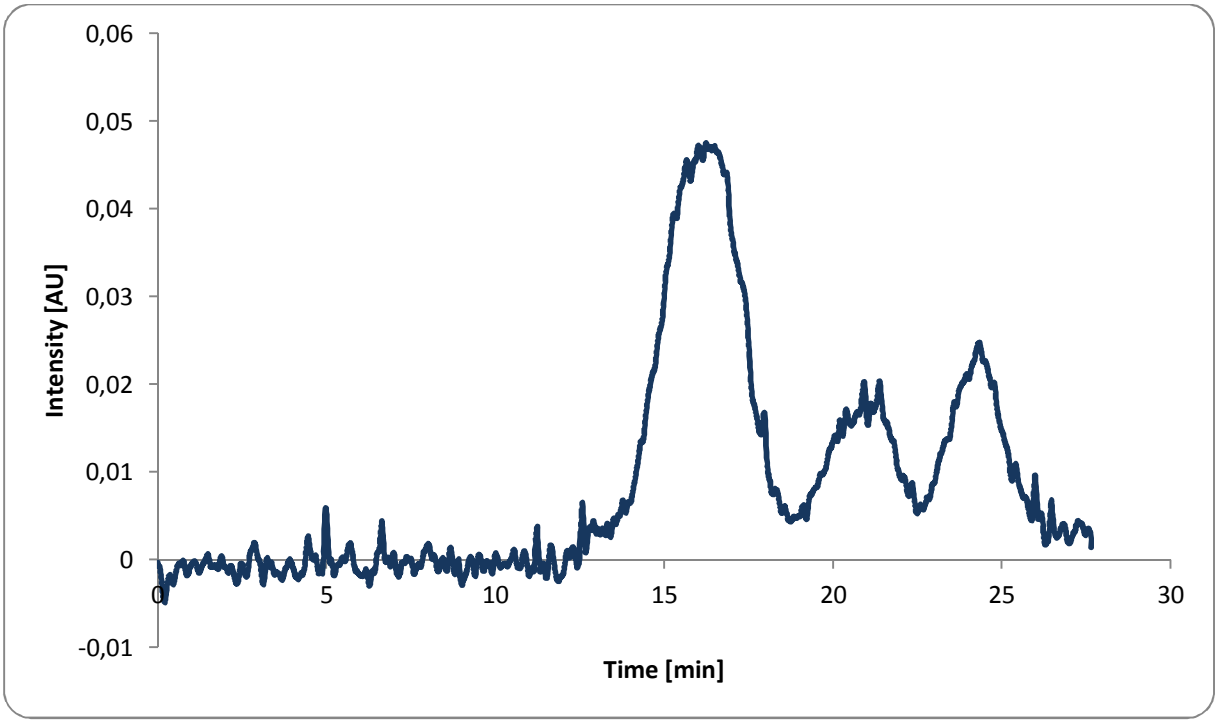

Figure 7.31: Separation of thiourea, naphthalene and anthracene in the 1 mm gap planar test cell; mobile phase: Cit:MeOH=1:19, voltage 10 kV[xxvi]

The results are not satisfying; however, one has to have an eye on the mobile phase. As mentioned already a couple of times, the influence of the mobile phase composition on the separation efficiency is remarkable.

Table 7.17: Results of the first separation in the 1 mm gap planar test cell

Substances	Retention time [min]	Plates [1/m]	Resolution
Thiourea	15.67	880	-
Naphthalene	20.92	2520	2.11
Anthracene	24.32	4290	1.64

[xxvi] Measurements carried out by R. Laskowski at TU Kaiserslautern 2011

Therefore, again some changes in the used mobile phase were made and finally H_2O:MeOH = 1:19 with 1% Cit buffer (25 mM) was used. The outcome is in good agreement with the results from the 0.3 planar test cell. Figure 7.32 shows the obtained electrochromatogram; Table 7.18 gives the figures of the separation.

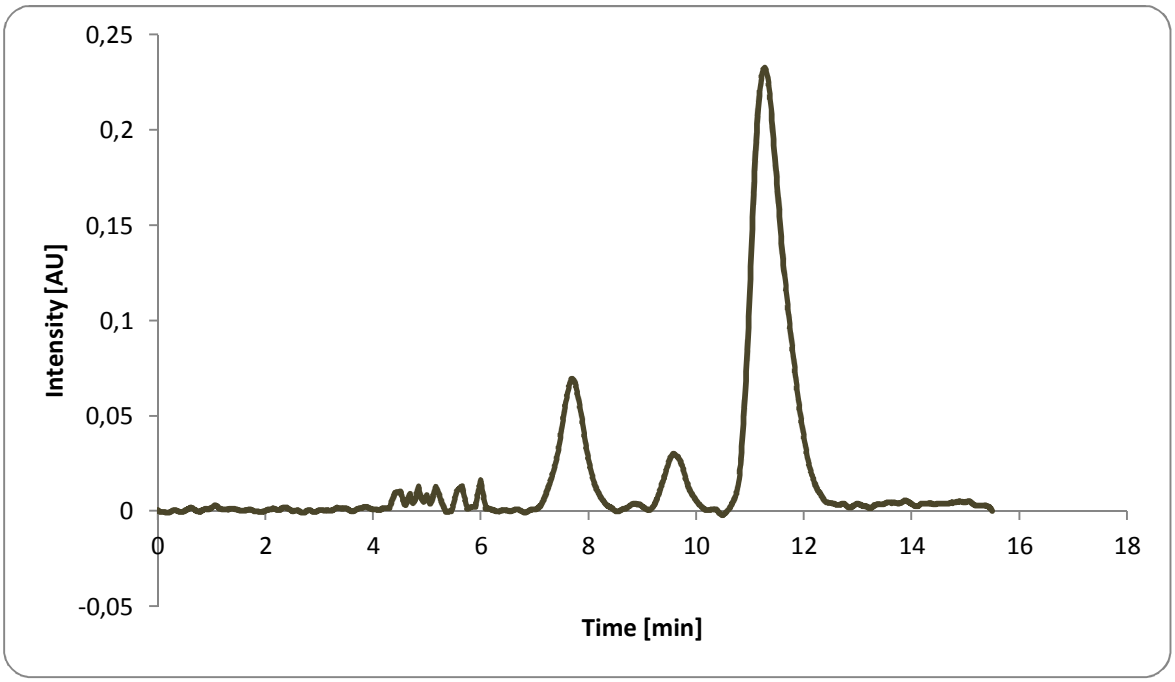

Figure 7.32: Separation of thiourea, naphthalene in the 1 mm gap planar test cell, mobile phase H_2O:MeOH=1:19 with 1% Cit buffer (25 mM), voltage 10kV[xxvii]

Table 7.18: Separation parameters of thiourea, naphthalene and anthracene in 1mm gap cell at 10 kV

Substances	Retention time [min]	Plates [1/m]	Resolution
Thiourea	7.70	6490	-
Naphthalene	9.59	11670	3.98
Anthracene	11.26	7770	2.99

The mobile phase of the second experiment has a water content significantly higher than the ones before. Therefore, the retention times are lower, the theoretical plate numbers are higher and the resolution is better than in the first experiment.

[xxvii] Measurements carried out by R. Laskowski at TU Kaiserslautern 2011

7.6.5. Separation of PAHs

After the good separation of the simple test system, the more complex test systems were separated in the planar test cell. The electrochromatogram is shown in Figure 7.33.

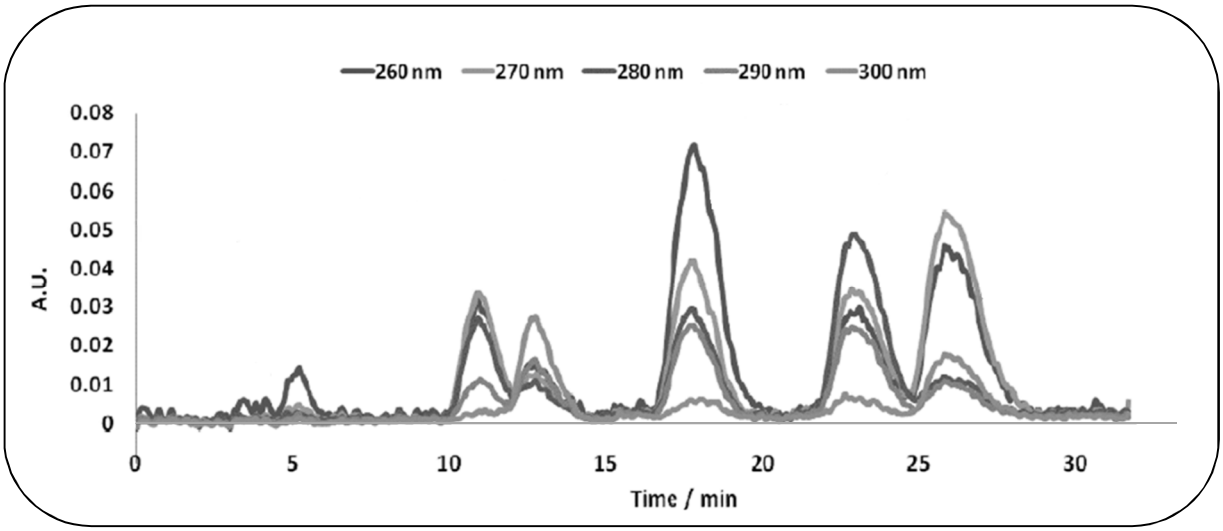

Figure 7.33: Separation of PAHs in the planar test cell, mobile phase: H_2O:MeOH:ACN = 1:3:1, voltage: 12 kV[xxviii]

One can clearly identify all the substances with the exception of phenanthrene and anthracene, the peak at 17.5 min, which could not be separated. The same problem occurred in the capillaries. However, there, one could identify two peaks, but the resolution was not satisfactory. In Figure 7.33, there is more than one diagram curve. This is due to the necessity to record the spectrum at more than one wavelength. The different substances absorb at different wavelength, respectively. The parameters can be looked up in Table 7.19.

[xxviii] Measurements carried out by R. Laskowski at TU Kaiserslautern 2011

Table 7.19: Parameters of separation of the PAH mixture obtained in the planar test cell with 1 mm gap

Substances	Retention time [min]	Plates [1/m]	Resolution
Thiourea	5.03	700	4.74
Naphthalene	10.95	1476	1.15
Acenaphthylene	12.67	1976	3.02
Phenanthrene + Anthracene	17.58	2795	2.75
Fluoranthene	22.74	3580	3.09
Pyrene	28.91	5787	4.74

7.6.6. Separation of phenols

Another task was the separation of the phenol mixture. As already assumed from the capillary experiments, the separation is not easy to accomplish. The electrochromatogram obtained is shown in Figure 7.34.

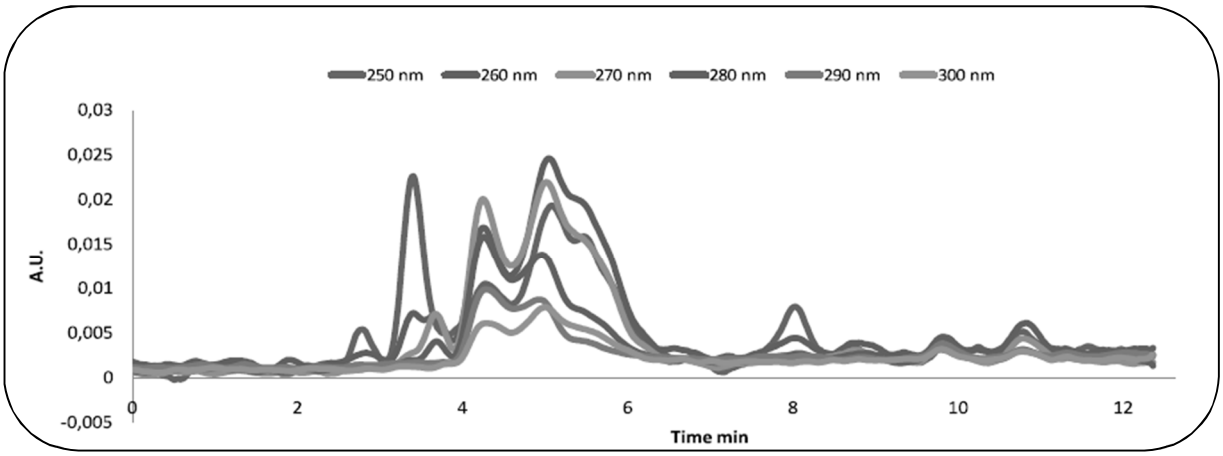

Figure 7.34: Separation of phenol mixture, mobile phase: H_2O:MeOH=1:9, voltage 12 kV[xxix]

The electrochromatogram does not show significant separation of the single substances, therefore it is refrained to present parameters of the electrochromatogram.

[xxix] Measurements carried out by R. Laskowski at TU Kaiserslautern 2011

7.7. Investigations in the annular geometry

The last task to undertake was the quantification of the separation efficiency in the annular geometry. First, the discharging of the liquid had to be examined. Therefore, a newly adapted system was built to test the elution behavior.[xxx] An outlet with 80 capillaries was constructed to check if the eluent is evenly discharged from the monolith. For this purpose the eluent is pushed into the system at the top of the system and the drops of the eluent are monitored at the outlet. A movie was taken to be able to exploit the discharging. A snapshot of this movie is shown in Figure 7.35.

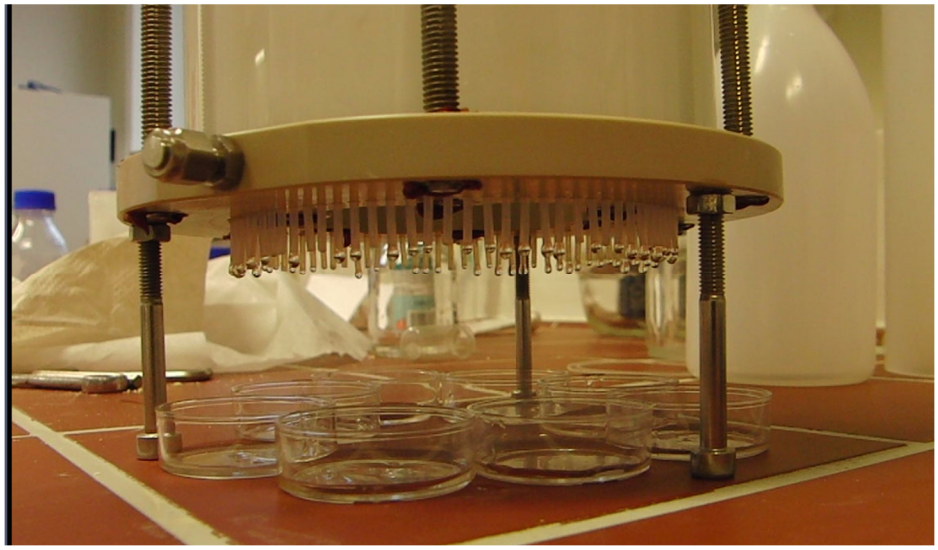

Figure 7.35: Snapshot a of the discharging eluent movie

From the movie and the snapshot shown, the fluid seems to be evenly distributed. However, to have actual values, the eluent was collected in eight different vessels and the amount was weighed. In average, 15 ml of MeOH were pumped through the annular monolith and the result of the vessels weighed is shown in Table 7.20. The statistical values are given in Table 7.21.

[xxx] Designed and manufactured by the Institut für Mikrotechnik Mainz GmbH

Table 7.20: Comparison of the discharged fluid collected at the outlet of the annular device

Number of vessel	Run 1 Weight [g]	Run 2 Weight [g]	Run 3 Weight [g]
1	2.77	1.18	1.65
2	1.19	1.29	1.40
3	1.99	1.76	1.87
4	1.10	0.49	1.36
5	1.36	1.55	0.87
6	1.42	2.81	1.47
7	1.07	1.70	2.93
8	1.06	1.00	2.26

Table 7.21: Mean value and RSD of discharged fluid at the outlet of the annular device

	Run 1	Run 2	Run 3
X_{mean} [g]	1.465	1.472	1.725
σ^2	0.36	0.46	0.40

When looking at these results, one has to remember that methanol is volatile and the amounts are not very big. However, the tendency shows satisfactory agreement. Another important issue is the stability of the monolith towards different eluents. A detailed study is given in the *Experimental* section, but to highlight the importance of it, the influence of storing the monolith in water is shown in Figure 7.36. In difference to that, it has to be mentioned that the short-term use of water as a mobile phase does not have a bad influence.

Figure 7.36: Damage of the monolith due to water storage

To ensure a homogeneous monolithic structure, another test could be examined in our lab. To visualize uniformity, the dye blue dextran was injected at the top of the annular geometry and pushed through the monolith. In Figure 7.37 the ring formed with the blue color ensures a nicely shaped system of through-pores and micropores.

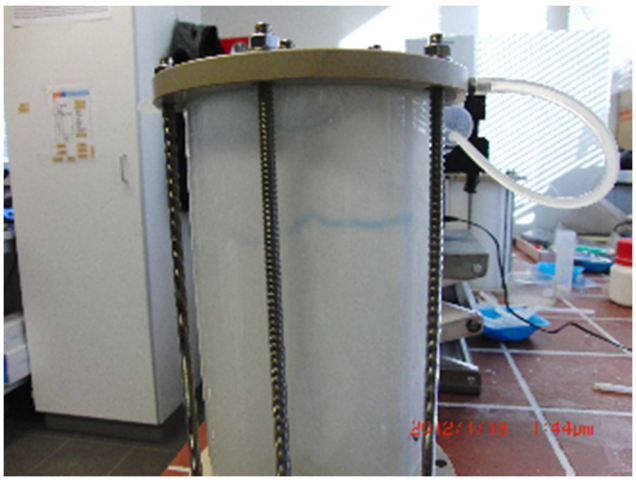

Figure 7.37: Blue dextran ring in annular monolith

Second, the volume flow was analyzed. Therefore, again three different compositions of mobile phases were used.

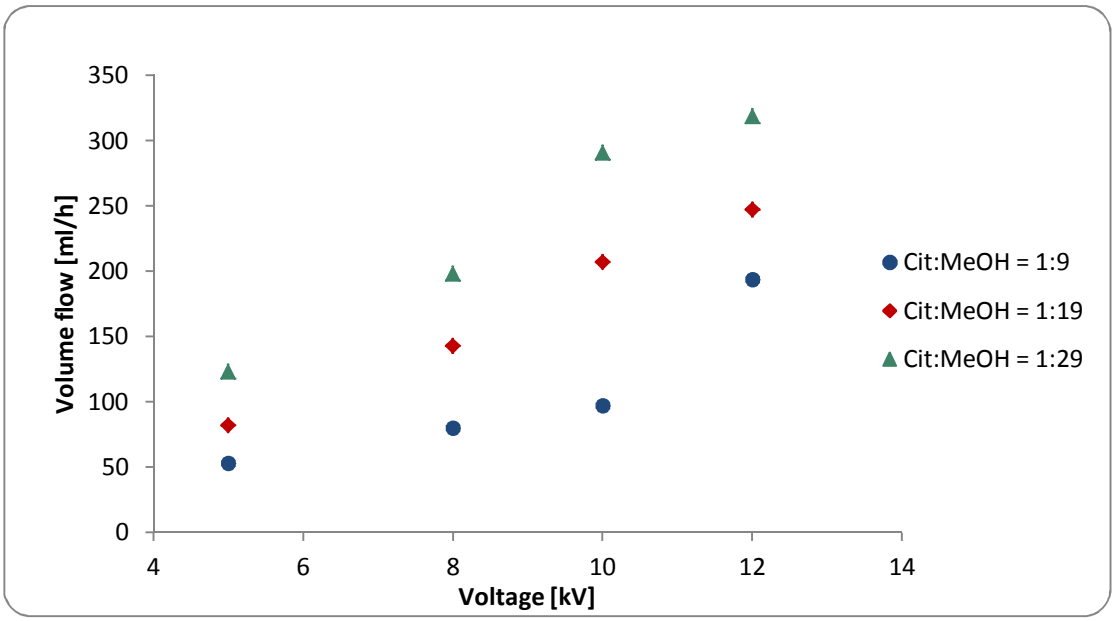

Figure 7.38: Comparison of volume flow of different mobile phases in the annular geometry[xxxi]

Decreasing the content of citrate buffer, i.e. the content the ionic strength, increases the volume flow. This knowledge can be used to adapt the application to different separation problem. The first results of separation were again accomplished with the dye system, shown in Figure 7.39 and Figure 7.40. Here, two different runs are documented, where one can see the influence of the homogeneity of the stationary phase on the separation bands. The bands in Figure 7.39 were obtained with a stationary phase prepared by manual pumping whereas Figure 7.40 shows the preparation after the standard preparation procedure. The separation bands of the second figure do not have the same lateral diffusion and therefore the bands are sharper and smaller.

[xxxi] Measurements carried out by R. Laskowski at TU Kaiserslautern 2011

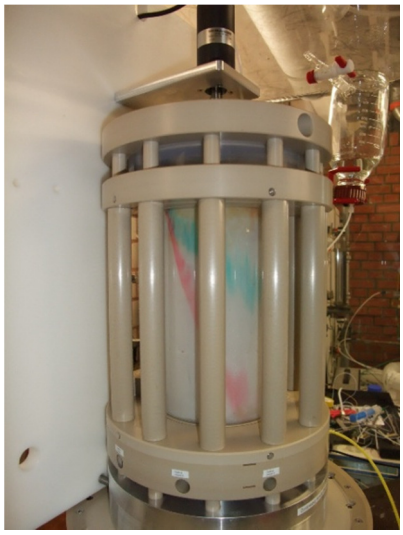

Figure 7.39: Separation of dyes in the annular geometry

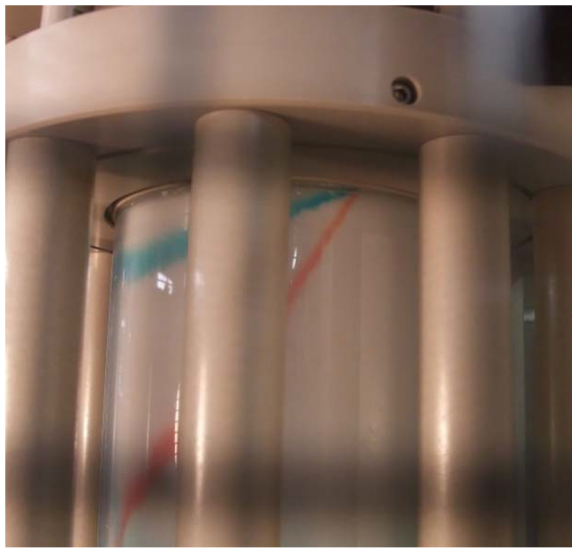

Figure 7.40: Separation of dyes in the annular geometry, detailed view

The dye separation is a good illustration of the principle itself. One can easily comprehend the theoretical approach explained in the *Introduction*.

Furthermore, the separation of the simple test system was possible in the annular geometry. The result can be seen in Figure 7.41. The concentrations of the analytes were 1 g/l each and the feed flow was 0.005 ml/h and 0.3°/s.

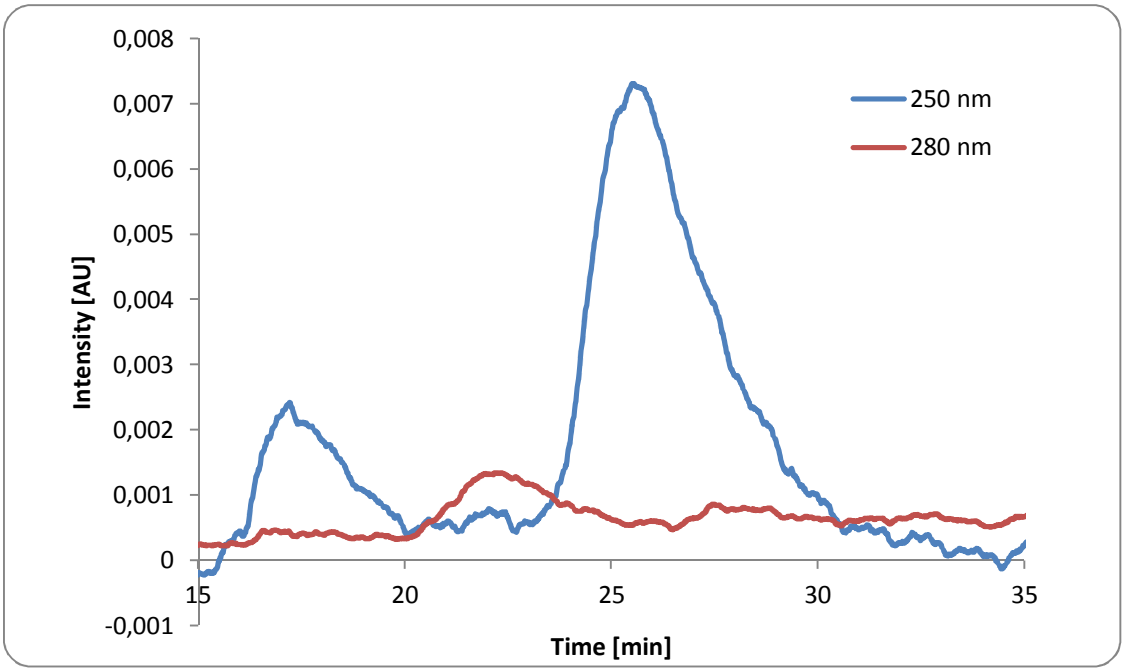

Figure 7.41: Separation of thiourea, naphthalene and anthracene in the annular geometry, mobile phase: Cit:MeOH=1:29, voltage 10 kV[xxxii]

In Table 7.22 the retention times, the plate numbers and the resolution of the standard test system are shown.

Table 7.22: Parameters of separation of the standard test system obtained in the annular geometry

Substances	Retention time [min]	Plates [1/m]	Resolution
Thiourea	17.07	1923	-
Naphthalene	21.97	2167	2.16
Anthracene	25.45	1253	1.11

7.8. Summary of separation in the different devices

The upscale presented – first from capillaries to two different gap sizes in the planar test cell, second from the test cell to two gap sizes in the annular geometry – shows the versatility of possible applications of the reversed phase particle-loaded monolith. The easiest molds to fill were the capillaries, which also explains the high numbers of experiments executed. Different test systems, namely a mixture of thiourea, naphthalene and anthracene, a mixture of PAHs, a mixture of alkylbenzenes and a mixture of phenols could be separated.

[xxxii] Measurements carried out by R. Laskowski at TU Kaiserslautern 2011

Additionally, tests concerning the mobile phase composition could be run in the capillaries. This was helpful in case of restrictions in solvent choice usable in the planar test cell and the annular chromatograph.

The next step of the scale-up showed the separation of the standard test system and the mixture of PAHs in the planar test cell. The separation parameters agree well with the results obtained from the capillaries, where for the standard test system plate numbers of up to 17 000 m^{-1} and for the PAHs mixture separation efficiencies of up to almost 6 000 m^{-1} could be achieved. The volume flow could be increased from 10 ml/h in the 0.3 mm gap to more than 40 ml/h in the 1 mm gap.

Although there has still work to be done concerning separation efficiency in the annular device, it is a powerful tool for future applications. Thiourea, naphthalene and anthracene could be separated with a separation efficiency of up to 2 100 and good resolution values could be obtained. A volume flow of more than 300 ml/h could be realized.

C) EXPERIMENTAL PART

8. General information

Deionized water was ultrapure water, 0.06 µS/cm.

FTIR spectra were recorded on a Bruker VERTEX 70 using a DLaTGS detector and an ATR unit: MVP Pro Star, Diamond crystal, resolution: 4cm^{-1}, 16 scans, 4000-600 cm^{-1}.

RAMAN spectra were recorded on a Perkin RamanStation 400F with a motorized XYZ Stage, Exposure Time: 10.00, Number of Exposures: 4, Laser Wavelength: 785.13 nm.

The **CE device** was a fully automated ^{3D}CE system (Agilent Technologies, CA, USA) equipped with a diode array detector (Wavelengths of 234, 240 and 450 nm were used for detection respectively).

For the online detection of the separation efficiency in the planar test cell a **UV-VIS spectrometer** (AVS-USB2000, Avantes Inc., Eerbeek, The Netherlands) with a 250–1000 nm range was employed, using a 200 µm glass fibres (Avantes UV/VIS, 200–750 nm, LEONI Fiber Optics GmbH, Germany). The light source was a UV-VIS-NIR source (Ocean Optics Inc., Dunedin, USA) with wave lengths ranging from 200 nm to 2000 nm. All measurements were performed at room temperature and in a dark environment.

The amounts of C and H were analyzed using an Elementar Vario El III device for **elemental analysis** with helium as carrier gas.

The **nitrogen physisorption analysis** was carried out on a Micromeritics ASAP 2010. The inner surface area was determined based on the BET method. The pore size distribution was determined using the BJH method applied to the adsorption isotherms.

Hg-porosimetry was carried out on a Demo AutoPore IV 9500 V1.06 (Micromeritics).

The **density** of the materials was determined using a Micromeritics He-pyknometer (AccuPyc 1340).

Microscope used was a microscope LEICA DM4000.

SEM/EDX was carried out with a FEI Quanta 600 FEG-ESEM system and a NORAN Vantage system with Si(Li)-detector (10 mm^2, PlexUs 0.65µm window, energy resolution 132eV).

The **Capillaries** of Agilent Technologies, CE standard capillary, 100 um, 40cm, 2/Pk

G 1600 – 60411 were filled with stationary phase.

For starting experiments, **Pasteuer pipettes** manufactured by VOLAC (reference: D812 230 mm ISO 7712) were used.

The **Microscope Slides** were 76x26 mm/ ready to use, cut by Menzel ISO 8037/1.The **commercial CEC capillary** was a CEC Cap HypC8 3µm, 100µm/25cm 2/PK.

9. List of chemicals used

Table 9.1: List of reagents used

Compound	Abbr.	Note	Company
3-aminopropyl-triethoxysilane	APTES	99%	Fluka
3-cyanopropyl-triethoxysilane	CPTES	98%	Aldrich
3-mercaptopropyl-functionalized silica gel	MPTMS	200-400 mesh	Aldrich
cetyltrimethyl-ammonium bromide	CTAB	98%	Sigma
diethylamine	DEA	puriss. pa ≥99.5%	Fluka
dimethylformamide	DMF	≥99.8%	Roth
polyethylenglycol 400	PEG	PH EUR	Fluka
tetraethoxysilane	TEOS	95%	Fluka
triethoxy(octyl)silane	C_8-TEOS	≥97.5%	Aldrich
tetramethyl orthosilicate	TMOS	98%	Aldrich

Table 9.2: List of solvents, acids and bases used

Compound	Abbr.	Note	Company
acetic acid	AA	99.8%	Aldrich
acetonitrile	ACN	≥99.5%	Roth
ammonium hydroxide solution	NH_4OH	puriss. pa 25 NH_3 basis	Sigma – Aldrich
citric acid	Cit	≥99.5%	Sigma – Aldrich
ethanol	EtOH	With 1% MEK	Roth
hydrochloric acid	HCl	≥32% p.a.	Roth
methanol	MeOH	99%	Roth
pyridine		≥99 %	Roth
sodium hydroxide	NaOH	≥99% p.a.	Roth
sulfuric acid	H_2SO_4	≥99.5%	Roth
tris(hydroxymethyl)-aminomethane	TRIS	pufferan ≥99.3%	Roth
water	H_2O	ultrapure water, 0.06 µS/cm	

Table 9.3: List of test molecules used

Compound	Note	Company
brilliant green	dye content 90%	Sigma
methyl red	ACS reagent	Sigma – Aldrich
naphthalene	98%	Fluka
anthracene	96%	Fluka
thiourea	99%,	Aldrich
acenaphthylene	75%	Aldrich
phenanthrene	98%	Aldrich
pyrene	98%	Aldrich
fluoranthene	98%	Aldrich
benzene	99.9%	Sigma-Aldrich
toluene	99.9%	Sigma-Aldrich
ethylbenzene	>99%	Fluka
propylbenzene	98%	Aldrich
butylbenzene	99%	Aldrich
pentylbenzene	99%	Aldrich
phenol	99.5%	Aldrich
3-(o-methoxyphenoxy)-1,2-propanediol	98%	Aldrich
3,5-dimethoxyphenol	99%	Aldrich
2-nitrophenol	99%	Fluka
2,5-dimethyl-4-(morpholinomethyl)-phenol	technical grade	Aldrich
2,4-dichloro-6-(5- isoxazolyl)-phenol	97%	Aldrich

10. Synthesis of different monolithic materials

10.1. Capillaries and Scale-up

All components listed in the tables were mixed in a vial for an hour at 40°C if not noted otherwise. After one hour, the mixture was cooled to room temperature and the catalyst was added. The capillaries were filled as shown in the chapter *Implementation*.

Table 10.1: Compounds and amounts of normal phase monolith

Compound	Abbreviation	Equiv.	Amount	Function
tetraethoxysilane	TEOS	1	0.4 ml	silica backbone
diethylamine	DEA	0.1	0.02 ml	catalyst
water	H_2O	4.9	0.16 ml	solvent
ethanol	EtOH	4.5	0.48 ml	solvent

Further improvements were made by adding a porogen, cetyltrimethylammonium bromide and a drying control chemical agent, dimethylformamide. The amounts are shown in the following table.

Table 10.2: Additional Chemicals for the normal phase monolith

Compound	Abbreviation	Equiv.	Amount	Function
cetyltrimethyl-ammonium bromide	CTAB	0.02	0.012 g	porogen
dimethylformamide	DMF	0.6	0.08 ml	drying control chemical agent

The amino functionalized monolith did not need any additional catalyst as the APTES initiated the polymerization. Amounts are shown in the following.

Table 10.3: Compounds and amounts of amino functionalized monolith

Compound	Abbreviation	Equiv.	Amount	Function
tetraethoxysilane	TEOS	1	0.223 ml	silica backbone
triethoxy(octyl)silane	C8-TEOS	1.4	0.300 ml	reversed phase mode
3-aminopropyl-triethoxysilane	APTES	0.5	0.050 ml	catalyst, amino groups
cetyltrimethyl-ammonium bromide	CTAB	0.04	15 mg	porogen
dimethylformamide	DMF	1.3	0.200 ml	drying control chemical agent
water	H_2O	3.5	0.063 ml	solvent
ethanol	EtOH	6	0.525 ml	solvent

The monolith was prepared with and without the addition of DMF.

The reversed phase monolith could be prepared in a one step and a two-step method. In the two-step approach, a silica backbone with the amounts of Table 10.1 was prepared and the alkyl groups were added by pumping a solution of octadecyltrichlorosilane (25 wt% in toluene) to give a C_{18}-functionality or of octyltrichlorosilane (25 wt% in toluene) to give C_8-functionality through the capillary.

The one step approach included mixing of all components except the catalyst for one hour at 60°C. The amounts are shown in Table 10.4.

Table 10.4: Compounds and amounts of the one step approach for the reversed phase monolith

Compound	Abbreviation	Equiv.	Amount	Function
tetraethoxysilane	TEOS	1	0.09 ml	silica backbone
triethoxy(octyl)silane	C_8-TEOS	0.4	0.05 ml	reversed phase mode
water	H_2O	1.4	0.01 ml	solvent
hydrochloric acid 0.5 N	HCl	0.3	0.01 ml	solvent, catalyst
methanol	MeOH	11	0.180 ml	solvent
diethylamine	DEA	0.5	0.02 ml	catalyst

For the planar test cell and the annular geometry the same mole equivalents as in the capillaries were used. The amounts were adapted depending on the mold needed.

As mentioned the monolithic material in the up-scaled devices was supported with the addition of silica particles. The amount was **15w%** of the precursor mixture. Before commercial Polygosil® particles were used, the particles were prepared in-house. In general, a normal phase monolith was prepared and crushed with a mortar. The particles were washed with methanol and added to the monolith.

Another approach was the preparation of Stöber particles.[148] In our case, we mixed methanol, saturated ammonium hydroxide and water together in a flask. While the solution was stirred on a magnetic stirrer, tetraethoxysilane was added dropwise. The formation of particles occurred within ten minutes. The particles obtained were smaller than 1 µm and the yield was low – only several mg in a solution of 10 ml. Therefore, this approach to prepare particles was neglected.

The C_8-C_8 capillaries were prepared with the precursor mixture mentioned in Table 10.4. The particles added in 15w% were Nucleosil®C_8 silica particles with a 5 µm diameter, produced by Macherey-Nagel GmbH & Co. KG, Düren, Germany.

The capillaries used in Figure 7.12 and Figure 7.13 were prepared with the precursor mixture shown in Table 10.4 **including** 0.02 equivalents of CTAB. In contrast to that the successional electrochromatograms were obtained with capillaries prepared with the same precursor mixture mentioned **without** additional CTAB. **No particles** were added to the precursor mixture used in the capillaries.

11. Characterization – details

To be able to understand all results given in the previous chapters, a summary of the sample abbreviation is given in this section. In general, sample descriptions can be derived from a systematic approach. Table 11.1 shows an overview of used classifications.

Table 11.1: Sample details of surface characterization

Sample name	Description
NP2	Normal phase monolith, number refers to the experiment
Amino 3	Amino functionalized monolith, number refers to experiment
C8_C81	C_8 functionalized monolith with C_8 functionalized particles embedded, number refers to experiment
C8 TEOS Mon	C_8 functionalized monolith, no CTAB added
C8 + PG rec	C_8 functionalized monolith with recycled PG particles embedded, 0.04 equivalent CTAB added
C8+27mg CTAB	C_8 functionalized monolith with addition of 27 mg CTAB
NP1+ctab	Normal phase monolith including 0.04 equivalents of CTAB
C8_1	C_8 functionalized monolith, 0.02 equivalents CTAB added
NP fct	Silica backbone, functionalized with C_8 groups in a second step
TMOS_1	Normal phase monolith, based on TMOS
27mg CTAB	C_8 functionalized monolith with addition of 27 mg CTAB
47mg CTAB	C_8 functionalized monolith with addition of 47 mg CTAB

12. Planar test cell – volume flow

A detailed list of the values obtained from the volume flow measurements is shown in Table 12.1.

Table 12.1: Number values of the volume flow measurement in 0.3 mm and 1 mm gap in the planar test cell; stationary phase: C_8-functionlized silica-based monolith including silica particles, mobile phase: Cit:MeOH = 1:29;

Voltage [kV]	0.3 mm gap, flow in [ml/h]	1 mm gap, flow in [ml/h]
5	6.31	21.75
8	9.38	34.80
10	13.50	43.50
12	16.37	52.21

13. Influence of different solvents on the monolithic material

To give an overview, which solvents can be used for chromatographic separation without endangering the monolithic material, Table 13.1 shows common eluents and their influence on the monolith.

Table 13.1: Eluents used in chromatography and their influence on the monolithic material

Eluent	Influence on monolith
methanol, ethanol	none, ok
n-hexane	none, ok
cyclohexane	none, ok
diethyl ether	none, ok
tetrahydrofuran	none, ok
acetone	none, ok
ethyl acetate	none, ok
isopropanol	none, ok
acetonitrile	none, ok
water	monolithic structure breaks
toluene	monolith swells
dimethylformamide	monolith swells
pyridine	monolithic structure breaks
dichloromethane	monolithic structure breaks
chloroform	monolith swells

14. Excursus

14.1. TMOS

Besides the pursuing of preparing monolithic materials on a TEOS basis, we also synthesized TMOS monoliths. Different recipes are presented in this section, referring to the comparison in the chapter Characterization.

The first attempt was to fill a capillary after Allen et al.[22] The amounts are shown in Table 14.1. All components expect ammonium hydroxide were mixed and stirred at 0°C for 45 min. The mixture was filled into the capillary and left for polymerization at 40°C overnight. Then, the capillary was flushed with ammonium hydroxide at 120°C for 60 min. This should ensure porosity of the monolith and give the possibility to functionalize the material in a second step.

Table 14.1: Recipe of TMOS monolith after Allen[22]

Compound	Abbreviation	Equiv.	Amount	Function
tetramethoxysilane	TMOS	1	0.5 ml	silica backbone
polyethylene glycole 10 000	PEG	0.004	0.1325 g	porogen
acetic acid 0.01 M	AA	0.6	0.1250 ml	solvent
ammonium hydroxide 0.01 M	NH_4OH		-	porogen

In our case, the silica backbone prepared was not porous in the first place. Therefore, a second TMOS monolith was prepared.

The second synthesis procedure is adapted from Tanaka et al.[149] The same components as in the previous recipe are stirred for 30 min at 0°C, filled into a mold and left for polymerization at 40°C for 24 hours. The capillary is washed with ammonium hydroxide for 3 hours at 120°C and dried at 330°C for 25 hours. The amounts are shown in Table 14.2.

Table 14.2: Recipe of TMOS monolith after Tanaka[149]

Compound	Abbreviation	Equiv.	Amount	Function
tetramethoxysilane	TMOS	1	4 ml	silica backbone
polyethylene glycole 10 000	PEG	0.004	1.06 g	porogen
acetic acid 0.01 M	AA	6.5	10 ml	solvent
ammonium hydroxide 0.01 M	NH_4OH		-	porogen

The same problem as in the first approach occurred. At first, the monolith was not permeable; after drying at elevated temperatures, the monolith shrunk significantly.

The third approach included a pore reagent from the beginning, namely urea. Due to the development of ammonia while heating the mixture, pores are formed. The components are shown in Table 14.3. The authors[31] mix all substances together and stir them for 45 min at 0°C. Then, the solution is filled into a capillary and left for polymerization at 40°C overnight. The next day, the capillary is dried at 120°C for 3 hours and again left at 330°C for 25 hours.

Table 14.3: Recipe of TMOS monolith after Motokawa[31]

Compound	Abbreviation	Equiv.	Amount	Function
tetramethoxysilane	TMOS	1	4 ml	silica backbone
polyethylene glycole 10 000	PEG	0.003	0.88 g	porogen
acetic acid 0.01 M	AA	6.5	10 ml	solvent
urea		0.5	0.9 g	porogen

Again, the material shrunk significantly and was not appropriate for our experiments.

14.2. Organic monolithic material

A further possibility to prepare monolithic material is the application of organic monomers. We followed a synthesis procedure of Schmid et al.[135] The capillary had to be pretreated with γ-methacryloxypropyltrimethoxysilane to introduce double bonds to the silica surface for covalent binding of the monolith to the inner walls. All components listed in Table 14.4 besides the polymerization starters were mixed and sonicated for 5 min. After TEMED and APODS were added, the solution was filled into a capillary and left for poylmeriaztion for 12 hours. In our case, we did not add any functionalized particles in contrast to the authors mentioned. Therefore, the obtained monolith shrunk and was not permeable and could not be used for our purpose.

Table 14.4: Recipe of organic monolith after Schmid[135]

Compound	Abbreviation	Equiv.	Amount	Function
piperazine diacrylamide	PAA	1.0	0.022 g	cross-linker
methacrylamide	MAA	1.9	0.018 g	monomer
ammonium sulfate	AS	0.7	0.01 g	medium
vinyl sulfonic acid 25%	VSA	0.3	0.012 ml	charge providing agent
TRIS buffer (50mM)	TRIS	0.2	0.4 ml	solvent
tetramethylenediamine	TEMED	0.5	0.005 ml	polymerization starter
ammonium peroxodisulfate	APODS	0.1	0.002 g	polymerization starter

In a second attempt, 15w% silica particles made from a NP TEOS monolith were added to enhance permeability. This could be achieved; however, the monolith shrunk again. Therefore, this approach was not further pursued.

15. Practical work – abbreviations

a	experimentally derived constant for Knox equation
A	eddy diffusion factor
ACN	acetonitrile
APIs	active pharmaceutical ingredients
APODS	ammonium peroxodisulfate
APTES	3-aminopropyltriethoxysilane
a_S	specific surface area
AS	ammonium sulfate
A_x	cross-sectional adsorbate area
b	experimentally derived constant for Knox equation
B	longitudinal diffusion factor
BET	Brunauer-Emmett-Teller
BJH	Barrett-Joyner-Halenda
C	BET constant; mass transfer resistance factor
c	concentration; experimentally derived constant for Knox equation
CAEC	continuous annular electrochromatography
c_m	concentration of the solute in the mobile phase
c_s	concentration of the solute in the stationary phase
C_8-TEOS	triethoxy(octyl)silane
CE	capillary electrophoresis
CEC	capillary electrochromatography
Cit	citrate buffer
CPTES	3-cyanopropyltriethoxysilane
CTAB	cetyltrimethylammonium bromide
D	pore mean diameter
d_c	column diameter
DEA	diethylamine
d_f	film thickness on stationary phase
D_M	diffusion coefficient of solute in the mobile phase

DMF	dimethylformamide
D_S	diffusion coefficient of solute in the stationary phase
d_p	particle diameter
D_w	diameter of the pore in Washburn equation
E	Giddings constant; electric field
EOF	electroosmotic flow
EtOH	ethanol
F	feed
FTIR	Fourier transform infrared spectroscopy
F_v	volume flow-rate
h	reduced plate height
H	plate height
H_2O	water, deionized
HCl	hydrochloric acid
HPLC	high performance liquid chromatography
HTPLC	high performance thin layer chromatography
k’	capacity ratio
K	distribution coefficient
K_F	Freundlich constant
K_H	Henry constant
K_L	Langmuir constant
L	length of the column
LC	liquid chromatography
M	molecular mass of the adsorbent
MAA	methacrylamide
m.e.	mol equivalents
MeOH	methanol
MPTMS	3-mercaptopropyltrimethoxysilane
n^a	gas amount absorbed at the relative pressure p/p^0
n^a_m	monolayer capacity
N_a	Avogadro constant

NaOH	sodium hydroxide
N	number of theoretical plates
OPLC	overpressured layer chromatography
p	pressure
P	partial pressure of adsorptive gas
p^0	saturation pressure
P_C	capillary pressure
PAA	piperazine diacrylamide
PAHs	poylcyclic aromatic hydrocarbons
PEC	planar electrochromatography
PEEK	polyether ether ketone
PEG	polyethylene glycol
PLOT	porous layer open tubular
PPEC	pressurized or closed planar electrochromatography
PSD	pore size distribution
q	constant; charge of the analyte
r	radius
r_h	hydraulic radius
RP	reversed phase
R_S	resolution
RSD	relative standard deviation
S	specific surface area
SEM	scanning electron microscope
SDS	sodium dodecyl sulfate
SMB	simulated moving bed
t	time
t_0	retention time of an unretained solute
TLC	thin layer chromatography
TMB	true moving bed
t_r	retention time
t_r'	corrected retention time

t_T, t_N, t_A	retention time of the tracer thiourea(Thio), naphthalene (Naph), anthracene (Anthr)
TEMED	tetramethylenediamine
TEOS	tetraethoxysilane
TLC	thin-layer chromatography
TMOS	tetramethoxysilane
tpv	total pore volume
TRIS	tris(hydroxymethyl)aminomethane
u	velocity of mobile phase
u_{eo}	electroosmotic flow
v	reduced velocity, velocity induced by electric field
V_0	dead volume
V_m	volume of the mobile phase
VMD	volume mean diameter
V_P	specific pore volume
V_r	retention volume
V_r'	corrected retention volume
V_s	volume of the stationary phase
V_S	volume of the pure solid
VSA	vinyl sulfonic acid 25%
W	band width
w_A, w_N	width of the anthracene and naphthalene peak at half height
w_b	width of the peak at the base
w_h	width of the peak at half height
X_{mean}	mean density value
α	selectivity
$\gamma_{(LV)}$	surface tension of the pore liquid at the liquid vapor interphase
Γ	adsorption function
γ	surface tension of mercury; constant considering hindrance factor of stationary phase
δ	thickness of the double layer

ε_0	permittivity through vacuum
ε_e	external porosity
$\varepsilon_P = \varepsilon_i$	internal porosity
ε_r	dielectric constant of the mobile phase
ε_t	total porosity
η	viscosity
Θ	contact angle of the liquid; surface coverage; angular coordinate
λ	packing uniformity factor
μ	electrophoretic mobility
μ_{EOF}	electroosmotic mobility
ξ	zeta-potential
ρ	density
σ	surface charge of the stationary phase
σ^2	standard deviation of mean density value, also RSD
ω	angular velocity

D) THEORETICAL APPROACH

16. Theoretical aspects of chromatography and simulation

As already mentioned in the introduction in part A, diffusion is a major aspect in the adsorption process of chromatographic separations. The beginnings of these considerations were called macroscopic models, which included deterministic equations of the necessary mass transport processes that could not be solved analytically.[150] Therefore, simplifying assumptions had to be made. The main idealization was the instantaneous equilibrium between mobile and stationary phase. In the relation to this Van Deemter found four classifications for chromatography: linear ideal, linear non-ideal, non-linear ideal and non-linear non-ideal.[63] Guiochon gives a closer description on the four distinctions.[35] In linear chromatography, the concentrations of a substance in the mobile and the stationary phase are proportional and the retention times are independent of the composition of the feed and the amount of the sample. In non-linear chromatography, the equilibrium isotherm of any compound depends on the other compounds in the sample and is therefore not linear. Whereas linear chromatography can be used for almost all analytical applications, non-linear chromatography accounts for preparative operations. In ideal chromatography, the axial dispersion is negligible and therefore, the rate of mass transfer kinetics is infinite. Accordingly, all the band profiles are only controlled by the thermodynamics of the phase equilibria. Ideal linear chromatography is a very simplified model and therefore utilized in practice whereas non-ideal linear chromatography is a powerful tool to have an insight on the influence of the thermodynamics on the band profiles. In non-ideal chromatography the column efficiency has a finite measurable value.

Reasonable solutions of these models can only be found for linear adsorption isotherms; therefore, two different approaches are stated for linear non-ideal chromatography. First, the plate theory considers the column segmented into different stages, where in every stage the equilibrium is reached. The plate theory is explained in detail in the chapter Introduction.

Second, the general rate model considers the column as a continuous piece and different transport processes like diffusion are incorporated. A complex array of kinetic equations is implemented. A detailed explanation is again given in the chapter Introduction. In close relation to this, the lumped kinetic model takes only one kinetic step into account – the rate determining one – whereas contributions of all other kinetic processes are lumped into the rate constant.[151] Further classifications can be made: the reactive model ignores the axial dispersion and the mass transfer kinetics are neglected due to their speed. The rate constants of adsorption and desorption are considered finite and are given by the second order Langmuir isotherms. This approach was developed by Henry Thomas.[152] An extension of the Thomas model is the reaction-dispersive model, where one mass balance and one kinetic equation are used. In contrast to the previous model, the solution has to be numerical. The transport-dispersive model on the other hand assumes very fast rates of adsorption and desorption processes and low mass transfer kinetics. In linear chromatography, the reactive-dispersive and the transport dispersive model are equivalent.[153]

Next to the classical models stochastic models were developed. In this molecular dynamic approach, every single molecule is tracked and the process describes the random movement along the chromatographic column.[154] The first to introduce this model for chromatography were Giddings and Eyring.[155] In their approach, the molecules travelling along the column run through random adsorption and desorption processes following a Poisson distribution.[153] The Monte Carlo method was used to describe either linear chromatography with the stochastic approach as well as non-linear chromatography.[156] The comparison with macroscopic models showed that the Monte Carlo simulations of non-linear chromatography equate to the Thomas model mentioned previously when dispersion in the mobile phase is neglected.[157] The authors demonstrated that the number of mass transfer units of the reactive-dispersion model is equivalent to the average number of adsorption-desorption steps of the stochastic approach.

The Monte Carlo method was developed after the Second World War in the 20th century. Although there had been experiments to take model sampling as approaches for problem solving before, the introduction of computers gave rise to the increasing research activity in this section.[158] Landau and Binder stated that with Monte Carlo methods the change of a

property of a system does not follow a given way but rather develops in a stochastic manner by generating random numbers.[159] More specifically, the probability of finding a certain configuration, $P_{NVT,}$ in this chain of random configurations, the Markov chain, is given by the Boltzmann equation:

$$P_{NVT}(\Gamma^N) \infty \exp[-\beta U(\Gamma^N)] \quad (36)$$

where $\beta=1/(k_BT)$, k_B is the Boltzmann constant and U is the intermolecular potential.[160]

In chromatography, as already describe by Dondi[156], the process includes following a molecule along its way through the column, where it can be adsorbed by the stationary phase and desorbed after a certain time step. The adsorption and desorption processes succeed a stochastic distribution and the elution peak can be seen as a histogram of the distribution of column residence time. Through Fourier transformation the Gaussian curve similar to the curves of the chromatogram is obtained.

Our approach is based on McGuffin et al., who studied the kinetic effects of the partition of molecules between the mobile and the stationary phase.[161,162] The main goal of this program is to identify the appropriate stationary phase for a given separation problem. Furthermore, the sequence of the substances eluted can be predicted. Details on the program are given in the following chapter.

17. Simulation approach

As explained in the previous part, our simulation approach is based on the Monte Carlo theory. Therefore, the molecules in the simulation are moving in a random manner, based on the Brownian motion. They can be transported through the column due to pressure or voltage. These possibilities can be adjusted up front. To give an overview of the operational sequence of the program, the flow sheet of the program is shown in Figure 17.1. The program presented is based on McGuffin et al.[162,163]

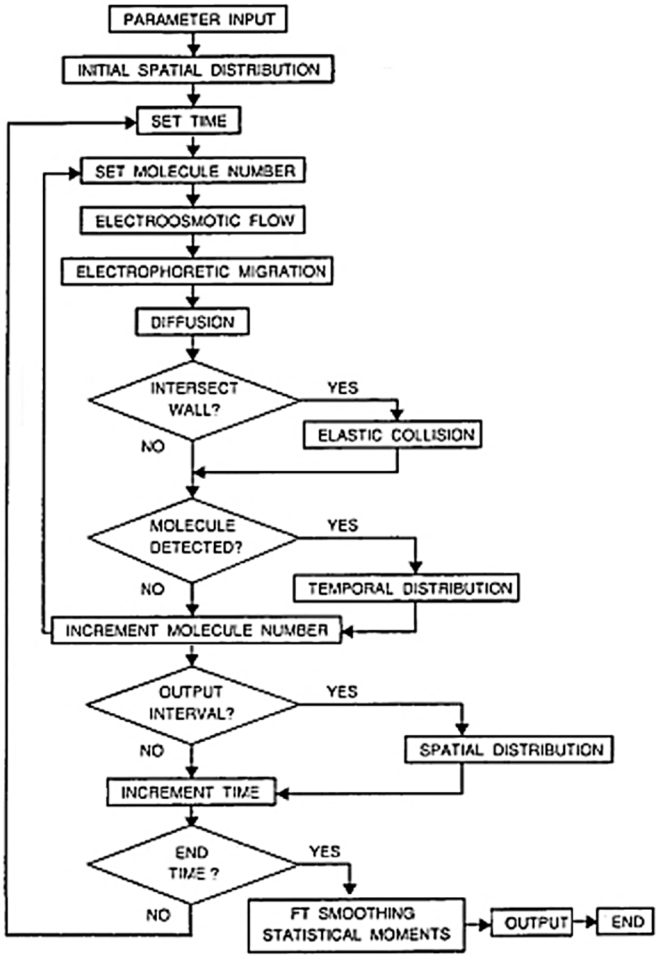

Figure 17.1: Flow sheet of the program, adapted from[162]

The parameters used in the program are grouped into system parameters, molecular parameters and computational parameters. The parameters are listed in Table 17.1. These parameters have to be defined to be able to perform the simulation. Details to the single values are given in the different sections.

Table 17.1: Simulation parameters

System parameters	
Radius of fluid phase	R
Length of fluid phase	L
Mean velocity of the fluid phase	v_0
Depth of surface phase	d_s
Pressure	P
Temperature	T_0
Electric field strength	E
Molecular parameters	
Diffusion coefficient	D_f, D_s
Distribution coefficient	K
Computational parameters	
Number of molecules	N
Time increment	t
Total simulation time	T

Besides the already specified algorithms used for transportation through the column, several other processes were implemented into the program. The molecules cover a certain distance in one time step, and the interactions with the wall or the stationary phase are considered. With every new time step, the process is repeated. The underlying transportation equation can be chosen by the operator. The retention of the molecules in the stationary phase is simulated with a probability distribution between the stationary and the mobile phase. Details are shown later in this chapter.

The initial distribution of the molecules, i.e. at the top of the column, has to be determined at the beginning. The molecules can be placed in a Gaussian, a random or rectangular distribution.

17.1. Detailed mathematical approach and validation

The different steps of the simulation program[xxxiii] are explained in detail and validation results are presented.

17.1.1. Positioning

In the beginning, the molecules have to be set in their starting positions and therefore, three types of distributions were used. These are shown in the following figures.

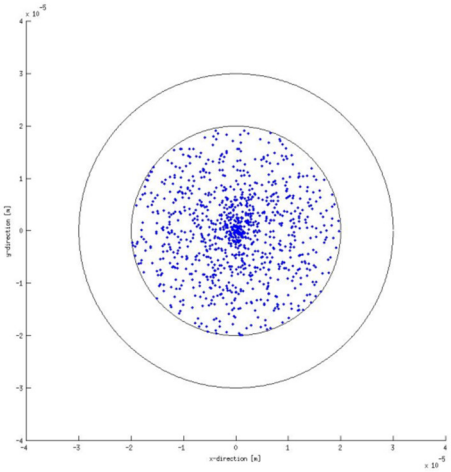

Figure 17.2: Random positioning of molecules

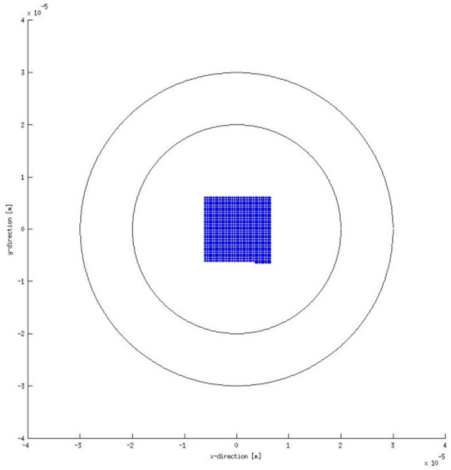

Figure 17.3: Rectangular positioning of molecules

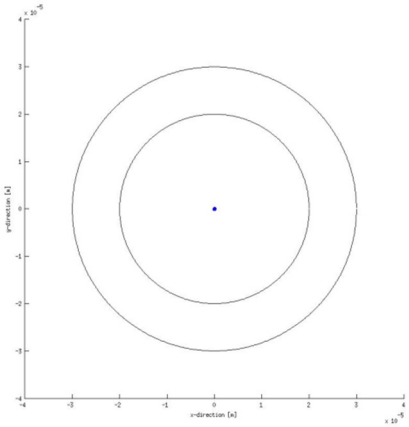

Figure 17.4: Gaussian positioning of molecules

[xxxiii] Basic program generated by Michael C. Gruber, TU Graz

17.1.2. Diffusion

After positioning, the algorithms for motion have to be implemented into the program. Three molecules, following the Brownian motion were tracked. The result is shown in Figure 17.5.

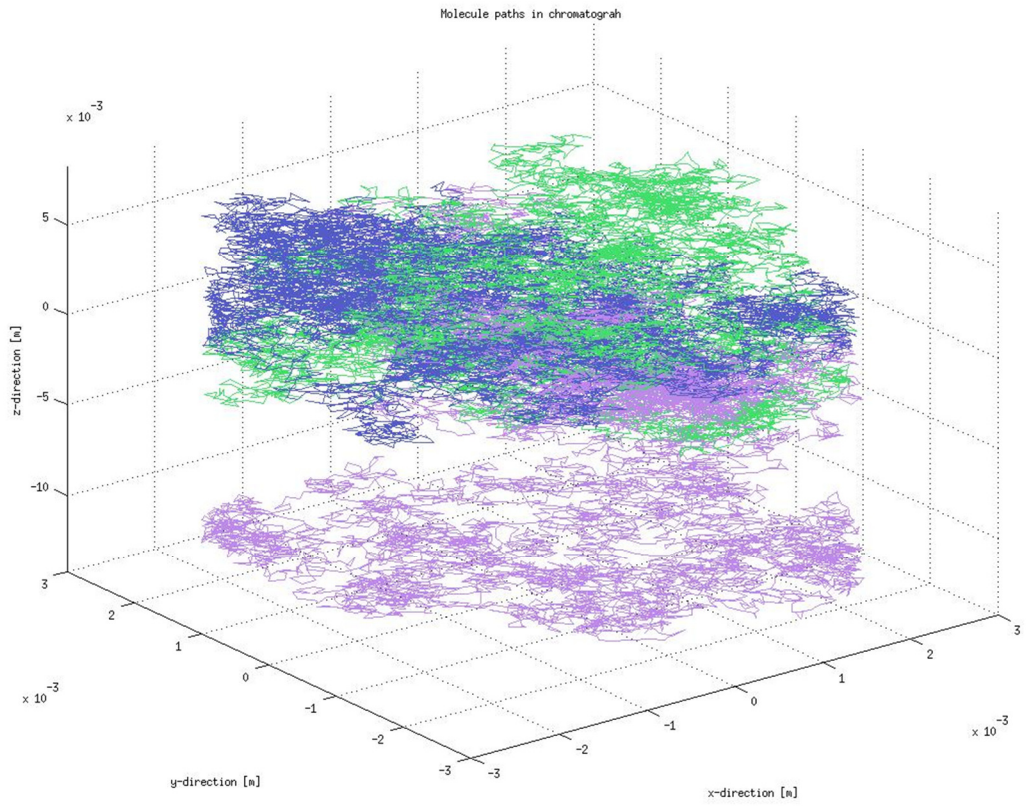

Figure 17.5: Tracked movement of three molecules

For diffusion, the Smoluchowski-Einstein equation was used (37).

$$\rho = \left(6D_{s,f}t\right)^{\frac{1}{2}} \qquad (37)$$

ρ is the radial distance travelled by a molecule in the time step t, D_s is the diffusion coefficient in the solid phase and D_f is the diffusion coefficient in the fluid phase.

For validation, the values calculated by the algorithm are compared to the theoretical results of the following equation:

$$\sigma^2 = 2D_f t, \quad z = 0 \qquad (38)$$

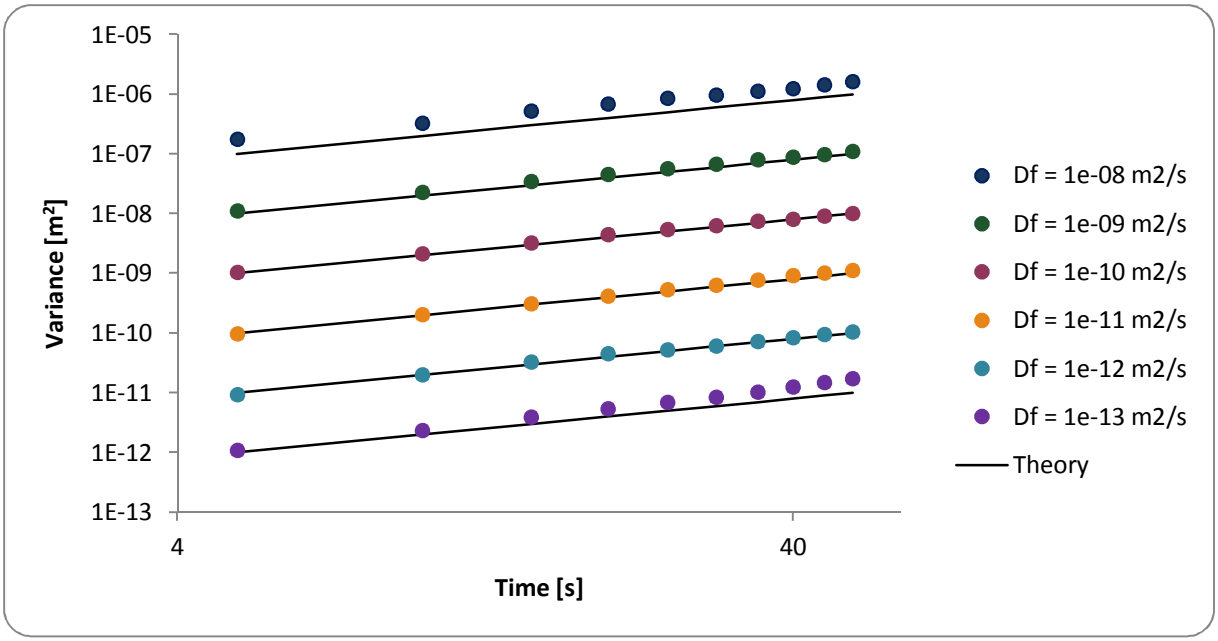

Figure 17.6: Validation of the diffusion algorithm by comparison of the variance with the theoretical prediction (see equation 3). Simulation conditions: N = 750, R = 2.0e-05 m, t_s = 1.0e-02 s;

Figure 17.6 shows the comparison of values simulated by the program (circles) and the theoretical prediction (straight line). The agreement is good within the range usually found in liquid chromatography, i.e, 1.0e-09 – 1.0e-11 m^2/s.[164]

17.1.3. Convection

As mentioned, the mean velocity, v_0, of the mobile phase in a cylindrical geometry can either be determined by the Hagen Poiseuille equation (39) – in a pressure driven system – or with the Smoluchowski equation (40) – in a system driven by voltage.

$$v_0 = \frac{R^2 P}{8\eta L} \quad (39)$$

$$v_0 = \frac{z_a D_f}{T_0 k_B} E \quad (40)$$

R is the radius of the capillary, P is the pressure, η is the viscosity and L is the length of the fluid phase. Furthermore, z_a is the charge of the electrolyte, T_0 is the absolute temperature, k_B is the Boltzmann constant, E is the electric field and D_f is the diffusion coefficient for the fluid phase, respectively.

The velocity profile in the cylindrical profile can be calculated with the Taylor-Aris equation (41), where r corresponds to the radius of the particle

$$v = 2v_0\left[1-\left(\frac{r}{R}\right)^2\right] \qquad (41)\,.$$

The validation for the convection algorithm in pressure induced flow could therefore be compared and validated via equation (41).

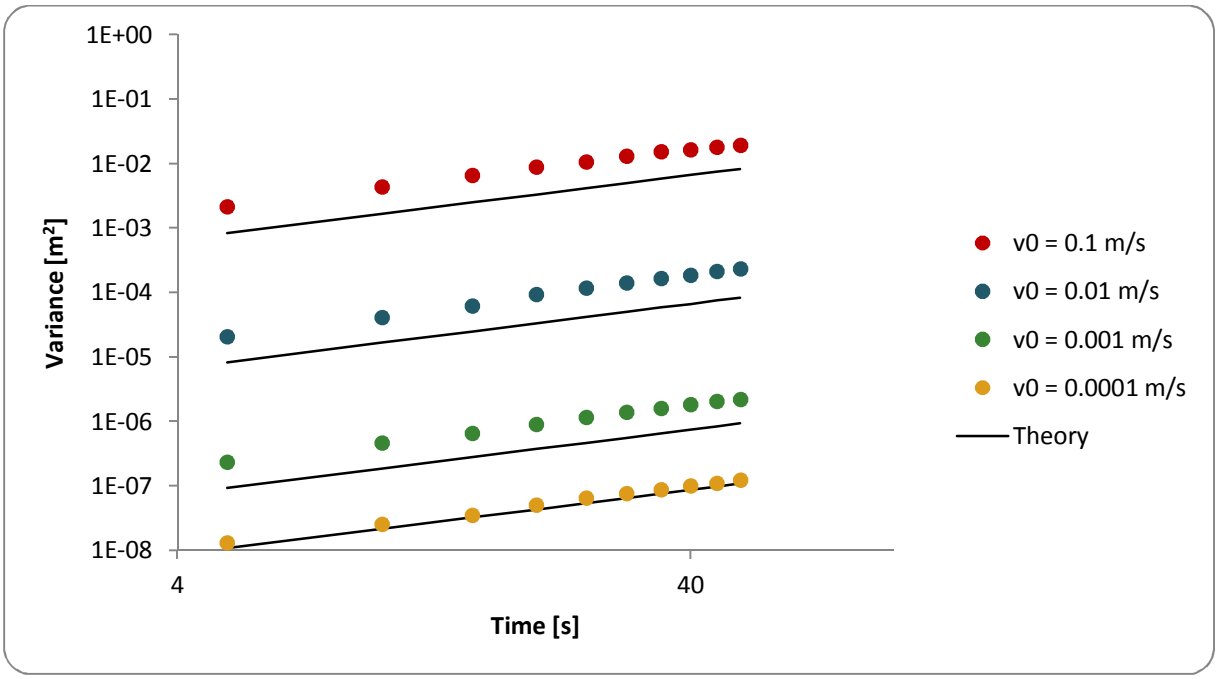

Figure 17.7: Validation of the convection algorithm with theory. $\sigma^2=2D_fT + R^2v_0^2T/(24D_f)$[162]; Simulation conditions: N = 750, R = 2.0e-05 m, t_s = 1.0e-02 s;

Figure 17.7 does not show the best agreement with higher velocities; however, with a velocity of v_0=0.0001 m/s an excellent agreement could be obtained. The reason for this discrepancy could be higher back pressures that were not considered in the program.

Moreover, the velocity can be adjusted with voltage. To calculate the velocity, the Rice-Whitehead equation is used:

$$v = v_0\left(1-\frac{I_0(\kappa r)}{I_0(\kappa R)}\right) \qquad (42)$$

where κ^{-1} is the Debye length and I_0 is the zero order modified Bessel function of the first kind. The mean velocity, v_0, can be calculated with the Helmholz-Smoluchowski equation (43)

$$v_0 = \frac{-\varepsilon\varepsilon_0\xi V}{\eta L} \qquad (43)$$

where ε is the permittivity of the fluid phase and ε_0 is the permittivity of vacuum, η is the viscosity of the fluid phase, V is the voltage and ξ is the zeta potential.

The zeta potential on silica surfaces in contact with an aqueous buffer is in the range of 100 to 150 mV.[165] The validation of the electrophoretic migration, which compares the deviation in the program to equation (37), is shown in Figure 17.8.

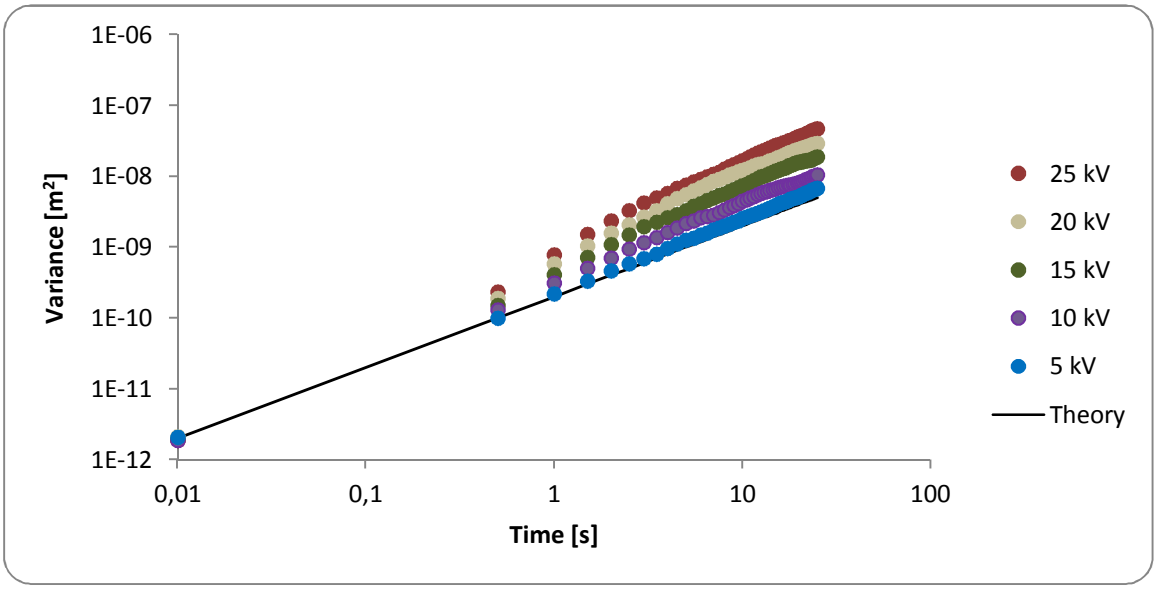

Figure 17.8: Validation of electrophoretic migration algorithm with equation (38); Simulation conditions: N = 750, R = 2.0e-05 m, t_s = 1.0e-02 s; D_f= 1.0e-10 m^2/s;

The agreement of theory and simulation is good with low voltage applied. However, when the voltage is increased, the program deviates from the theory. This can be due to an increased mobility of the solutes and therefore higher deviation values compared to the theory.

17.1.4. Retention

The retention is implemented into the system via a probability function. The possibility of the transfer of the molecules from mobile to stationary phase or vice versa is given by

$$P_{f-s} = K\left(\frac{D_s}{D_f}\right)^{\frac{1}{2}} \text{ and } P_{s\text{-}f} = 1 \qquad (44)$$

which indicates the transfer of the molecule from fluid to solid phase and

$$P_{f-s} = K^{-1}\left(\frac{D_f}{D_s}\right)^{\frac{1}{2}} \text{ and } P_{f\text{-}s} = 1 \qquad (45)$$

which indicates the transfer from solid to fluid phase, respectively.

K is the distribution coefficient in both cases. Depending on the diffusion and the distribution coefficient, a probability is calculated in the beginning and the probability functions are plotted.

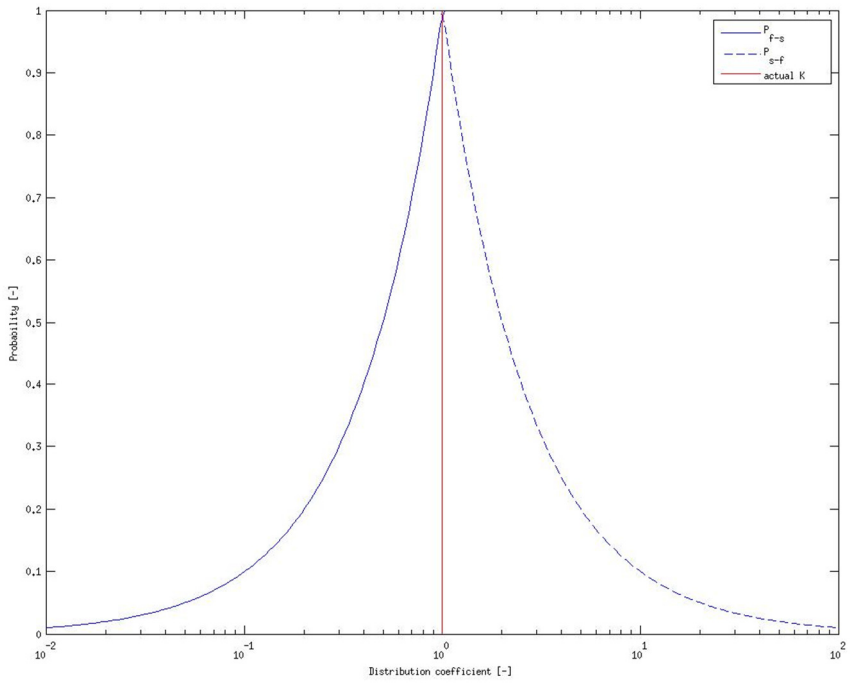

Figure 17.9: Probability function with two identical diffusion coefficients and K=1

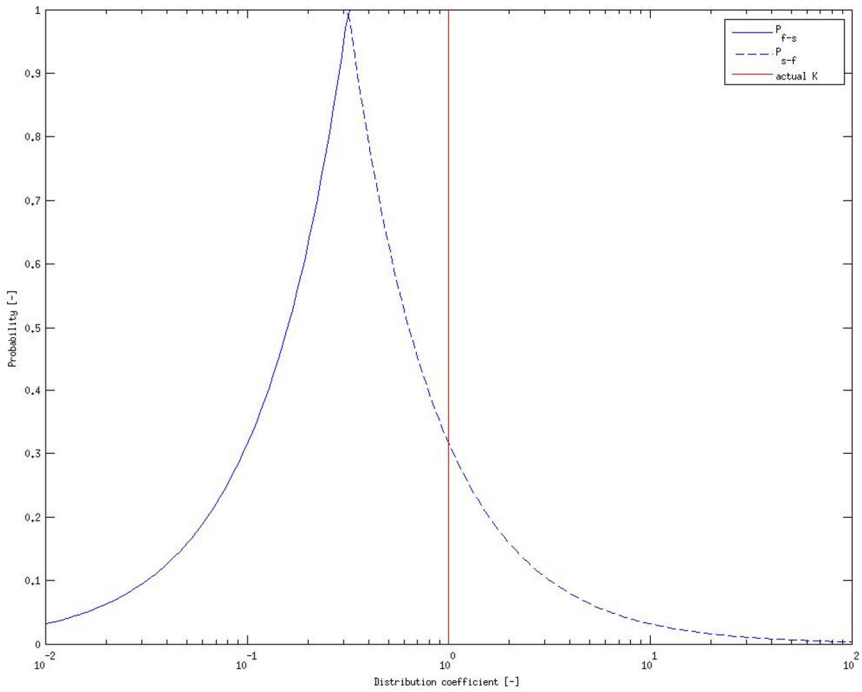

Figure 17.10: Probability function where D_s is higher than D_f. K=1

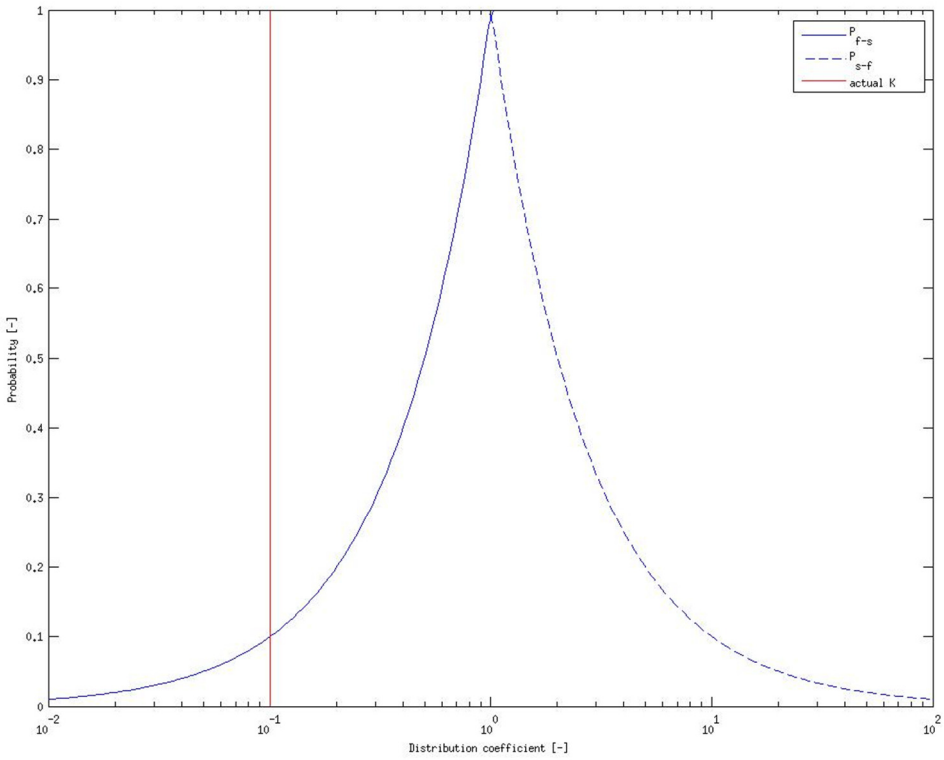

Figure 17.11: Probability function with D_s=D_f and K=0.1

The preceding figures should demonstrate how the initial parameters influence the simulation. Depending on the properties of the analytes different aspects have to be taken into account. Therefore, the determination of these properties is of major importance.

17.2. Output of the program

The main output of the program is the spatial distribution of the molecules over time. The molecule population is summed up in discrete elements and smoothed by Fourier transformation. An example is shown in Figure 17.12.

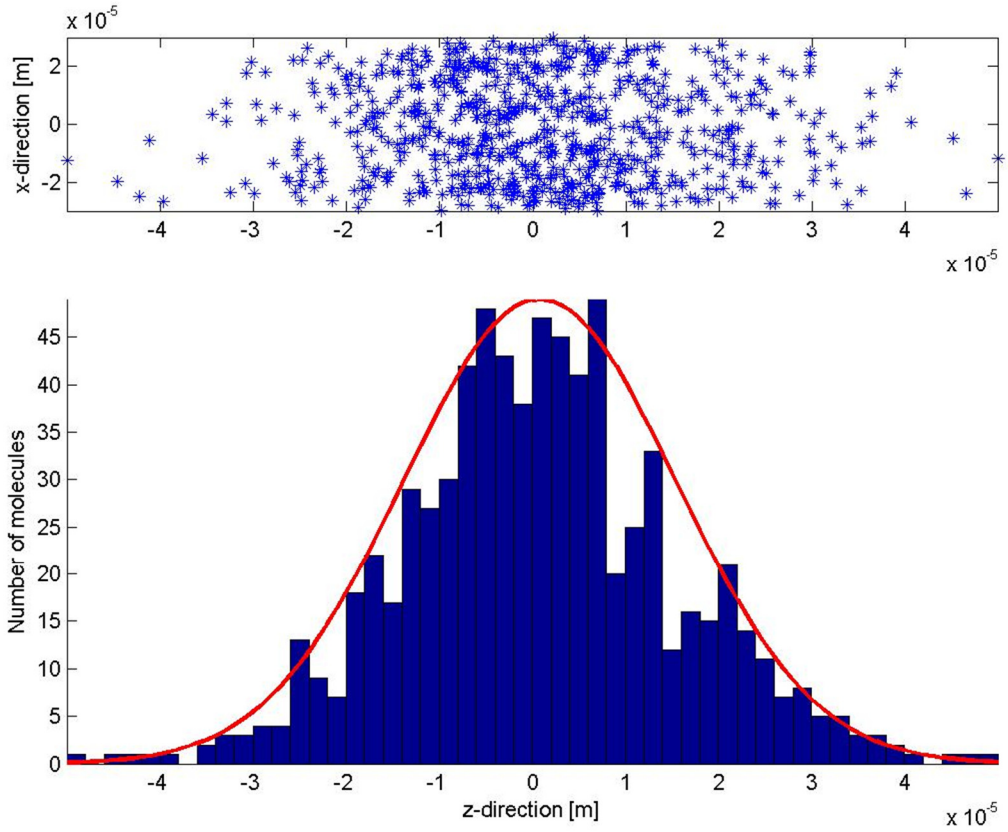

Figure 17.12: Spatial distribution of the molecules at the beginning of the simulation in the computational domain (top) and the segmented and smoothed zone profile along the z axis.

The general approach includes the distribution of a solute X between the solid and the fluid phase. Therefore, rate constants can be calculated. Equation (46) shows the relationships of the solute in the two phases.

$$X_f \underset{k_{s\text{-}f}}{\overset{k_{f\text{-}s}}{\rightleftharpoons}} X_s \qquad (46)$$

In equilibrium, the distribution coefficient K is proportional to the ratio of the first order rate constants, $k_{s\text{-}f}$ and $k_{s\text{-}f}$ and further is related to the molecules, N, in the solid and the fluid phase, see Equation (47). V_s and V_f are the volumes of the solid and the fluid phase, respectively.

$$\frac{KV_s}{V_f} = \frac{k_{f-s}}{k_{s-f}} = \frac{N_s}{N_f} \qquad (47)$$

Until the equilibrium is reached, the situation can be described by a kinetic model. The approach is shown in Equation (48).

$$\frac{d(N_f)}{dt} = k_{s-f}N_s - k_{f-s}N_f \qquad (48)$$

In the beginning, all molecules start from the fluid phase, therefore, the solution for the kinetic model equation is shown in (49).

$$\frac{(N_f)_t}{(N_f)_0} = \frac{k_{s-f} + k_{f-s}\exp[-T(k_{f-s} + k_{s-f})]}{k_{f-s} + k_{s-f}} \qquad (49)$$

This equation can predict the rate constants if the distribution is known and if the rate constants are known, the distribution can be calculated with the non-linear least square method at any given time. This is the main aspect of the program. The rate constants of the adsorption-desorption process are determined for any given separation problem. The output of the program is shown in Figure 17.13.

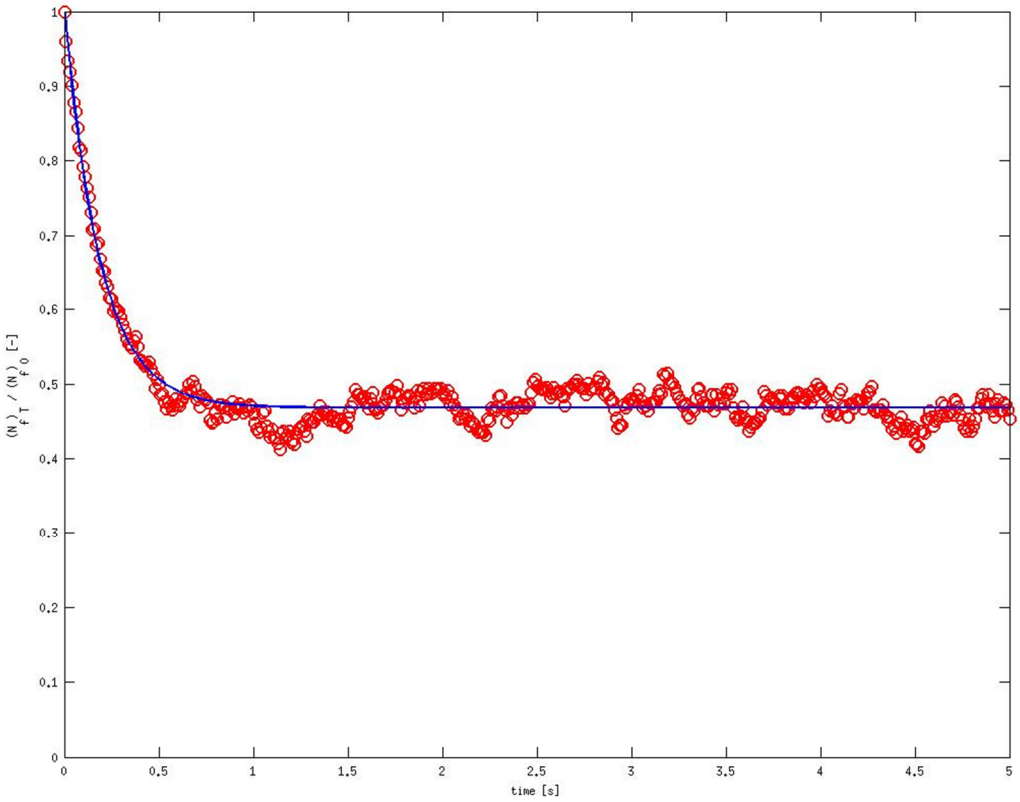

Figure 17.13: Determination of equilibrium rate of the solute from the fluid phase as a function of time, the red circles are the values of the simulation; the solid curve is fitted with non-linear regression analysis

Figure 17.13 shows an example of the equilibrium distribution of solutes between the solid and the fluid phase with the rate constants $k_{s\text{-}f}$ = 2.2804 s^{-1} and $k_{f\text{-}s}$ = 2.5781 s^{-1}. The velocity was calculated with the Hagen-Poiseuille equation and resulted in 9.025e-03 m/s. The number of molecules was 750, K = 1.0, D_f = 3.5e-10 m^2/s and D_s = 1.8e-10 m^2/s.

17.3. Simulation of the test system anthracene/naphthalene

The main idea of the program was to simulate the separation of different substances. Therefore, the main properties of these substances have to be known. Our test system is a mixture of anthracene and naphthalene. The properties needed for the simulation are given in Table 17.2.

The diffusion coefficients used are based on the partition of the molecules in an octanol/water mixture and represent the reversed phase stationary phase.

Table 17.2: Properties of the test system anthracene/naphthalene

	Diffusion coefficient fluid, D_f [cm^2/s][xxxiv]	**Diffusion coefficient Solid, D_s [cm^2/s]** [xxxv]	**Distribution coefficient [-]**
Anthracene	$7.74 \cdot 10^{-06}$	$5.9 \cdot 10^{-06}$	4.5 [xxxvi]
Naphthalene	$7.50 \cdot 10^{-06}$	$6.0 \cdot 10^{-06}$	3.3 [xxxvii]

As already mentioned, two different modes of operation can be adjusted in the program, the pressure-driven flow or the electroosmotic flow. One has to consider that in experiments, capillaries of a micrometer diameter are usually used in capillary electrochromatography or ultra-high pressure devices due to the high backpressure. Furthermore, as already shown in Figure 17.13, the equilibrium is achieved after approximately one second. Therefore, the rate constants of the solutes are calculated after 2 seconds in the following. To underline this possibility, the determination of the equilibrium rates themselves is shown in comparison in the specific section.

17.3.1. Pressure-driven flow

A separation of the test system with the properties shown in Table 17.2 was simulated. The mobile phase was pushed through the system with a velocity of 0.0001 m/s, which corresponds to a pressure of 1108 Pa. The rate constants obtained with the program were k_{sf} = 1.6758 s^{-1} and k_{fs} = 8.2490 s^{-1} for anthracene and k_{sf} = 2.2856 s^{-1} and k_{fs} = 8.0084 s^{-1} for naphthalene. The equilibrium rates are compared in Figure 17.14. The separation of the substances can be shown in a chromatogram-like figure, where the mean value and the deviation of the molecules at the end of the simulations are compared, as shown in Figure 17.15. This separation was received after 200s.

[xxxiv] Data from http://www.depreportingsvcs.state.pa.us/ReportServer/Pages/ReportViewer.aspx?%2fCPP%2fChemicals
[xxxv] based on[166]
[xxxvi] Data from http://www.inchem.org/documents/icsc/icsc/eics0825.htm
[xxxvii] taken from: *REPORT ON CARCINOGENS, ELEVENTH EDITION,* http://ntp.niehs.nih.gov/ntp/roc/toc11.html

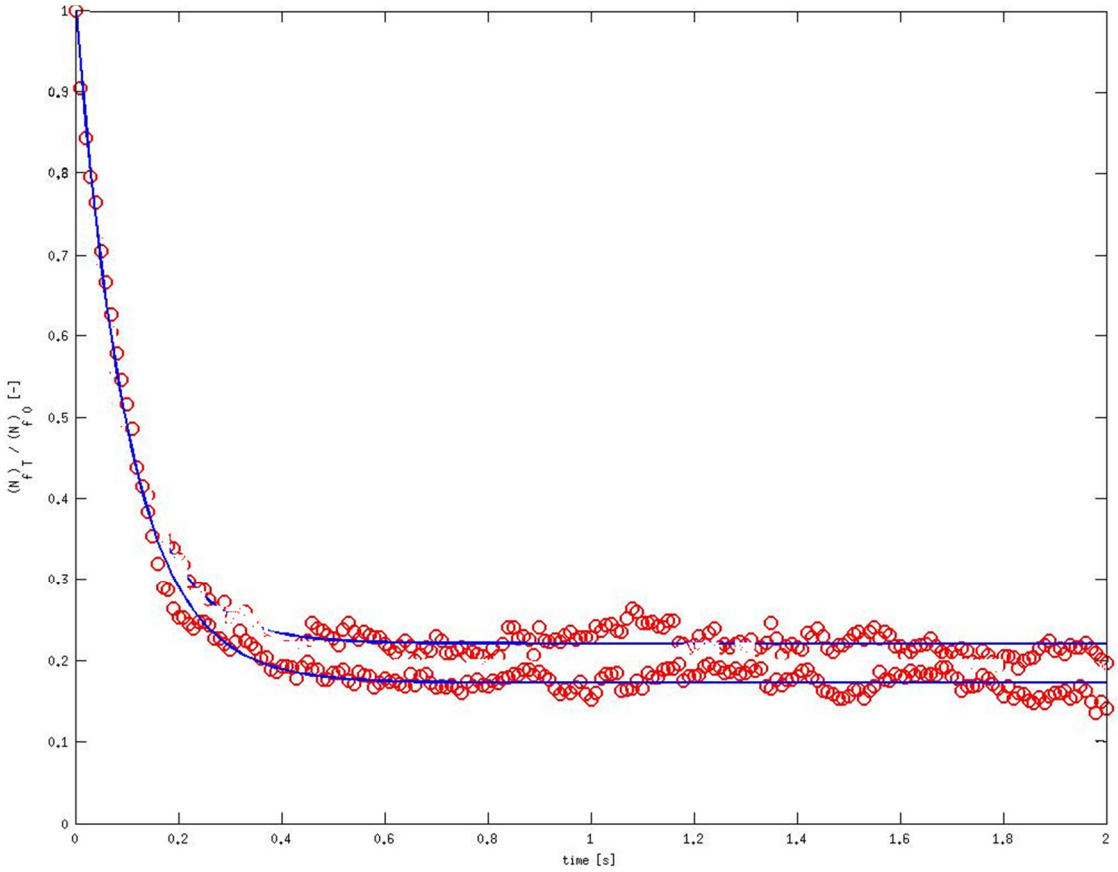

Figure 17.14: Equilibrium rates of naphthalene (top) and anthracene (bottom) from the fluid phase as a function of time, the red circles are the values of the simulation; the solid curve is fitted with non-linear regression analysis; v_0 = 0.0001 m/s.

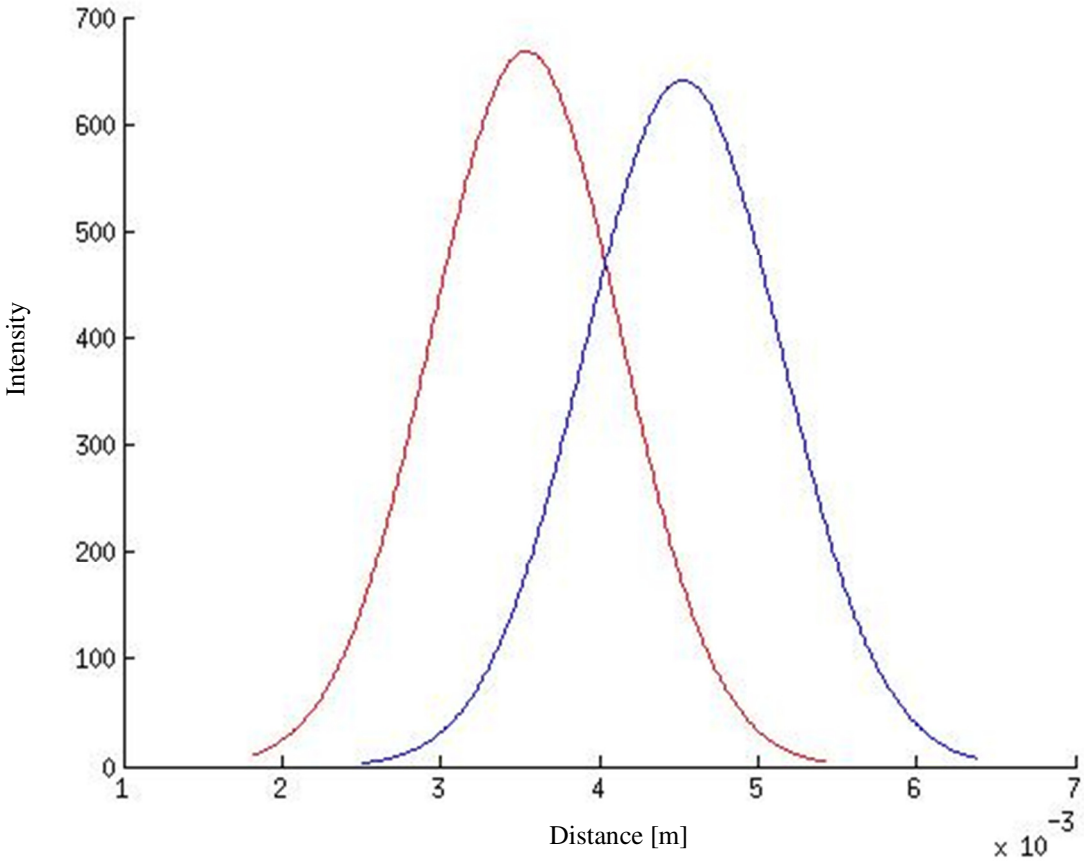

Figure 17.15: Solute zone profile of naphthalene (blue) and anthracene (red). Simulation parameters: Number of molecules N_a=750, N_n=750; radius of fluid phase R = 2.0e-05 m; depth of surface phase d_s = 1.0e-05 m; T = 200s; t = 1.0e-02s, v_0 = 0.0001 m/s;

In the next simulation, the velocity was increased to 0.001 m/s, which corresponds to a pressure of 11080 Pa. Figure 17.17 shows that the separation efficiency increases after 200s of simulation time. The equilibrium rates are shown in Figure 17.16. The rate constants for anthracene are k_{sf} = 1.7214 s^{-1} and k_{fs} = 8.9519 s^{-1} and for naphthalene k_{sf} = 1.3678 s^{-1} and k_{fs} = 8.3317 s^{-1}.

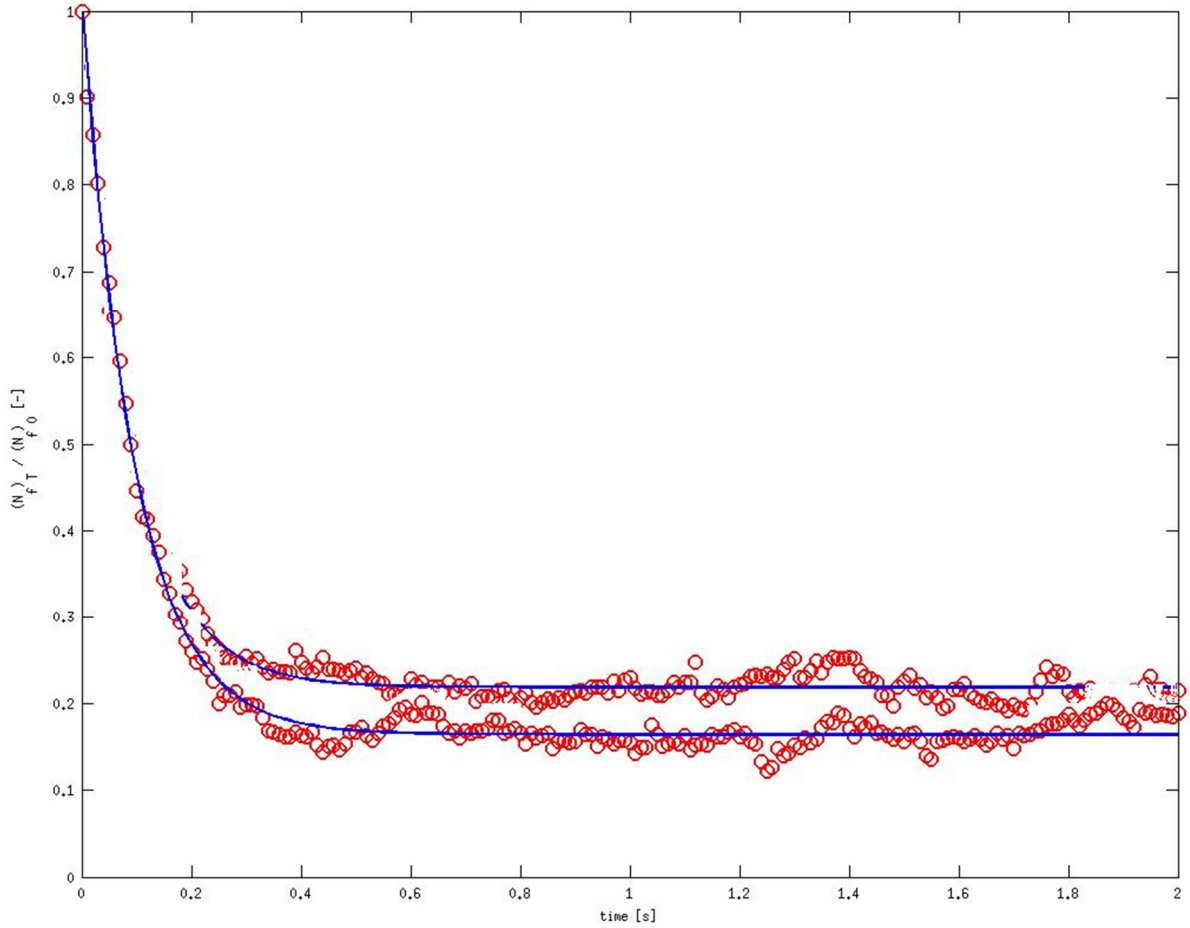

Figure 17.16: Equilibrium rates of naphthalene (top) and anthracene (bottom) from the fluid phase as a function of time, the red circles are the values of the simulation; the solid curve is fitted with non-linear regression analysis; v_0 = 0.001 m/s.

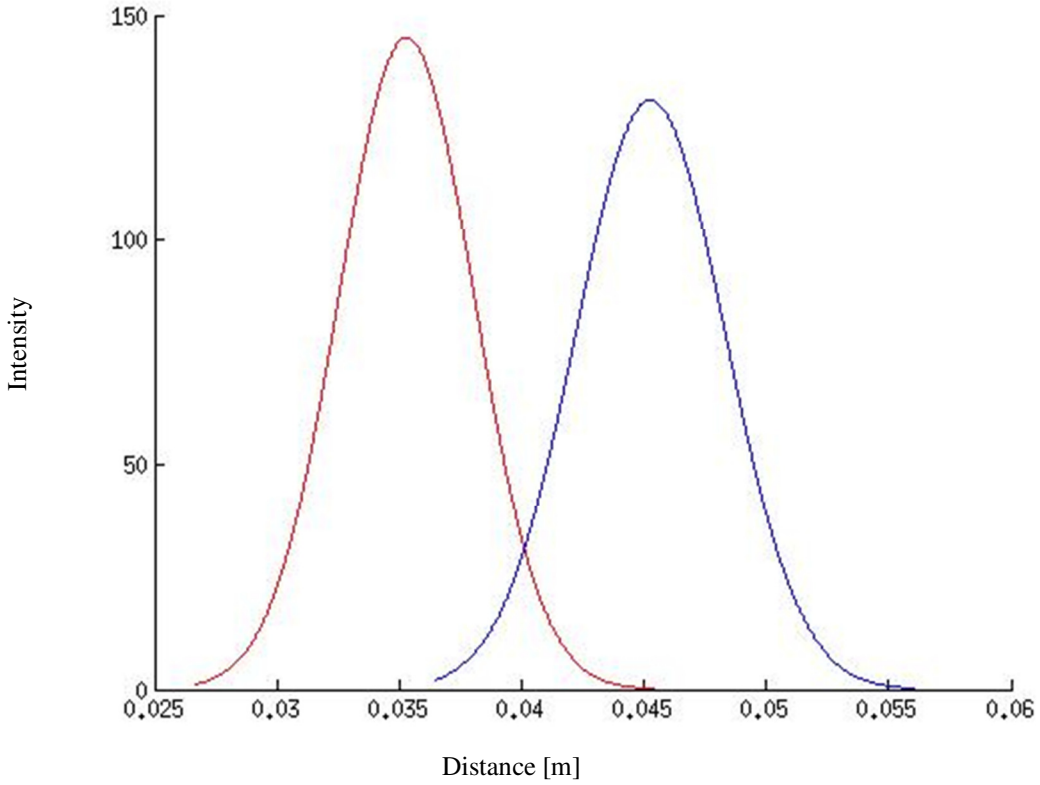

Figure 17.17: Solute zone profile of naphthalene (blue) and anthracene (red). Simulation parameters: Number of molecules N_a=750, N_n=750; radius of fluid phase R = 2.0e-05 m; depth of surface phase d_s = 1.0e-05 m; T = 200s; t = 1.0e-02s, v_0 = 0.001 m/s;

If we consider the advance of the simulation and include the length of capillary, i.e, 25 cm, into the calculation, the peak of naphthalene will show at the detector around 18 minutes. If we further consider the low pressure – compared to high performance liquid chromatography – and that the column simulated is an open tubular layer column, this result can be compared to conventional capillary chromatography.[167]

17.3.2. Electroosmotic flow

To illustrate the influence of the applied voltage, two simulations at two different voltages are shown. Furthermore, the equilibrium rates of the solutes are shown to make clear that equilibrium is reached after approximately one second. The first figure, Figure 17.18, shows the equilibrium rates at 5 kV. Figure 17.19 shows the calculated chromatogram after 200s simulation time. The rate constants for anthracene are k_{sf} = 1.5684 s^{-1} and k_{fs} = 7.8912 s^{-1}. The rate constants for naphthalene are k_{sf} = 2.3845 s^{-1} and k_{fs} = 8.6580 s^{-1}. The velocities for the solutes are $v_{0,n}$ = 1.320e-04 m/s and $v_{0,a}$ = 1.279e-04 m/s.

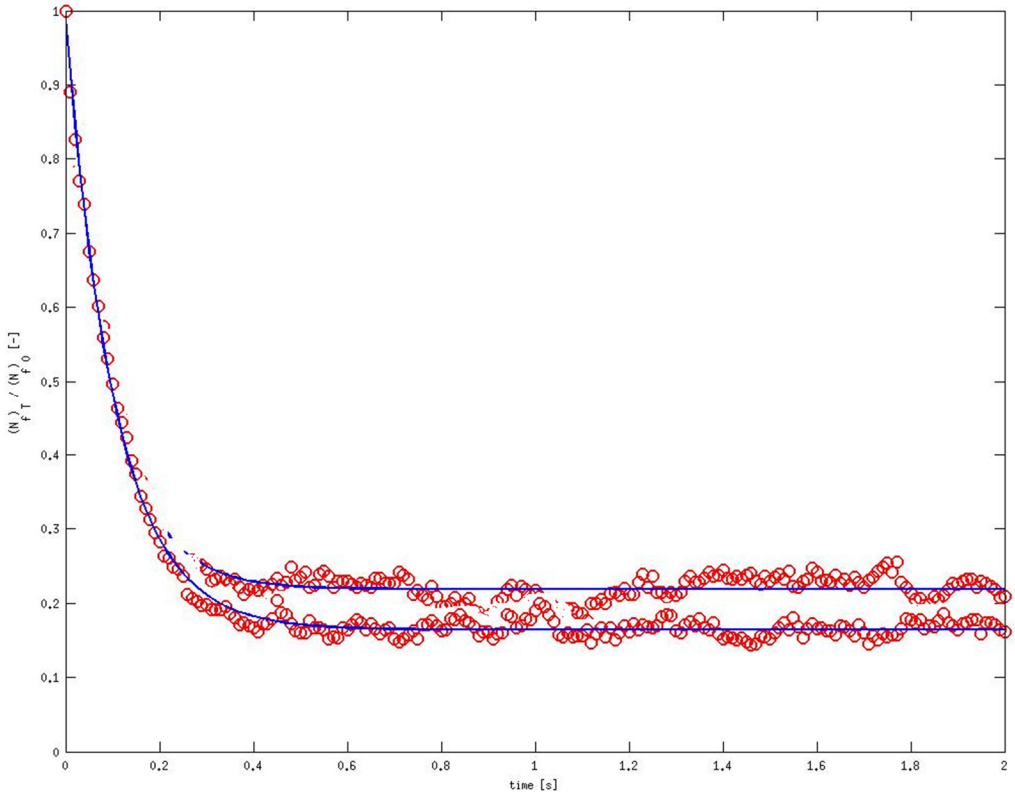

Figure 17.18: Equilibrium rates of naphthalene (top) and anthracene (bottom) from the fluid phase as a function of time, the red circles are the values of the simulation; the solid curve is fitted with non-linear regression analysis; V = 5 kV.

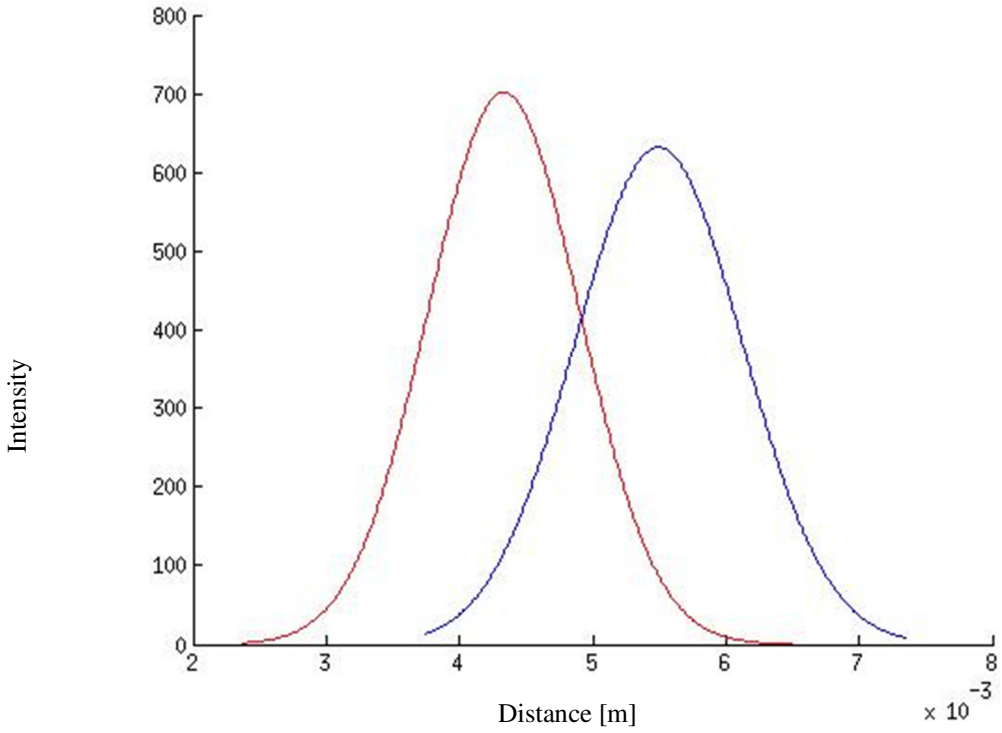

Figure 17.19: Solute zone profile of naphthalene (blue) and anthracene (red). Simulation parameters: Number of molecules N_a=750, N_n=750; radius of fluid phase R = 2.0e-05 m; depth of surface phase d_s = 1.0e-05 m; T = 200s; t = 1.0e-02s, V = 5 kV/m;

To compare the results, a separation was simulated with an applied voltage of 20 kV/m. The same properties as in the previous simulation were used and the separation is again shown after 200s. The equilibrium rates are shown in Figure 17.20. The rate constants for anthracene are k_{sf} = 1.6311 s^{-1} and k_{fs} = 8.5390 s^{-1}. The rate constants for naphthalene are k_{sf} = 2.2965 s^{-1} and k_{fs} = 7.9809 s^{-1}. The calculated mean velocities of the components are $v_{0,a}$ = 5.117e-04 m/s and $v_{0,n}$ = 5.281e-04 m/s, respectively. Figure 17.21 shows the calculated chromatogram of anthracene and naphthalene.

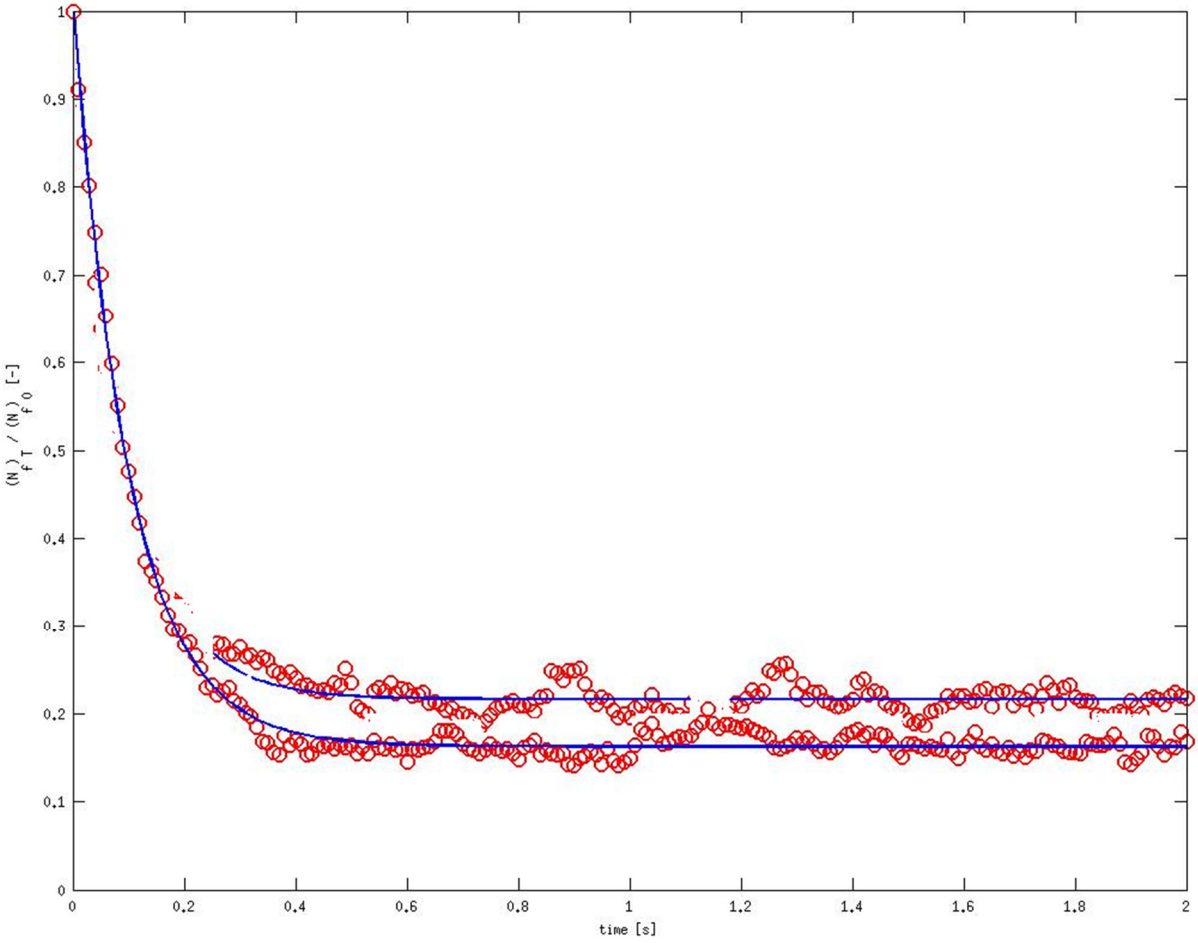

Figure 17.20: Equilibrium rates of naphthalene (top) and anthracene (bottom) from the fluid phase as a function of time, the red circles are the values of the simulation; the solid curve is fitted with non-linear regression analysis; V = 20 kV.

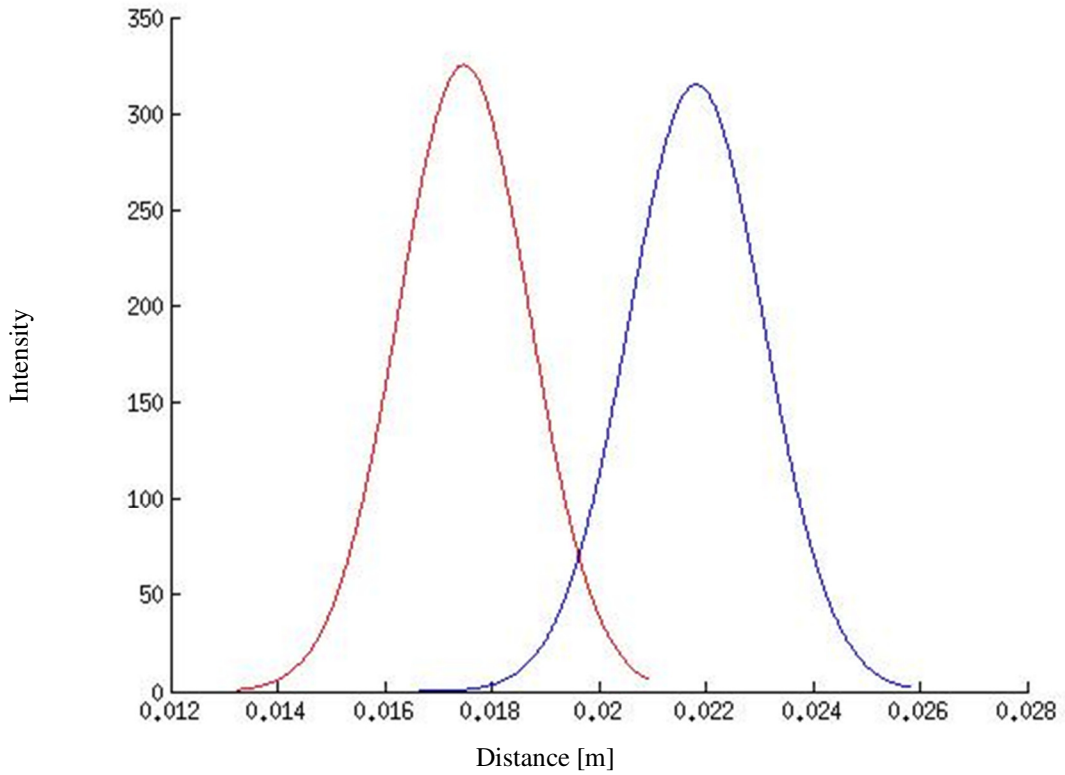

Figure 17.21: Solute zone profile of naphthalene (blue) and anthracene (red). Simulation parameters: Number of molecules N_a=750, N_n=750; radius of fluid phase R = 2.0e-05 m; depth of surface phase d_s = 1.0e-05 m; T = 200s; t = 1.0e-02s, V = 20 kV/m;

As expected, naphthalene is eluted first from the column. In comparison to the pressure induced flow in the capillary, the advance of the substances in the electroosmotic driven flow is not as far after the same amount of simulation time. A reason for that could be the porous layer open-tubular column used in the simulation and producing only a low electroosmotic flow velocity. Then again, common porous layers range around 0.7 µm in width, whereas in the simulation the layer is 10 µm thick.[168] This can have a major influence on the flow velocity.

17.4. Summary of the simulation program

In this chapter, the development of a simulation program was documented. This program includes algorithms for diffusion, convection and retention mechanisms in a chromatographic separation. These algorithms were validated by comparing them to theory and showed reasonable good agreement. To simulate a standard test system, in our case naphthalene and anthracene, diffusion coefficients and properties of these molecules were

inserted into the program. The rate constants of the distribution of these molecules between a mobile and reversed phase stationary phase could be calculated. Furthermore, an actual chromatogram could be obtained for a pressure-driven and an electroosmotic flow driven separation process. These chromatograms show the expected separation behavior of naphthalene and anthracene in a reversed phase chromatographic system.

18. Simulation – abbreviations

$D_{f,s}$	diffusion coefficient
E	electric field strength
I_0	zero order modified Bessel function of the first kind
k_B	Boltzmann constant
$k_{f\text{-}s}$, $k_{f\text{-}s}$	kinetic rate constants
K	distribution coefficient
L	length of the fluid phase
$N_{s,f}$	molecules in the solid, fluid phase
P	applied pressure
$P_{f\text{-}s}$, $P_{s\text{-}f}$	probability of transfer
$P_{NVT}(\Gamma^N)$	Boltzmann equation
r	radius of the particle
R	radius of the fluid phase
t	time increment
T	total simulation time; temperature
T_0	absolute temperature
U	intermolecular potential
v	velocity profile
v_0	mean velocity
$V_{s,f}$	volume of the solid, fluid phase
$X_{s,f}$	solute in fluid or solid phase
z	distance along the z axis
z_a	charge of solute
ε	permittivity in the fluid
ε_0	permittivity in vacuum
κ^{-1}	Debye length
η	viscosity of the fluid phase
μ_q	electrophoretic mobility
ξ	zeta-potential
ρ	radial distance

σ^2	variance

19. Reference List

1. Jacobsen, T.; Wertheimer, A. *Modern Pharmaceutical Industry: A Primer;* Jones and Bartlett Publisher Canada: 2010.

2. Kazakevich, Y.; LoBrutto, R. *HPLC for Pharmaceutical Scientists;* John Wiley and Sons, Inc.: 2007.

3. Bigelow, J. Bioanalytical Tools for Drug Analysis. In *Pharmacology*, Miles, H., William Messer and Kenneth BachmannA, Kenneth, B., Eds.; Academic Press: San Diego, 2009; pp 279-302.

4. Erni, F. Use of high-performance liquid chromatography in the pharmaceutical industry. *Journal of Chromatography A* **1990,** *507* (0), 141-149.

5. Dunn, P.; Wells, A.; Williams, M. *Green Chemistry in Pharmaceutical Industry;* Wiley - VCH, Verlag GmbH & Co. KGaA Germany: 2010.

6. Hjerten, S.; Liao, J. L.; Zhang, R. High-performance liquid chromatography on continuous polymer beds. *Journal of Chromatography A* **1989,** *473* (0), 273-275.

7. Svec, F.; Peters, E. C.; Sykora, D.; Frechet, J. M. J. Design of the monolithic polymers used in capillary electrochromatography columns. *Journal of Chromatography A* **2000,** *887* (1-2), 3-29.

8. Heck, R. M.; Gulati, S.; Farrauto, R. J. The application of monoliths for gas phase catalytic reactions. *Chemical Engineering Journal* **2001,** *82* (1-3), 149-156.

9. Hosoya, K.; Bendo, M.; Tanaka, N.; Watabe, Y.; Ikegami, T.; Minakuchi, H.; Nakanishi, K. An application of silica-based monolithic membrane emulsification technique for easy and efficient preparation of uniformly sized polymer particles. *Macromolecular Materials and Engineering* **2005,** *290* (8), 753-758.

10. Vazquez, M.; Paull, B. Review on recent and advanced applications of monoliths and related porous polymer gels in micro-fluidic devices. *Analytica Chimica Acta* **2010,** *668* (2), 100-113.

11. Huang, X. J.; Yuan, D. X. Recent Developments of Extraction and Micro-extraction Technologies with Porous Monoliths. *Critical Reviews in Analytical Chemistry* **2012,** *42* (1), 38-49.

12. Svec, F. Less common applications of monoliths: Preconcentration and solid-phase extraction. *Journal of Chromatography B-Analytical Technologies in the Biomedical and Life Sciences* **2006,** *841* (1-2), 52-64.

13. Zheng, M. M.; Lin, B.; Feng, Y. Q. Hybrid organic-inorganic octyl monolithic column for in-tube solid-phase microextraction coupled to capillary high-performance liquid chromatography. *Journal of Chromatography A* **2007,** *1164* (1-2), 48-55.

14. Svec, F. Capillary Electrochromatography: A Rapidly Emerging Separation Method. In *Advances in Biochemical Engineering/Biotechnology Vol. 76*, Springer Verlag Berlin Heidelberg: 2002.

15. Svec, F. Capillary column technology: Continuous polymer monoliths. In *Journal of Chromatography Library - Capillary Electrochromatography*, Volume 62 ed.; Svec, F., Deyl, Z., Eds.; Elsevier: 2001; pp 183-240.

16. Maruska, A.; Kornysova, O. Continuous beds (monoliths): stationary phases for liquid chromatography formed using the hydrophobic interaction-based phase separation mechanism. *Journal of Biochemical and Biophysical Methods* **2004,** *59* (1), 1-48.

17. Guiochon, G. Monolithic columns in high-performance liquid chromatography. *Journal of Chromatography A* **2007,** *1168* (1–2), 101-168.

18. Buchmeiser, M. R. Polymeric monolithic materials: Syntheses, properties, functionalization and applications. *Polymer* **2007,** *48* (8), 2187-2198.

19. Xu, L.; Sun, Y. Protein separation by open tubular capillary electrochromatography employing a capillary coated with phenylalanine functionalized tentacle-type polymer under both cathodic and anodic electroosmotic flows. *Journal of Chromatography A* **2008,** *1183* (1-2), 129-134.

20. Lun, Z. H.; Deng, Q. L.; Yan, C.; Gao, R. Y. Molecularly imprinted polymer monolithic column separation of isomers and analogues of vanillin by capillary electrochromatography. *Chinese Journal of Chemistry* **2006,** *24* (3), 442-444.

21. Liu, Z. S.; Xu, Y. L.; Yan, C.; Gao, R. Y. Capillary electrochromatography of molecularly imprinted monolithic column using p-hydroxybenzoic acid as templates. *Chinese Chemical Letters* **2004,** *15* (12), 1469-1472.

22. Allen, D.; El Rassi, Z. Silica-based monoliths for capillary electrochromatography: Methods of fabrication and their applications in analytical separations. *Electrophoresis* **2003,** *24* (22-23), 3962-3976.

23. Colon, L. A.; Burgos, G.; Maloney, T. D.; Cintron, J. M.; Rodriguez, R. L. Recent progress in capillary electrochromatography. *Electrophoresis* **2000,** *21* (18), 3965-3993.

24. Hayes, J. D.; Malik, A. Sol–Gel Monolithic Columns with Reversed Electroosmotic Flow for Capillary Electrochromatography. *Anal. Chem.* **2000,** *72* (17), 4090-4099.

25. Nakanishi, K.; Soga, N. Phase Separation in Gelling Silica–Organic Polymer Solution: Systems Containing Poly(sodium styrenesulfonate). *Journal of the American Ceramic Society* **1991,** *74* (10), 2518-2530.

26. Hench, L. L.; West, J. K. The Sol-Gel Process. *Chemical Reviews* **1990,** *90* (1), 33-72.

27. Siouffi, A. M. Silica gel-based monoliths prepared by the sol-gel method: facts and figures. *Journal of Chromatography A* **2003,** *1000* (1-2), 801-818.

28. Aggarwal, P.; Tolley, H. D.; Lee, M. L. Monolithic bed structure for capillary liquid chromatography. *Journal of Chromatography A* **2012,** *1219*, 1-14.

29. Puy, G.; Roux, R.; Demesmay, C.; Rocca, J. L.; Iapichella, J.; Galameau, A.; Brunel, D. Influence of the hydrothermal treatment on the chromatographic properties of monolithic silica capillaries for nano-liquid chromatography or capillary electrochromatography. *Journal of Chromatography A* **2007,** *1160* (1-2), 150-159.

30. Brinker, C. J.; Scherer, G. W. *Sol-Gel Science;* Academic Press, INC.: 1990.

31. Motokawa, M.; Kobayashi, H.; Ishizuka, N.; Minakuchi, H.; Nakanishi, K.; Jinnai, H.; Hosoya, K.; Ikegami, T.; Tanaka, N. Monolithic silica columns with various skeleton sizes and through-pore sizes for capillary liquid chromatography. *Journal of Chromatography A* **2002,** *961* (1), 53-63.

32. Hertz, A.; FitzGerald, V.; Pignotti, E.; Knowles, J. C.; Sen, T.; Bruce, I. J. Preparation and characterisation of porous silica and silica/titania monoliths for potential use in bone replacement. *Microporous and Mesoporous Materials* **2012,** *156*, 51-61.

33. Unger, K. K. Pore structure of silica. In *Journal of Chromatography Library Volume 16*, Unger, K. K., Ed.; 1979.

34. Unger, K. K. Silica columns - packing procedures and performance characteristics. In *Journal of Chromatography Library Volume 16*, Unger, K. K., Ed.; 1979.

35. Guiochon, G.; Fellinger, A. The Mass Balance Equation of Chromatography and Its General Properties. In *Fundamentals of Preparative and Nonlinear Chromatography*, Elsevier B.V.: 2006.

36. Unger, K. K.; Tanaka, N. Comparison of the Performance of Particle-Packed and Monolithic Columns. In *Monolithic Silicas in Separation Science*, Wiley-VHC: 2011.

37. Al-Bokari, M.; Cherrak, D.; Guiochon, G. Determination of the porosities of monolithic columns by inverse size-exclusion chromatography. *Journal of Chromatography A* **2002,** *975* (2), 275-284.

38. Sing, K. S. W.; Everett, D. H.; Haul, R. A. W.; Moscou, L.; Pierotti, R. A.; Rouquerol, J.; Siemieniewska, T. Reporting Physisorption Data for Gas Solid Systems with Special Reference to the Determination of Surface-Area and Porosity (Recommendations 1984). *Pure and Applied Chemistry* **1985,** *57* (4), 603-619.

39. Jandera, P.; Urban, J. Characterisation of Pore Structure and Its Impact on the Chromatographic Properties of Organic Polymer Monolithic Capillary Columns. In *Monolithic Chromatography and its Modern Application*, Wang, P. G., Ed.; 2010.

40. Barbosa-Cánovas, G.; Ortega-Rivas, E.; Juliano, P.; Ya, H. *Food Powders: Physical Properties, Processing, and Functionality;* Kluwer Academic/Plenum Publisher New York: 2005.

41. Tadanaga, K.; Minami, T. Measurement of Gas Adsorption and Permeability of Sol-Gel Materials. In *Handbook of Sol-Gel Science and Technology*, Sakka, S., Ed.; Kluwer Academic Publisher: 2005.

42. Brunauer, S.; Emmett, P. H.; Teller, E. Adsorption of gases in multimolecular layers. *J. Am. Chem. Soc.* **1938,** *60*, 309-319.

43. Condon, J. *Surface Area and Porosity Determinations by Physisorption;* Elsevier B.V.: 2006.

44. Lowell, S.; Shields, J.; Thomas, M. T. M. Surface Area Analysis from the Langmuir and BET Theories. In *Characterization of Porous Solids and Powders: Surface Area, Pore Size and Density*, Kluwer Academic Publishers: 2004.

45. Allen, T. Surface Determination by Gas Adsorption. In *Particle Size Measurement, Volume 2*, Chapman and Hall: 1997.

46. Washburn, E. W. The dynamics of capillary flow. *Physical Review* **1921,** *17* (3), 273-283.

47. DePhillips, P.; Lenhoff, A. M. Pore size distributions of cation-exchange adsorbents determined by inverse size-exclusion chromatography. *Journal of Chromatography A* **2000,** *883* (1–2), 39-54.

48. Tanaka, N.; Kobayashi, H.; Ishizuka, N.; Minakuchi, H.; Nakanishi, K.; Hosoya, K.; Ikegami, T. Monolithic silica columns for high-efficiency chromatographic separations. *Journal of Chromatography A* **2002,** *965* (1-2), 35-49.

49. Saito, H.; Nakanishi, K.; Hirao, K.; Jinnai, H. Mutual consistency between simulated and measured pressure drops in silica monoliths based on geometrical parameters obtained by three-dimensional laser scanning confocal microscope observations. *Journal of Chromatography A* **2006,** *1119* (1–2), 95-104.

50. Roux, R.; Jaoude, M. A.; Demesmay, C.; Rocca, J. L. Optimization of the single-step synthesis of hybrid C-8 silica monoliths dedicated to nano-liquid chromatography and capillary electrochromatography. *Journal of Chromatography A* **2008,** *1209* (1-2), 120-127.

51. Glenn, K. M.; Lucy, C. A.; Haddad, P. R. Ion chromatography on a latex-coated silica monolith column. *Journal of Chromatography A* **2007,** *1155* (1), 8-14.

52. Skudas, R.; Grimes, B. A.; Machtejevas, E.; Kudirkaite, V.; Kornysova, O.; Hennessy, T. P.; Lubda, D.; Unger, K. K. Impact of pore structural parameters on column performance and resolution of reversed-phase monolithic silica columns for peptides and proteins. *Journal of Chromatography A* **2007,** *1144* (1), 72-84.

53. O Riordain, C.; Gillespie, E.; Connolly, D.; Nesterenko, P. N.; Paull, B. Capillary ion chromatography of inorganic anions on octadecyl silica monolith modified with an amphoteric surfactant. *Journal of Chromatography A* **2007,** *1142* (2), 185-193.

54. Lämmerhofer, M.; Gargano, A. Monoliths with chiral surface functionalization for enantioselective capillary electrochromatography. *Journal of Pharmaceutical and Biomedical Analysis* **2010,** *53* (5), 1091-1123.

55. Zheng, Y.; Wang, X.; Ji, Y. Monoliths with proteins as chiral selectors for enantiomer separation. *Talanta* **2012,** *91* (0), 7-17.

56. Chen, M. L.; Zheng, M. M.; Feng, Y. Q. Preparation of organic–inorganic hybrid silica monolith with octyl and sulfonic acid groups for capillary electrochromatograhpy and application in determination of theophylline and caffeine in beverage. *Journal of Chromatography A* **2010,** *1217* (21), 3547-3556.

57. Ye, F.; Wang, S.; Zhao, S. Preparation and characterization of mixed-mode monolithic silica column for capillary electrochromatography. *Journal of Chromatography A* **2009,** *1216* (51), 8845-8850.

58. Scott, R. P. W. *Liquid Chromatography Column Theory;* John Wiley and Sons: 1992.

59. Cazes, J.; Scott, R. P. W. *Chromatography Theory;* Marcel Dekker, Inc.: 2002.

60. Butt, H.-J.; Graf, K.; Kappl, M. *Physics and Chemistry of Interfaces;* 2003.

61. Snyder, L. R.; Dolan, J. W. *High-Performance Gradient elution: The Practical Application of the Linear-Solvent-Strength Model;* John Wiley and Sons: 2007.

62. Braithwaite, A.; Smith, F. J. *Chromatographic methods;* 5 ed.; Kluwer Academic Publisher: 1999.

63. Vandeemter, J. J. Citation Classic - Longitudinal Diffusion and Resistance to Mass-Transfer As Causes of Non-Ideality in Chromatography. *Current Contents/Engineering Technology & Applied Sciences* **1981,** (3), 16.

64. Sadek, P. C. *Illustrated Pocket Dictionary of Chromatography;* Wiley - Interscience: 2004.

65. Giddings, J. C. The role of lateral diffusion as a rate-controlling mechanism in chromatography. *Journal of Chromatography A* **1961,** *5* (0), 46-60.

66. Giddings, J. C. Reduced plate height equation: a common link between chromatographic methods. *Journal of Chromatography A* **1964,** *13* (0), 301-304.

67. Cazes, J. *Encyclopedia of Chromatography;* Marcel Dekker, INC. 2004.

68. Golay, M. J. E. Height Equivalent to A Theoretical Plate of An Open Tubular Column Lined with A Porous Layer - A Generalized Equation. *Anal. Chem.* **1968,** *40* (2), 382.

69. Li, S. F. Y. *Capillary Electrophoresis: Principles, Practice and Applications;* Elsevier Science Publishers: 1992.

70. Bartle, K. D.; Cikalo, M. G.; Robson, M. M. An Introduction to Capillary Electrochromatography. In *Capillary Electrochromatography*, Bartle, K. D., Myers, P., Eds.; The Royal Society of Chemistry: 2001.

71. Rice, C. L.; Whitehead, R. Electrokinetic Flow in a Narrow Cylindrical Capillary. *J. Phys. Chem.* **1965,** *69* (11), 4017-4024.

72. Cikalo, M. G.; Bartle, K. D.; Robson, M. M.; Myers, P.; Euerby, M. R. Capillary electrochromatography. *Analyst* **1998,** *123* (7), 87R-102R.

73. Enlund, A. M.; Hagman, G.; Isaksson, R.; Westerlund, D. Capillary electrochromatography of basic compounds in pharmaceutical analysis. *Trac-Trends in Analytical Chemistry* **2002,** *21* (6-7), 412-427.

74. Paul, P. H.; Garguilo, M. G.; Rakestraw, D. J. Imaging of Pressure- and Electrokinetically Driven Flows through Open Capillaries. *Anal. Chem.* **1998,** *70* (13), 2459-2467.

75. Li, S.; Lloyd, D. K. Packed-capillary electrochromatographic separation of the enantiomers of neutral and anionic compounds using +¦-cyclodextrin as a chiral selector: Effect of operating parameters and comparison with free-solution capillary electrophoresis. *Journal of Chromatography A* **1994,** *666* (1–2), 321-335.

76. Lelievre, F.; Yan, C.; Zare, R. N.; Gareil, P. Capillary electrochromatography: operating characteristics and enantiomeric separations. *Journal of Chromatography A* **1996,** *723* (1), 145-156.

77. Kitagawa, S.; Tsuda, T. Effects of pH and organic solvent on chromatographic behavior in capillary electrochromatography. *J. Micro. Sep.* **1994,** *6* (2), 91-96.

78. Colon, L. A.; Reynolds, K. J.; Alicea-Maldonado, R.; Fermier, A. M. Advances in capillary electrochromatography. *Electrophoresis* **1997,** *18* (12-13), 2162-2174.

79. Dongqing, L. Experimental studies of electroosmotic flow. In *Interface Science and Technology. Electrokinetics in Microfluidics*, Volume 2 ed.; Dongqing, L., Ed.; Elsevier: 2004; pp 354-462.

80. Johnson, C. M.; McKeown, A. P.; Euerby, M. R. Modes of CEC separation. In *Journal of Chromatography Library. Capillary Electrochromatography*, Volume 62 ed.; Deyl, Z., Svec, F., Eds.; Elsevier: 2001; pp 87-110.

81. Schwartz, H.; Wanders, B. Capillary Electrophoresis. In *Handbook of HPLC*, Katz, E., Eksteen, R., Eds.; Dekker: 1998.

82. Ye, M.; Zou, H.; Liu, Z.; Ni, J. Separation of acidic compounds by strong anion-exchange capillary electrochromatography. *Journal of Chromatography A* **2000,** *887* (1–2), 223-231.

83. Hostettmann, K. Preparative Pressure Liquid Chromatography. In *Preparative Chromatography Techniques: Applications in Natural Product Isolation*, Hostettmann, K., Marston, A., Eds.; Springer-Verlag Berlin: 1998.

84. Snyder, L. R.; Kirkland, J. J. *Introduction to modern liquid chromatography;* John Wiley and sons, INC: 1979.

85. Rathore, A.; Velayudhan, A. *Scale-up and Optimization in Preparative Chromatography: Principles and Biopharmaceutical Applications;* Marcel Dekker, Inc.: 2002.

86. Wall, P. *Thin Layer Chromatography: A Practical Approach;* The Royal Society of Chemistry: 2005.

87. Nurok, D. Planar electrochromatography. *Journal of Chromatography A* **2004,** *1044* (1-2), 83-96.

88. Srivastava, M. *High-Performance Thin Layer Chromatography (HPTLC);* Spinger Verlag Berlin: 2011.

89. Nyiredy, S. Preparative Thin-Layer Chromatography. In *Handbook of Thin-Layer Chromatogprahy*, Marcel Dekker, Inc.: 2003.

90. Howard, A. G.; Shafik, T.; Moffatt, F.; Wilson, I. D. Electroosmotically driven thin-layer electrochromatography on silica media. *Journal of Chromatography A* **1999,** *844* (1–2), 333-340.

91. Nurok, D.; Koers, J. M.; Carmichael, M. A. Role of buffer concentration and applied voltage in obtaining a good separation in planar electrochromatography. *Journal of Chromatography A* **2003,** *983* (1-2), 247-253.

92. Dzido, T. H.; Plocharz, P. W.; Slazak, P.; Halka, A. Progress in planar electrochromatography. *Analytical and Bioanalytical Chemistry* **2008,** *391* (6), 2111-2118.

93. Dzido, T. H.; Mroz, J.; Jozwiak, G. W. Adaptation of a horizontal DS chamber to planar electrochromatography in a closed system. *Jpc-Journal of Planar Chromatography-Modern Tlc* **2004,** *17* (6), 404-410.

94. Dzido, T. H.; Plocharz, P. W.; Slazak, P. Apparatus for pressurized planar electrochromatography in a completely closed system. *Anal. Chem.* **2006,** *78* (13), 4713-4721.

95. Nurok, D.; Koers, J. M.; Novotny, A. L.; Carmichael, M. A.; Kosiba, J. J.; Santini, R. E.; Hawkins, G. L.; Replogle, R. W. Apparatus and initial results for pressurized planar electrochromatography. *Anal. Chem.* **2004,** *76* (6), 1690-1695.

96. Tate, P. A.; Dorsey, J. G. Linear voltage profiles and flow homogeneity in pressurized. planar electrochromatography. *Journal of Chromatography A* **2006,** *1103* (1), 150-157.

97. Sherma, J. Planar Chromatography. *Anal. Chem.* **2010,** *82* (12), 4895-4910.

98. Nishizawa, H.; Tahara, K.; Miyamori, S.; Motegi, Y.; Shoji, T.; Abe, Y. True moving bed chromatography: solid-liquid multi-stage counter-current extraction. *Journal of Chromatography A* **1999,** *849* (1), 61-69.

99. Guiochon, G.; Shirazi, D.; Fellinger, A. *Fundamentals of Preparative and Nonlinear Chromatography;* Academic Press: 2006.

100. Bart, H. J.; Pilz, S. *Industrial Scale Natural Products Extraction;* Wiley-VCH: 2011.

101. Schulte, M.; Strube, J. Preparative enantioseparation by simulated moving bed chromatography. *Journal of Chromatography A* **2001,** *906* (1–2), 399-416.

102. Klatt, K. U.; Hanisch, F.; D++nnebier, G. Model-based control of a simulated moving bed chromatographic process for the separation of fructose and glucose. *Journal of Process Control* **2002,** *12* (2), 203-219.

103. Rajendran, A.; Paredes, G.; Mazzotti, M. Simulated moving bed chromatography for the separation of enantiomers. *Journal of Chromatography A* **2009,** *1216* (4), 709-738.

104. Minceva, M.; Pais, L. S.; Rodrigues, A. E. Cyclic steady state of simulated moving bed processes for enantiomers separation. *Chemical Engineering and Processing* **2003,** *42* (2), 93-104.

105. Schmidt-Traub, H.; Seidel-Morgenstern, A. *Preparative Chromatography;* Wiley-VCH: 2012.

106. Hilbrig, F.; Freitag, R. Continuous annular chromatography. *Journal of Chromatography B-Analytical Technologies in the Biomedical and Life Sciences* **2003,** *790* (1-2), 1-15.

107. Bart, H. J.; Messenbock, R. C.; Byers, C. H.; Prior, A.; Wolfgang, J. Continuous chromatographic separation of fructose, mannitol and sorbitol. *Chemical Engineering and Processing* **1996,** *35* (6), 459-471.

108. Wankat, P. C. The relationship between one-dimensional and two-dimensional separation processes. *AIChE J.* **1977,** *23* (6), 859-867.

109. Uretschlager, A.; Jungbauer, A. Preparative continuous annular chromatography (P-CAC), a review. *Bioprocess and Biosystems Engineering* **2002,** *25* (2), 129-140.

110. Wolfgang, J. Continuous Annular Chromatography. In *Modern Advances in Chromatography*, Freitag, R., Ed.; 2002.

111. Brozio, J.; Bart, H. J. Heat transfer and hydrodynamics in preparative continuous annular chromatography (P-CAC). *Chemical Engineering & Technology* **2000,** *23* (10), 893-899.

112. Brozio, J.; Bart, H. M. A rigorous model for annular chromatography. *Chemical Engineering & Technology* **2004,** *27* (9), 962-970.

113. Tobiska, L.; Thiele, A. Numerical Simulation of Annular Chromatography. In *Mathematics. Key Technology for the Future*, Jäger, W., Krebs, H.-J., Eds.; Spinger Verlag Berlin: 2002.

114. Braunbruck, M. Development of a stationary phase for continuous annular electrochromatography. Master Thesis Graz University of Technology, 2009.

115. Waksmundzka-Hajnos, M.; Petruczynik, A.; Hawryl, A. Comparison of chromatographic properties of cyanopropyl-, diol- and aminopropyl- polar-bonded stationary phases by the retention of model compounds in normal-phase liquid chromatography systems. *Journal of Chromatography A* **2001,** *919* (1), 39-50.

116. Kazoka, H. HPLC separation of some purine and pyrimidine derivatives on Chromolith Performance Si monolithic column. *Journal of Biochemical and Biophysical Methods* **2007,** *70* (1), 15-21.

117. Adachi, T.; Sakka, S. Preparation of Monolithic Silica-Gel and Glass by the Sol-Gel Method Using N,N-Dimethylformamide. *Journal of Materials Science* **1987,** *22* (12), 4407-4410.

118. Ma, X. D.; Sun, H. W.; Yu, P. A novel way for preparing high surface area silica monolith with bimodal pore structure. *Journal of Materials Science* **2008,** *43* (3), 887-891.

119. Rao, A. P.; Rao, A. V. Study the influence of drying control chemical additives on the physical and optical properties of nanocrystalline cadmium sulfide-doped tetraethylorthosilicate silica xerogels. *Journal of Materials Synthesis and Processing* **2002,** *10* (1), 7-16.

120. Ding, G. S.; Da, Z. L.; Yuan, R. J.; Bao, J. J. Reversed-phase and weak anion-exchange mixed-mode silica-based monolithic column for capillary electrochromatography. *Electrophoresis* **2006,** *27* (17), 3363-3372.

121. Rieux, L.; Niederlander, H.; Verpoorte, E.; Bischoff, R. Silica monolithic columns: Synthesis, characterisation and applications to the analysis of biological molecules. *Journal of Separation Science* **2005,** *28* (14), 1628-1641.

122. Ikegami, T.; Horie, K.; Jaafar, J.; Hosoya, K.; Tanaka, N. Preparation of highly efficient monolithic silica capillary columns for the separations in weak cation-exchange and HILIC modes. *Journal of Biochemical and Biophysical Methods* **2007,** *70* (1), 31-37.

123. Watanabe, Y.; Ikegami, T.; Horie, K.; Hara, T.; Jaafar, J.; Tanaka, N. Improvement of separation efficiencies of anion-exchange chromatography using monolithic silica capillary columns modified with polyacrylates and polymethacrylates containing tertiary amino or quaternary ammonium groups. *Journal of Chromatography A* **2009,** *1216* (44), 7394-7401.

124. Lubda, D.; Lindner, W. Monolithic silica columns with chemically bonded tert-butylcarbamoylquinine chiral anion-exchanger selector as a stationary phase for enantiomer separations. *Journal of Chromatography A* **2004,** *1036* (2), 135-143.

125. Minakuchi, H.; Nakanishi, K.; Soga, N.; Ishizuka, N.; Tanaka, N. Octadecylsilylated porous silica rods as separation media for reversed-phase liquid chromatography. *Anal. Chem.* **1996,** *68* (19), 3498-3501.

126. Ishizuka, N.; Minakuchi, H.; Nakanishi, K.; Soga, N.; Nagayama, H.; Hosoya, K.; Tanaka, N. Performance of a monolithic silica column in a capillary under pressure-driven and electrodriven conditions. *Anal. Chem.* **2000,** *72* (6), 1275-1280.

127. Hara, T.; Kobayashi, H.; Ikegami, T.; Nakanishi, K.; Tanaka, N. Performance of monolithic silica capillary columns with increased phase ratios and small-sized domains. *Anal. Chem.* **2006,** *78* (22), 7632-7642.

128. Dulay, M. T.; Kulkarni, R. P.; Zare, R. N. Preparation and characterization of monolithic porous capillary columns loaded with chromatographic particles. *Anal. Chem.* **1998,** *70* (23), 5103-5107.

129. Fujimoto, C. Preparation of fritless packed silica columns for capillary electrochromatography. *Hrc-Journal of High Resolution Chromatography* **2000,** *23* (1), 89-92.

130. Kato, M.; Onda, Y.; Sakai-Kato, K.; Toyoka, T. Simultaneous analysis of cationic, anionic, and neutral compounds using monolithic CEC columns. *Analytical and Bioanalytical Chemistry* **2006,** *386* (3), 572-577.

131. Allen, D.; El Rassi, Z. Capillary electrochromatography with monolithic silica column: I. Preparation of silica monoliths having surface-bound octadecyl moieties and their chromatographic characterization and applications to the separation of neutral and charged species. *Electrophoresis* **2003,** *24* (3), 408-420.

132. Tanaka, N.; Nagayama, H.; Kobayashi, H.; Ikegami, T.; Hosoya, K.; Ishizuka, N.; Minakuchi, H.; Nakanishi, K.; Cabrera, K.; Lubda, D. Monolithic silica columns for HPLC, micro-HPLC, and CEC. *Hrc-Journal of High Resolution Chromatography* **2000,** *23* (1), 111-116.

133. Xie, S.; Allington, R.; Frechet, J.; Svec, F. Porous Polymer Monoliths: An Alternative to Classical Beads. In *Modern Advances in Chromatography*, 76 ed.; Freitag, R., Ed.; Springer Berlin / Heidelberg: 2002; pp 87-125.

134. Dulay, M. T.; Quirino, J. P.; Bennett, B. D.; Kato, M.; Zare, R. N. Photopolymerized sol-gel monoliths for capillary electrochromatography. *Anal. Chem.* **2001,** *73* (16), 3921-3926.

135. Schmid, M. G.; Koidl, J.; Wank, P.; Kargl, G.; Zohrer, H.; Gubitz, G. Enantioseparation by ligand-exchange using particle-loaded monoliths: Capillary-LC versus capillary electrochromatography. *Journal of Biochemical and Biophysical Methods* **2007,** *70* (1), 77-85.

136. Liapis, A. I.; Meyers, J. J.; Crosser, O. K. Modeling and simulation of the dynamic behavior of monoliths. Effects of pore structure from pore network model analysis and comparison with columns packed with porous spherical particles. *Journal of Chromatography A* **1999,** *865* (1-2), 13-25.

137. Ishizuka, N.; Minakuchi, H.; Nakanishi, K.; Soga, N.; Tanaka, N. Designing monolithic double-pore silica for high-speed liquid chromatography. *Journal of Chromatography A* **1998,** *797* (1-2), 133-137.

138. Buchmeister, M. R. *Polymeric Materials in Organic Synthesis and Catalysis;* Wiley-VCH: 2003.

139. Ruike, M.; Houzouji, M.; Motohashi, A.; Murase, N.; Kinoshita, A.; Kaneko, K. Pore structure of porous silicon formed on a lightly doped crystal silicon. *Langmuir* **1996,** *12* (20), 4828-4831.

140. Chen, M. L.; Zheng, M. M.; Feng, Y. Q. Preparation of organicΓÇôinorganic hybrid silica monolith with octyl and sulfonic acid groups for capillary electrochromatograhpy and application in determination of theophylline and caffeine in beverage. *Journal of Chromatography A* **2010,** *1217* (21), 3547-3556.

141. Planeta, J.; Moravcova, D.; Roth, M.; Karísek, P.; Kahle, V. Silica-based monolithic capillary columns: Effect of preparation temperature on separation efficiency. *Journal of Chromatography A* **2010,** *1217* (36), 5737-5740.

142. Saito, H.; Kanamori, K.; Nakanish, K.; Hirao, K. Real space observation of silica monoliths in the formation process. *Journal of Separation Science* **2007,** *30* (17), 2881-2887.

143. Yan, L. J.; Zhang, Q. H.; Feng, Y. Q.; Zhang, W. B.; Li, T.; Zhang, L. H.; Zhang, Y. K. Octyl-functionalized hybrid silica monolithic column for reversed-phase capillary electrochromatography. *Journal of Chromatography A* **2006,** *1121* (1), 92-98.

144. Tang, Q.; Xin, B.; Lee, M. L. Monolithic columns containing sol–gel bonded octadecylsilica for capillary electrochromatography. *Journal of Chromatography A* **1999,** *837* (1ΓÇô2), 35-50.

145. Xu, L.; Lee, H. K. Preparation, characterization and analytical application of a hybrid organic–inorganic silica-based monolith. *Journal of Chromatography A* **2008,** *1195* (1–2), 78-84.

146. Banko, C. Production of stationary phases for the purification of fine chemicals and active pharmaceutical ingredients with electrochromatography. Master Thesis Graz University of Technology, 2012.

147. Qu, Q. S.; He, Y. Z.; Gan, W. E.; Deng, N.; Lin, X. Q. Electrochromatography with a 2.7 mm inner diameter monolithic column. *Journal of Chromatography A* **2003,** *983* (1-2), 255-262.

148. Stöber, W.; Fink, A.; Bohn, E. Controlled growth of monodisperse silica spheres in the micron size range. *Journal of Colloid and Interface Science* **1968,** *26* (1), 62-69.

149. Tanaka, N.; Nagayama, H.; Kobayashi, H.; Ikegami, T.; Hosoya, K.; Ishizuka, N.; Minakuchi, H.; Nakanishi, K.; Cabrera, K.; Lubda, D. Monolithic Silica Columns for HPLC, Micro-HPLC, and CEC. *J. High Resol. Chromatogr.* **2000,** *23* (1), 111-116.

150. Lapidus, L.; Amundson, N. R. Mathematics of Adsorption in Beds .6. the Effect of Longitudinal Diffusion in Ion Exchange and Chromatographic Columns. *Journal of Physical Chemistry* **1952,** *56* (8), 984-988.

151. Golshan-Shirazi, S.; Guiochon, G. Comparison of the various kinetic models of non-linear chromatography. *Journal of Chromatography A* **1992,** *603* (1–2), 1-11.

152. Thomas, H. C. Heterogeneous Ion Exchange in a Flowing System. *J. Am. Chem. Soc.* **1944,** *66* (10), 1664-1666.

153. Felinger, A.; Cavazzini, A.; Dondi, F. Equivalence of the microscopic and macroscopic models of chromatography: stochastic–dispersive versus lumped kinetic model. *Journal of Chromatography A* **2004,** *1043* (2), 149-157.

154. Felinger, A. Molecular dynamic theories in chromatography. *Journal of Chromatography A* **2008,** *1184* (1-2), 20-41.

155. Giddings, J. C.; Eyring, H. A Molecular Dynamic Theory of Chromatography. *Journal of Physical Chemistry* **1955,** *59* (5), 416-421.

156. Dondi, F.; Munari, P.; Remelli, M.; Cavazzini, A. Monte Carlo Model of Nonlinear Chromatography. *Anal. Chem.* **2000,** *72* (18), 4353-4362.

157. Cavazzini, A.; Dondi, F.; Jaulmes, A.; Vidal-Madjar, C.; Felinger, A. Monte Carlo Model of Nonlinear Chromatography: Correspondence between the Microscopic Stochastic Model and the Macroscopic Thomas Kinetic Model. *Anal. Chem.* **2002,** *74* (24), 6269-6278.

158. Allen, M. P.; Tildesley, J. Monte Carlo Methods. In *Computer Simulation of Liquids*, Allen, M. P., Ed.; 1987.

159. Landau, D.; Binder, K. *A Guide to Monte Carlo Simulations in Statistical Physics;* Cambridge Universtiy Press: 2000.

160. Smit, B.; Maesen, T. L. M. Molecular simulations of zeolites: Adsorption, diffusion, and shape selectivity. *Chemical Reviews* **2008,** *108* (10), 4125-4184.

161. McCalley, D. V. Comparison of conventional microparticulate and a monolithic reversed-phase column for high-efficiency fast liquid chromatography of basic compounds. *Journal of Chromatography A* **2002,** *965* (1-2), 51-64.

162. McGuffin, V. L.; Wu, P. R. Three-dimensional molecular simulation of chromatographic separations. *Journal of Chromatography A* **1996,** *722* (1-2), 3-17.

163. Hopkins, D. L.; McGuffin, V. L. Three-dimensional molecular simulation of electrophoretic separations. *Anal. Chem.* **1998,** *70* (6), 1066-1075.

164. Novák, J.; Janák, J. Basic processes in chromatography. In *Liquid Column Chromatography: A survey of modern techniques and applications*, Macek, K., Deyl, Z., Janák, J., Eds.; Elsevier Scientific Publishing Company: 1975.

165. McGuffin, V. L. Theory of chromatography. In *Journal of Chromatography Library: Fundamentals and applications of chromatography and related differential migration methods*, Volume 69 ed.; Heftmann, E., Ed.; Elsevier: 2004; pp 1-93.

166. Sawatsky, N.; Feng, Y.; Dudas, M. J. Diffusion of 1-naphthol and naphthalene through clay materials: Measurement of apparent exclusion of solute from the pore space. *Journal of Contaminant Hydrology* **1997,** *27* (1–2), 25-41.

167. Tsuda, T. Electroosmosis and Electrochromatography. In *Electric Field Application*, VCH Verlagsgesellschaft Weinheim, Germany: 2008.

168. Crego, A. L.; Martinez, J.; Marina, M. L. Influence of mobile phase composition on electroosmotic flow velocity, solute retention and column efficiency in open-tubular reversed-phase capillary electrochromatography. *Journal of Chromatography A* **2000,** *869* (1–2), 329-337.

SUMMARY AND OUTLOOK

This thesis depicts the development of a stationary phase for continuous annular electrochromatography. This task was embedded in the CAEC research project, co – financed by the 7th Framework Programme of the European Commission.

In the beginning, different monolithic backbones like inorganic and organic monomers and different functionalization possibilities of silica-based monoliths like amino groups and normal phase were investigated. The C_8-functionalized silica-based monolithic column including porous silica particles showed the best properties for our approach. This reversed phase material was characterized with FTIR spectroscopy, nitrogen physisorption and mercury intrusion and elemental analysis was performed. The results of the characterization showed

- a loading of **3.8 µmol/m^2** C_8-groups for the reversed phase
- a density of the C_8-functionlalized material including silica particles of **1.30 cm^3/g**
- a BET surface area up to **170 m^2/g**
- and a porosity up to **83%.**

The reversed phase stationary phase was implemented into different molds, namely capillaries for capillary electrochromatography, a planar test cell and in between to glass cylinders for the annular prototype. Figure I shows all three molds filled with the developed stationary phase.

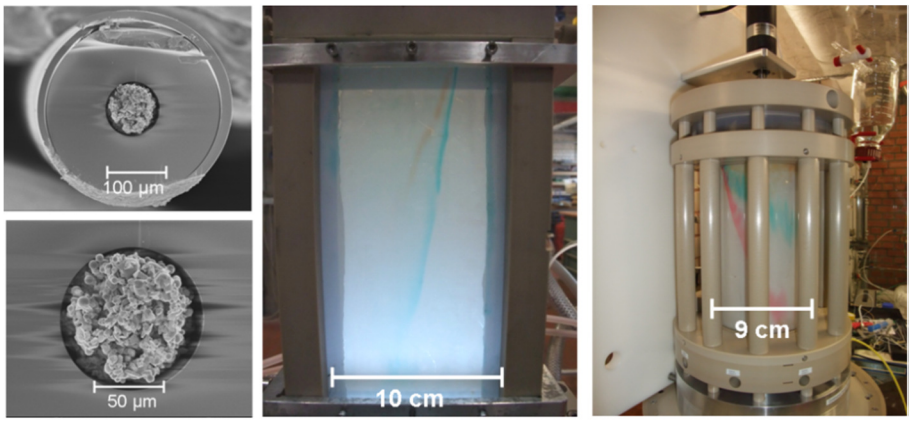

Figure I: Pictures of capillaries for CEC (left), the planar test cell (middle) and the annular prototype, filled with C_8-functionalized stationary phase

Besides the physical properties of the monolithic materials the separation efficiency in the different molds were investigated. Therefore, a standard test system was used, namely thiourea, naphthalene and anthracene. Furthermore, more complex systems, i.e., a mixture of polycyclic aromatic hydrocarbons, a mixture of alkylbenzenes and a mixture of phenols were separated in the capillaries. Separation efficiencies in the capillaries up to

- **39 000** per meter for the PAHs
- **25 000** per meter for the alkylbenzenes and
- **30 000** per meter could be achieved for the phenol mixture.

In the planar test cell, the standard test system and the PAHs mixture could be separated with high resolution values and plate numbers up to **15 000** per meter for the standard test system could be achieved. The volume flow was increased from 10 ml/h in the 0.3 mm gap to more than **40 ml/h** in the **1 mm** gap.

In the annular geometry, a volume flow of more than **300 ml/h** could be obtained. Furthermore, the resolutions of the standard test system were higher than **1**.

The second part of this work deals with the development of a **simulation program** to predict the **interactions of solute molecules with the mobile and the stationary phase**. Therefore, property parameters for the standard test system, namely naphthalene and anthracene, and for the reversed phase stationary phase were inserted into the program developed. The output of the program gives

- the calculated **rate constants** of the solutes and
- actual **chromatograms** of the separation of the test molecules.

Therefore, this program can provide predictions of the separation behavior on different stationary phases.

Thus, the project CAEC is completed. However, there has still work to be done to improve the separation efficiency in the annular prototype. Furthermore, the prototype has to be validated with industrial separation problems. Therefore, a follow-up project is planned between the Graz University of Technology and the Kaiserslautern University of Technology. This should not only increase efficiency of already presented materials, but develop new ones for specific separation problems with the know-how acquired in this work task.